Otto Scheibelhofer, BSc

Combining Rheometric Powder Characterization Techniques with Near Infrared Spectroscopy based on Experimental Design and Multivariate Data Analysis

MASTER THESIS

For obtaining the academic degree
Diplom-Ingenieur

Master Programme of
Technical Physics

Graz University of Technology

Graz University of Technology

Supervisor:

Ao.Univ.-Prof. Mag. Dr.rer.nat. Robert Schennach

Institute of Solid State Physics

Graz, October 2010

Otto Scheibelhofer, BSc

Kombination von pulverrheometrischen Methoden mit Nahinfrarotspektroskopie mittels statistischer Versuchsplanung und multivariater Datenanalyse

MASTERARBEIT

zur Erlangung des akademischen Grades
Diplom-Ingenieur

Masterstudium Technische Physik

Graz University of Technology

Technische Universität Graz

Betreuer:

Ao.Univ.-Prof. Mag. Dr.rer.nat. Robert Schennach

Institut für Festkörperphysik

Graz, Oktober 2010

EIDESSTATTLICHE ERKLÄRUNG

Ich erkläre an Eides statt, dass ich die vorliegende Arbeit selbstständig verfasst, andere als die angegebenen Quellen/Hilfsmittel nicht benutzt, und die den benutzten Quellen wörtlich und inhaltlich entnommene Stellen als solche kenntlich gemacht habe.

Graz, am ……………………………   ……………………………………………………..
                                                                          (Unterschrift)

STATUTORY DECLARATION

I declare that I have authored this thesis independently, that I have not used other than the declared sources / resources, and that I have explicitly marked all material which has been quoted either literally or by content from the used sources.

……………………………   ……………………………………………………..
        date   (signature)

Acknowledgement

Abstract

Flow and blending of pharmaceutical powders is a complex process, as the behaviour significantly changes with processing history, mixer type and process scale up. Therefore, knowledge of the powder attributes and their influence on the mixing is essential.

In this work, a comprehensive characterization of powders based on Design of Experiments was carried out with the FT4 Powder Rheometer. Pure powders and powder blends have been investigated thoroughly, in order to establish Multivariate Data Analysis models, more precisely using Partial Least Squares Regression, for a multitude of different parameters. Using the advantage of the FT4, i.e., higher reproducibility than traditional methods like shear cell tests and flow through a funnel, sound models were developed and examined.

Complementary, blending processes have been investigated by near infrared spectroscopy, at different critical positions. Finally, an attempt to establish connections between rheological parameters of blends and blending attributes has been made.

Kurzfassung

Fließ- und Mischverhalten von pharmazeutischen Pulvern ist ein komplexer Prozess, da sich das Verhalten abhängig von vorangegangenen Prozessen, Mischertypen, sowie zwischen Laboraufbauten und Industrieanlagen signifikant ändert. Daher ist das Wissen um Pulvereigenschaften und ihren Einfluss auf das Mischen notwendig.

In dieser Arbeit wurde eine Charakterisierung von Pulvern, basierend auf statistischer Versuchsplanung, mittels des FT4 Pulverrheometers durchgeführt. Reine Pulver und Pulvergemische wurden umfassend untersucht, in der Absicht, mittels multivariater Datenanalyse, der Partial Least Squares Regression, Modelle für unterschiedliche Parameter zu erstellen. Den Vorteil der höheren Reproduzierbarkeit des FT4, gegenüber traditionellen Methoden wie Scherzelle und Trichterfluss, nutzend, wurden fundierte Modelle erstellt und evaluiert.

Ergänzend wurden Mischprozesse mittels Nahinfrarot-Spektroskopie, an verschiedenen kritischen Positionen untersucht. Schlussendlich wurde der Versuch unternommen, Verbindungen zwischend den rheologischen Parametern von Mischungen und den Mischgrößen herzustellen.

Table of Contents

Nomenclature and Abbreviations

Nomenclature

Scalars are denoted with small letters a, vectors are bold-face $\boldsymbol{a}$, matrices are noted in capital letters A, and tensors are double-underlined $\underline{\underline{a}}$. A hat $\hat{a}$ indicates, that the value is predicted. Rheological parameters are noted down in capital abbreviations AAA.

Abbreviations

α, β	regression coefficients	k	wavenumber
χ^2	χ^2-distribution	k	number of factors
λ	wavelength	l	number of wavenumbers
ν	degrees of freedom	$LogC$	LogFit of Compressbility
ϕ_i	surface charge density	M	number of responses
σ^2	variance	MCC	Microcrystalline cellulose
σ_{ii}	normal stress	MPS	Major Principal Stress
τ_{ij}	shear stress	M_{AS}	mixture performance
τ_0	cohesion	n	number of tappings
φ_e	effective angle of internal friction	N	number of samples
φ_i	angle of internal friction	N_{ij}	parameter values
ϱ	density	p	desired concentration
A	number of principal components	P	loading matrix
a	inclination	$P8$	Permeability at 8 kPa (Pressure Drop)
A, B, C	factors	$PD2$	Poured Density at -2 deg
AEE	Aeration End Energy	$Q_r(x)$	cumulative particle size distribution
AIF	Angle of Internal Friction	$q_r(x)$	particle size density distribution
$AIFE$	Effective Angle of Internal Friction	r	number of samples taken
AR	Aeration Ratio	R	half factor range
ASA	Acetylsalicylic acid	s	number of parameter values
a_k	spectral intensity	SE	Specific Energy
BFE	Basic Flow Energy	SI	Stability Index
$BFE2$	Basic Flow Energy at -2 deg	s^2	empirical variance
CBD	Conditioned Bulk Density	T	score matrix
CE	Consolidated Energy (250 taps)	TAB	Lactose monohydrate
Coh	Cohesion	U	contact potential
d	distance	UYS	Unconfined Yield Strength
E	residual matrix	v	air speed
F	Force	V	volume
f	number of center points	W	van-der-Waals energy
ffc	flow function constant	x	Particle size
Flu	Fluidisation Point	x	realisation of factor
FRI	Flow Rate Index	x_i	concentration in sample i
HR	Hausner Ratio	y	realisation of response
I	intensity		

1. Introduction

(a) Powder Avalanche in the Suisse Alps [1]
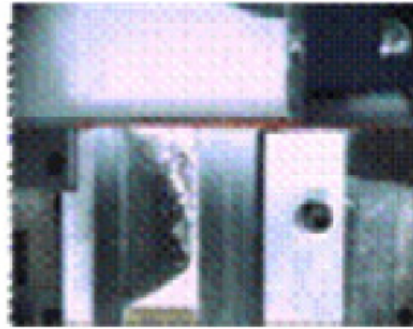
(b) Shoe filling for tablet pressing [2]

Figure 1.1.: Occurrence of powder flow in nature and industry on vastly different scales.

1.1. A castle built of sand

Powders accompany our existence, and it is astonishing how often they are encountered in daily live. The dust found under the bed, the flour bread is made of, the cement houses are built with and the ingredients tablets are made of, all share the same attribute, that they are granular materials. They consist of an often uncountable number of smaller individual particles, every particle with its own distinct shape and properties. This makes powders difficult to understand and describe, and very often unpredictable.

A bulk of powder sitting as a conical heap on a surface is very different from the same powder gliding down a chamfer. Describing powders and their behaviours is a necessary and challenging goal in widely diverse fields of applications, whereof two are representatively shown in figure 1.1. Avalanches are an example of powder flow, and the properties of the snow flakes determine path and hazardousness of such an avalanche. Contrary, for shoe filling, fast and homogeneous powder flow should be achieved for a very small amount of powder, in order to fill the die fast and completely.

To characterize powders, a lot of different attributes have to be taken into account. Furthermore, environmental influences can change powders' behaviours drastically. Adding some water to dry sand, enables the construction of stable walls of sand and the

building of beautiful castles, but an additional drop of water may lead to the formation of mud and losing the shape of the castle.

Blending different powders can be a very difficult task, or sometimes even impossible. The annoyance of unmixed muesli for breakfast is a common and well known problem. A more severe challenge is the blending uniformity for pharmaceutical powders, because within a tablet the right fractions and distributions of substances must be contained, to not lead to overdose or being useless. Furthermore, most pharmaceutical powders are plain white, and not distinguishable with the plain eye, so spectroscopic methods must be used for identifying these powders.

The difficult descriptions of powders and the whole lot of information contained in spectra lead to huge amounts of data, which have to be dealt with, so a statistical approach is necessary. The experiments have to be performed in an organized and predefined way, providing reliable statistics. As well, the analysis of this pool of data, heavily relies on mathematics and computation to be possible, and should follow the aim, to reduce the amount of data, and to distinguish between important and unnecessary information.

A general understanding of powders and reliable methods for measuring their attributes, and the attributes of blends, is crucial. Mostly this is true for the pharmaceutical industry, to improve the processes involved in tablet production, make them more reliable, less costly and reduce the produced waste. And somewhat this knowledge helps in building sandcastles too.

1.2. QbD and PAT

Constant process monitoring and taking corrective actions instead of end-product testing, the set up of sound mathematical models, and the development of knowledge-based procedures is labelled with the term *Process Analytical Technology (PAT)*, which is defined as "System for Designing, Controlling and Analysing Manufacturing". PAT has been enabled and enforced in the pharmaceutical industry via the PAT-initiatives of the US Federal Food and Drug Administration (FDA) and the *Quality by Design (QbD)* guidelines by the International Conference on Harmonization [3, 4].

The aim of PAT is to perform measurements in real-time, continuously and non-invasive. The prime example is the usage of Infrared-Spectroscopy. Often mid-infrared is used for liquids and solutions and near-infrared for solid materials, due to different penetration depths [5]. Furthermore the measured data have to be analysed, to gain valuable process parameters. This can be done by using *Multivariate Data Analysis (MVDA)*, for example *Principle Component Analysis (PCA)* or *Partial Least Squares Regression (PLS)* [3]. The quality of the product shall further not be tested at the end, and then be classified as good or waste, but critical process parameters should be supervised and controlled. Understanding the process via these parameters enables to ensure process quality. PAT enables to optimize the process and the quality of the product the same way [3].

QbD provides the technical and regulatory framework for PAT [5]. Understanding and redesigning of future processes in industry is covered by QbD, having the aim, not only to discover failures using quality control, but to redesign the process in such a way, that failures should not emerge, or even design new processes using QbD-methodology [3, 5].

1.3. Scope of this work

The scope of this work is to establish a connection between two different PAT-tools.

On the one hand, there is the FT4 Powder Rheometer (Freeman Technology, UK) to determine physical properties of powders off-line. This device is already used to define and classify raw materials [6]. As the counterpart, there is *near-infrared-spectroscopy (NIRS)*, already used for supervising blending or process parameters [7].

A lot of different topics from different research fields have to be combined to pursue this goal and are presented in this work. An overview of the topics and used methods, with references to the according chapters, is given here:

- Powders do have a lot of relevant properties, those investigated in this work are described in section 2.2. The physical properties are investigated with the FT4 powder rheometer introduced in section 2.2.3. Blending of powder is theoretically described in section 2.2.4, and is controlled by near-infrared-spectroscopy, explained in section 2.3.

- Due to the large amount of parameters a Design of Experiments, as will be introduced in section 3.1 is set up. For analysing the experiments, methods of multivariate data analysis, as introduced in section 3.2, are necessary.

- First the physical powder properties were investigated, analysed, and modelled as is described in section 4.

- Then blending is investigated via NIRS, and the characteristic blending parameters connected to the physical properties, as explained in section 5.

2. Understanding and characterizing powders and blends

2.1. The physics of powders

The understanding of powders, or more precisely, particulate or granular solids, is a crucial, but nonetheless very challenging task in modern industry. The science of particulate solids lies within an intersection of process and civil engineering and involves mechanics as well as chemistry [8].

The fundamental problem for particulate science are the length and time scales. Large scale objects are treated as single elements, whereas fluids are treated as continua. For particles, there are three different length and time scales, that of the process equipment, that of the particles, and that of subparticulate phenomena, for example cohesion. Furthermore which length scale is dominant can change rather rapidly, for example, macroscopic failure[1] under stress is a large-scale process, whereas the flow field after failing is better described on the scale of individual particles [8].

This problem is reflected in the possible measurement techniques, which range from fundamental ones, like looking at the individual particle shapes, up to macroscopic tests, like the *Hausner ratio*, which are easy to perform, but are influenced by such a lot of parameters, that it is very difficult and often impossible to relate it to other properties of a material [8].

Due to their complex behaviour, powders cannot be described by just a single number or parameter, but a lot of properties have to be taken into account [9].

2.1.1. Microscopic view of powders

Powders can be seen as a two-phase system. The disperse phase consists of the individual particles, whereas air builds the continuous phase. The behaviour of powders is determined by the particle properties and interactions at the interfaces. Unfortunately, due to the large number of particles, the description of powders from the physical principles is often impossible, however a lot of achievements have been made recently [10].

Interparticulate Forces

Van-der-Waals-Forces are a result of dipole-interactions of atoms and molecules. They are dependent on the distance and size of particles, as well as on the substances the

---

[1]To fail means in the context of granular materials, to not be static any more and start to flow.

particles are made of [11].

Electrostatic Forces are a result of different potentials on the surface of particles. A distinction between insulators and conductors is necessary [11].

Liquid bridges appear in moist bulk solids in the contact area of particles, when low viscous liquids are present. The particles are attracted to each other as a consequence of surface tension and capillary forces. The force imposed by liquid bridges depends strongly on the amount of liquid present [12].

Van-der-Waals and liquid-bridge forces are strong for very low distances, but decrease rapidly with increasing distance. Electrostatic forces are weaker than those two for very close distances, but do not decrease that fast. In contrast, gravity is proportional to the third power of the particle diameter, and is therefore unimportant for small particles, but dominant for larger ones [11]. Models for forces acting on a sphere, with diameter x, in distance d to a wall are, as taken from [10]:

$$\text{van-der-Waals:} \qquad F = \frac{W}{16\pi}\frac{x}{d^2} \tag{2.1}$$

$$\text{electrostatic (conductor):} \qquad F = \frac{\pi}{2}\varepsilon_0\varepsilon U^2 \frac{x}{d} \tag{2.2}$$

$$\text{electrostatic (insulator):} \qquad F = \frac{\pi}{2}\frac{\phi_1\phi_2}{\varepsilon_0\varepsilon}x^2 \tag{2.3}$$

$$\text{gravitation:} \qquad F = \frac{\pi}{6}\varrho_t g x^3, \tag{2.4}$$

where U is the contact potential, ϕ_i are the surface charge densities, ϱ_t the density of the particle, and $W = 5\,\text{eV}$ the van-der-Waals-interaction energy [10]. A comparison of those forces can be seen in figure 2.1.

The flowability of a powder is determined by the ratio of adhesive forces and gravitational forces. If powders are compressed, particles are brought in contact to each other, or even deform, enlarging the contact area. For that reason, the properties of powders are influenced by processes in the past [11].

2.1.2. Particle size distribution

For determining particle size distributions, most methods are based on an optical approach, just allowing the analysis of projections of particles. As particles are usually not perfectly spherical, a diameter has to be defined. This can be done by different means. Either a certain length on the projection is taken, or an equivalent diameter is calculated[2] [10].

Particles are classified into size classes based on this diameter. Usually the *cumulative particle size distribution* $Q_r(x)$ is of interest, where the fraction of the particles, which have a larger diameter than x are indicated. The derivative of this curve

$$q_r(x) = \frac{\mathrm{d}Q_r(x)}{\mathrm{d}x} \tag{2.5}$$

---

[2]A detailed list of diameters can be found in [10].
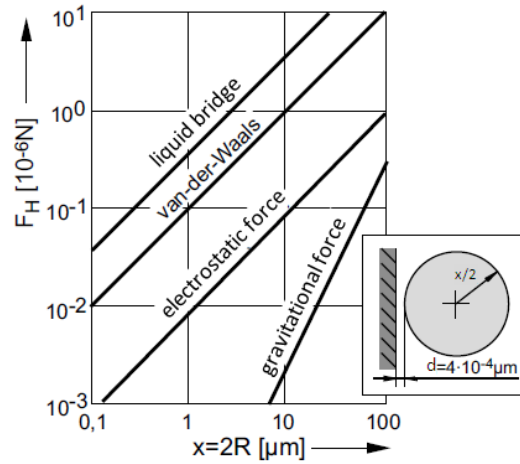
Figure 2.1.: Forces acting on a particle near a wall, in dependence of particle size, adapted from [11].

is the *particle size density distribution* [10, 13]. Examples for distributions can be seen in appendix A.3. However, the fraction can also be defined differently in the following ways: [10]

$Q_0(x)$ The fraction of *number* of particles with a diameter smaller than x.

$Q_2(x)$ The fraction of *projected area* by particles with a diameter smaller than x.

$Q_3(x)$ The fraction of *volume (or mass)* of particles with a diameter smaller than x.

Important characteristics of such a distribution are the *median* x_{50}, where 50 % of the particle distribution are located below and above. Opposing, the *modal value* x_h is the diameter, which occurs most times [10].

Particle size distribution via QicPic

The used device in this work for determining the particle size density distribution consists of several subunits, all manufactured by Sympatec GmbH (System-Partikel-Technik, Germany). Particle samples are filled into a funnel and retrieved with a constant rate by a vibrating chute with the VIBRI-module. Then they are dispersed using the RODOS dry-dispersion module. Agglomerates are broken up and an aerosol beam is generated. This beam is then analysed in the actual QicPic-unit. A light source produces flashes, and pictures of the passing particles are taken with a frequency of up to 500 Hz. The pictures are then analysed, and particles identified and classified in Windox [14].

Examples of the created particle size distributions can be found in chapter A.3. In this case, the method of *Diameter of Circle of Equal Projection Area (EQPC)* was

used. In this method the diameter of an observed particle is defined as the diameter of a circle that covers the same area than the projection of the particle [13].

χ^2-**homogeneity test**

To test, if different particle size distributions stem from the same population, a χ^2-homogeneity test was performed. The H_0-hypothesis is: *All distributions are the same.* For r samples taken, with s parameter values N_{ij}, the critical value χ^2_{crit} is calculated via

$$\chi^2_{\text{crit}} = \sum_{i=1}^{r} \sum_{j=1}^{s} \frac{(N_{ij} - N_i N_j)/N^2}{N_i N_j / N}, \tag{2.6}$$

where

$$N = r \cdot s, \tag{2.7}$$

$$N_i = \sum_{j=1}^{s} N_{ij}, \tag{2.8}$$

$$N_j = \sum_{i=1}^{r} N_{ij}. \tag{2.9}$$

The null hypothesis is rejected, when

$$\chi^2_{\text{crit}} > \chi^2_{(r-1)(s-1),1-\alpha}, \tag{2.10}$$

where α is the level of significance [15].

2.2. Macroscopic powder parameters

The macroscopic characterization of powders is usually based on continuum mechanics [11]. An overview of traditional macroscopic powder tests is given in [16]. Focus is put firstly on the parameters gained by shear cell tests, and secondly on the tests performed with the FT4 powder rheometer.

2.2.1. Density and porosity

Beforehand, attention is brought to the density of powders. As powders usually contain entrained air, different values for density exist.

The *bulk density* ϱ_b is the ratio of the total mass m_{tot}, divided by the total volume V_{tot} of an amount of bulk solid. It is different from the *true density* ϱ_t, which is the density of the particles.

The *porosity* ε is defined as the ratio of the total volume a bulk solid takes up, and the clear space between the particles, as following

$$\varepsilon = \frac{V_{\text{inter-particle voids}} + V_{\text{intra-particle voids}}}{V_{\text{tot}}}, \tag{2.11}$$

so the different densities can be related as follows

$$\varrho_b = (1 - \varepsilon) \cdot \varrho_t, \tag{2.12}$$

when possible fluid entrainments are neglected [11].

2.2.2. Shear cell tests

The shear cell test was first introduced by Jenike, and is widely used to determine powder parameters [11].

Construction of Mohr circles from stress values

First the Mohr circle and its relation to the stress tensors shall be described.

For a finite volume of powder, simplified as a cube, different stresses can act on every of the six surfaces, as is indicated in figure 2.2. The normal vector of the plane in the front of the image is parallel to the z-axis. The stresses therefore carry the index z. A force can now act in direction of the z axis, normal on the plane, and is noted down as σ_{zz}, or often just short as σ_z. Compressing forces are defined positive in bulk solid mechanics, as opposed to other technical areas. Furthermore, forces can act parallel along the plane, inducing shear forces, τ_{zx} and τ_{zy}.
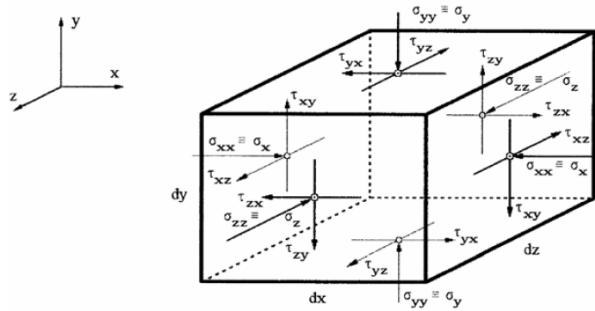
Figure 2.2.: Representation of normal and shear stresses on a bulk solid [10].

The stress tensor can be noted down as

$$\underline{\underline{\sigma}} = \begin{pmatrix} \sigma_{xx} & \tau_{xy} & \tau_{xz} \\ \tau_{yx} & \sigma_{yy} & \tau_{yz} \\ \tau_{zx} & \tau_{zy} & \sigma_{zz} \end{pmatrix}, \tag{2.13}$$

[17] and because of momentum balance, it is valid that

$$\tau_{xy} = -\tau_{yx}. \tag{2.14}$$

A diagonalization of the matrix is possible, resulting in no shear stresses. The resulting normal stresses $\sigma_1, \sigma_2, \sigma_3$ are called *principal stresses*. Per definition σ_1 is the

largest one, and called *Major Principal Stress (MPS)*, whereas σ_2 is the smallest one, called *Minor Principal Stress* [10]. The principal stresses are eigenvalues of the stress tensor, and the eigenvectors are the principal axes along which these stresses act.
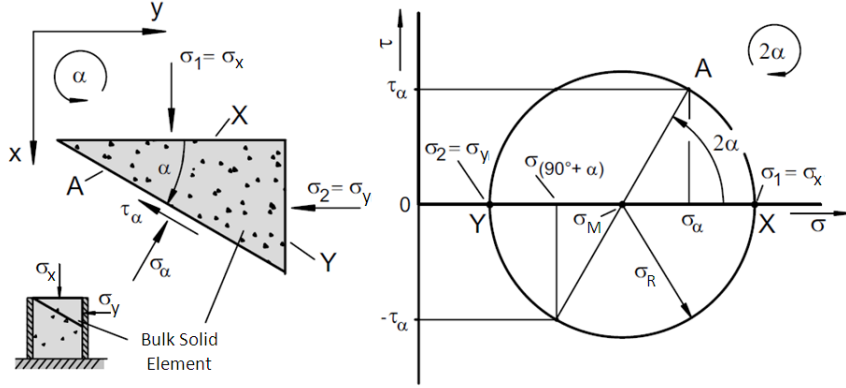
Figure 2.3.: Shear and stress values on a Mohr circle for a bulk solid element, adopted from [11].

A two-dimensional case for a bulk solid element under stress can be seen in figure 2.3. Here the applied stresses are σ_x and σ_y. The relations between shear and normal stresses can be displayed in the shear-stress $(\sigma - \tau)$-plane. The stresses then transform to so-called *Mohr circles*. A point on the Mohr circle displays the shear and normal stress acting on a plane intersecting the powder with the angle α. The corresponding plane is indicated in the Mohr circle with 2α in counter-clockwise direction and the according shear and stress values are called σ_α and τ_α [10]. The equation for the Mohr circle is

$$\tau^2 + (\sigma - \sigma_M)^2 = \sigma_R^2, \tag{2.15}$$

where

$$\sigma_M = (\sigma_x + \sigma_y)/2 = (\sigma_1 + \sigma_2)/2 \tag{2.16}$$

denotes the centre of the Mohr circle and

$$\sigma_R = \sqrt{\left(\frac{(\sigma_y - \sigma_x)}{2}\right)^2 + \tau^2} = \frac{\sigma_1 - \sigma_2}{2} \tag{2.17}$$

the radius of the circle. The stresses, acting in a certain direction can be described as

$$\sigma_x = \sigma_M + \sigma_R \cdot \cos 2\alpha \tag{2.18}$$
$$\sigma_y = \sigma_M - \sigma_R \cdot \cos 2\alpha \tag{2.19}$$
$$\tau_{xy} = \sigma_R \cdot \sin 2\alpha. \tag{2.20}$$

Therefore, principal stresses can be determined using the measurable applied stress values

$$\sigma_1 = \frac{\sigma_x + \sigma_y}{2} + \sqrt{\left(\frac{(\sigma_y - \sigma_x)}{2}\right)^2 + \tau^2} = \sigma_M + \sqrt{\sigma_R^2 + \tau^2} \qquad (2.21)$$

$$\sigma_2 = \frac{\sigma_x + \sigma_y}{2} - \sqrt{\left(\frac{(\sigma_y - \sigma_x)}{2}\right)^2 + \tau^2} = \sigma_M - \sqrt{\sigma_R^2 + \tau^2} \qquad (2.22)$$

$$\tan 2\alpha = \frac{2\tau}{\sigma_y - \sigma_x}. \qquad (2.23)$$

It can be seen, that for a given uni-axial normal stress, the maximal shear appears at an angle of $\alpha = 45°$ to the normal stress. A charged cube of bulk solid will evolve a diagonal plain of fail [10].

Construction of Mohr circles from shear cell data

The working principle of all shear cells is, to shear two planes of powders against each other. The original shear cell designed by Jenike was a lateral shear cell, however it is mostly replaced by annular shear cells nowadays [11]. An example of a modern shear cell is the shear cell module of the FT4 (Freeman Technology, UK) seen in figure 2.4.
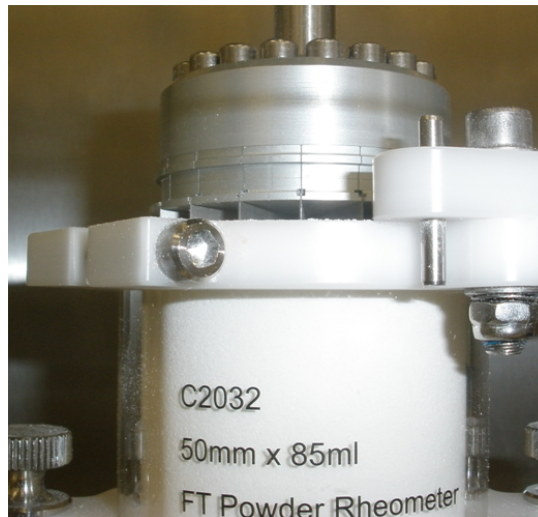
Figure 2.4.: Shear cell module of the FT4 Powder Rheometer

A shear cell test follows the following routine [11]:

1. The powder is preconsolidated with a certain load.

2. The powder is presheared, e.g. the head pressing on the powder starts rotating with a certain angular speed. A shear plane develops in the powder bed and after some time the point of stationary flow is reached.

3. The consolidation force is then lowered. Then shearing starts again. A certain torque can be applied before the powder starts to flow. This is called the point of failure.

4. Preshear cycles (with the original loading) and shear cycles (with subsequently less loading) are performed alternately. Usually preshear torque is lowering with every cycle, due to particle rearrangement. Therefore the torque for the failure point i is corrected with

$$\tau_{\text{corrected},i} = \tau_i \cdot \frac{\tau_{\text{preshear},i}}{\overline{\tau}_{\text{preshear}}}, \tag{2.24}$$

where $\overline{\tau}_{\text{preshear}}$ is the mean of all preshear torque values. In the FT4 this is called pro-rating [6, 11].

5. The points of failure and the point of stationary flow are then carried over to the $\sigma - \tau$-plane for Mohr circle construction.

Actual data gained by shear cells can be seen for a traditional cell in figure 2.5 and for a test with the FT4 in figure 2.6.

An actual Mohr plot can be seen in figure 2.7, with the important parameters indicated. The measured points are charted in the shear-stress diagram. A linear regression is applied, to fit a straight line through this point, displayed as

$$\tau = \tau_0 + a \cdot \sigma, \tag{2.25}$$

where τ_0, the intersection with the shear stress axis, is called *Cohesion*. The line is called the *yield locus*. Below this line, the powder bed is stable, above the applied stresses lead to failure. The *Angle of Internal Friction* ϕ_i is defined as

$$\phi_i = \arctan\left(\frac{\mathrm{d}\tau}{\mathrm{d}\sigma}\right). \tag{2.26}$$

It is then possible to construct the minor Mohr circle, which intersects the origin, is tangent to the yield locus, and intersects the normal stress axes at the *Unconfined Yield Strength* σ_c, with

$$\sigma_c = 2\tau_0 \tan\left(\frac{\pi}{4} + \frac{\phi_i}{2}\right). \tag{2.27}$$

The end Mohr circle is tangent to the yield locus and contains the point of stationary flow (σ_{st}, τ_{st}), therefore we can get the following equations for centre and radius of the end Mohr circle:

$$\sigma_M = \left(\sigma_{st}\left(1 + a^2\right) + a\tau_0\right) - \sqrt{\left(\sigma_{st}\left(1 + a^2\right) + a\tau_0\right)^2 - \left(\left(\sigma_{st}^2 - \tau_{st}^2\right)\left(1 + a^2\right) - \tau_0^2\right)} \tag{2.28}$$

$$\sigma_R = \frac{a}{\sqrt{1 + a^2}}\left(\sigma_M + \frac{\tau_0}{a}\right) \tag{2.29}$$

$$\sigma_1 = \sigma_M + \sigma_R. \tag{2.30}$$

Figure 2.5.: Data gained by a traditional shear cell test. The horizontal axis represents time (from right to left), however the axis is not continuous, as the measurement is stopped in between for changing consolidation weights etc. The vertical axis shows shear force, of which shear stress can be calculated.

The endpoint of the yield locus, that is the intersection of the yield locus with the end Mohr circle, can be derived by

$$\sigma_E = \frac{a}{1+a^2} \left(\frac{\sigma_M}{a} - \tau_0 \right) \tag{2.31}$$

$$\tau_E = \tau_0 + \frac{a}{1+a^2} (\sigma_M - a\tau_0) \tag{2.32}$$

and finally it is possible to construct the *Effective Angle of Internal Friction*,

$$\phi_e = \arcsin\left(\frac{\sigma_R}{\sigma_M} \right) = \arcsin\left(\frac{a}{1+a^2} \left(1 + \frac{\tau_0}{a\sigma_M} \right) \right), \tag{2.33}$$

which is tangent to the end-Mohr circle and goes through the origin [10].

Parameters gained by shear cell tests

The parameters gained by the shear cell test and their informative value shall be presented shortly. [10, 11]

Figure 2.6.: Shear cell data gained by the FT4. The upper graph represents force values, the lower graph shear values. Both abscissae represent time (from left to right as opposed to figure 2.5).

Major Principle Stress (MPS): The largest normal stress appearing in the powder.

Unconfined Yield Stress (UYS): The applied normal stress under which a powder starts to flow.

Angle of Internal Friction (AIF): The change of the yield locus with the applied normal stress.

Effective Angle of Internal Friction(AIFE): Approximatively, all end Mohr circles, for different consolidation stresses should be tangent to this line. This value is extensively used for hopper design.

Cohesion (Coh): A quantity for the strength of the inter-particulate forces.

One widely used index for describing the flowability of a powder is the flow function constant *ffc*, gained by

$$ffc = \frac{\sigma_1}{\sigma_c}. \tag{2.34}$$

Its classification can be found in appendix A.4. By doing measurements for different consolidation stresses, the flow function curve can be constructed, describing the flowability of a powder in dependence of its consolidation [11].
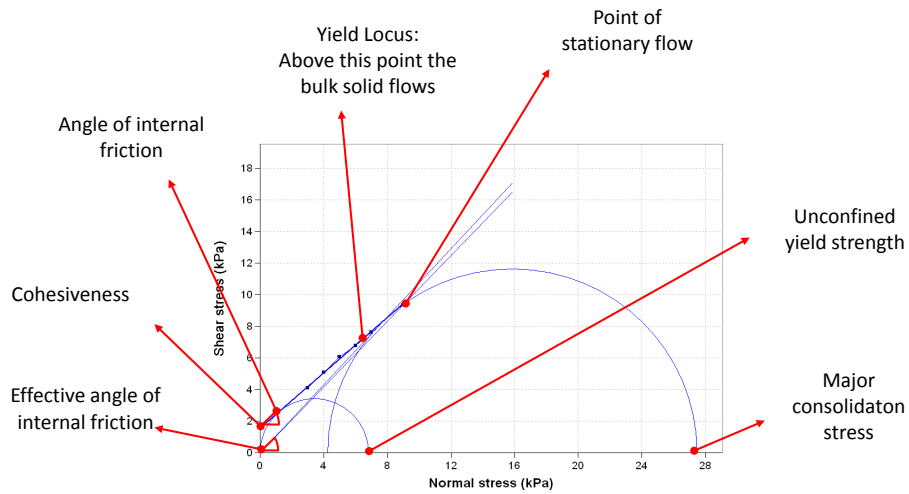
Figure 2.7.: Mohr plot with important parameters indicated.

Mohr plot analysis is just valid for the applied consolidation stress. Furthermore a lot of assumptions are used, for example the linearity of the yield locus, even down to no applied normal stress, which is not true in reality [11].

2.2.3. The FT4 Powder Rheometer

The FT4 offers a variety of possible tests, in a standardized way, to allow powder testing and characterization consistently and independent of the operator [6].

The centrepiece of the FT4 is a blade following a defined helical path, like in figure 2.8, through a powder bed. Usually before any test, the blade stirs through the powders numerous times, called the conditioning cycle, bringing the powder to a defined state, rarely influenced by the filling of the vessel, or previous handling of the powder [6].

In the following the tests performed with the FT4 and the parameters gained are listed and described shortly.

The mass of the powder is measured for every test. Most tests have a point, where the vessel is split and the superfluous powder dumped, to have a defined volume. In this case the *Conditioned Bulk Density (CBD)* can be calculated [6].
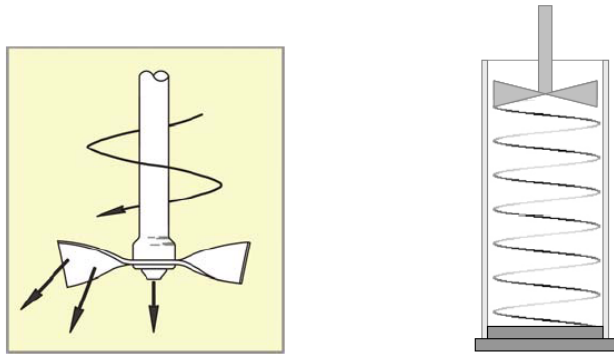
Figure 2.8.: Schematic drawing of the blade of the FT4 following (up and down) a helical path [6].

Stability and Variable Flow Rate

When conditioning, the blade is going down in a clockwise motion, splitting the powder and introducing a conditioned state. In contrast, when doing a test cycle, the blade moves counter-clockwise, creating an area of high stress in front of the moving blade [6].

For measuring stability, conditioning and test cycles are performed alternately seven times. Just small changes should be seen in energy during the test cycles, otherwise it is very likely that de-aeration, attrition or segregation has occurred [6].

A *Stability Index (SI)* is defined by

$$SI = \frac{\text{Energy of Test 7}}{\text{Energy of Test 1}}, \tag{2.35}$$

which should be in the range of 0.9 - 1.1. The energy the blade invested in the last test cycle is defined as the *Basic Flowability Energy (BFE)*. In contrast the energy, when the blade is moving up is recorded, (actually the mean of cycle 6 and 7 is taken,) and divided by the mass of the powder, gaining the *Specific Energy (SE)*. As opposed to *BFE*, which is influenced by the compressibility of a powder, *SE* depends mainly on the cohesion, and other particle characteristics.

Finally the tip speed of the blade is slowed down in the last four additional cycles, effecting the incorporated energy. The *Flow Rate Index (FRI)* is defined as

$$FRI = \frac{\text{Energy at } 100\,\text{mm/s tip speed}}{\text{Energy at } 10\,\text{mm/s tip speed}}, \tag{2.36}$$

and is influenced by the amount of entrapped air and the interlocking of particles [6].

Aeration

During the aeration test, air is pressed through a sieve at the bottom of the powder bed. The amount of air is varied and tests with the blade are simultaneously carried out. The air forms channels through the powder bed, particles are separated and the mechanical interlocking is removed, making cohesive forces the dominant one. An example thereof can be seen in figure 2.9, the blade was moving from right to left and is now positioned at the left visible edge of the vessel. The blade is trailed by air bubbles, which are rising in the powder bed. At a certain air velocity, the powder is fluidized and behaves more like a liquid. This point can be determined by the fact, that the inserted energy of the powder has reached a minimum and does not change any more [6, 9]. Parameters gained are the *Aeration Ratio AR_v*, which is the ratio of the basic flow energy for no air flow and energy for air speed v. This energy is called the *aeration energy AE_v* [6].
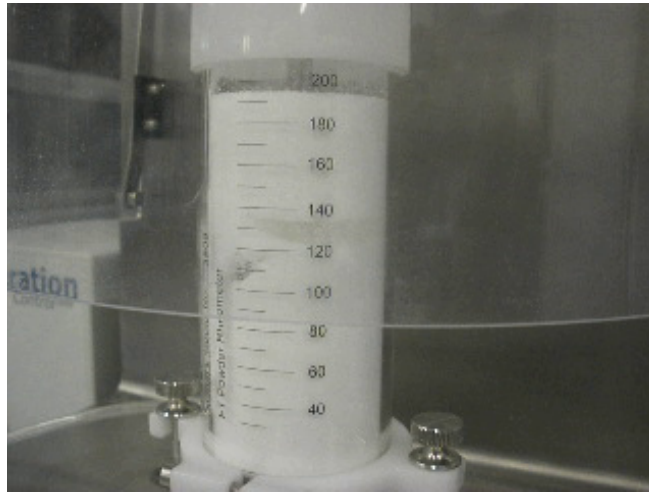
Figure 2.9.: Performance of an Aeration test. The blade and the trailing air bubbles in the powder bed can be seen.

Consolidation

Consolidation of the powder happens by tapping. Basic flow energy after tapping n times is called *Consolidated Energy $CE_{tap,n}$*. Density of the powder after tapping and splitting is noted as *Tapped Density TD*. Therefore it is possible to calculate the *Consolidation Index (CEI)* [6]

$$CEI_{\text{tap},n} = \frac{CE_{\text{tap},n}}{BFE} \tag{2.37}$$

and the *Hausner Ratio (HR)* [18]

$$HR = \frac{CBD}{TD}. \tag{2.38}$$

Compressibility

A vented piston compresses the powder and the position of the piston is measured, therefore giving the volume of the compressed powder sample. Important parameters are the *Compressibility Cp*, which is the change in volume after compression, often noted in %. The bulk density of course increases with the applied normal stress. An example for Compressibility for two differently behaving powders and a blend thereof can be seen in figure 2.10. Finally a *Compressibility Index CpI* is defined [6] as

$$CpI = \frac{\varrho_{\text{after compression}}}{CBD}. \tag{2.39}$$

Therefore those two parameters are related via

$$Cp = V \left(1 - \frac{1}{CpI}\right) \cdot 100\%, \tag{2.40}$$

where $V = 85\,\text{ml}$ is the vessel volume.
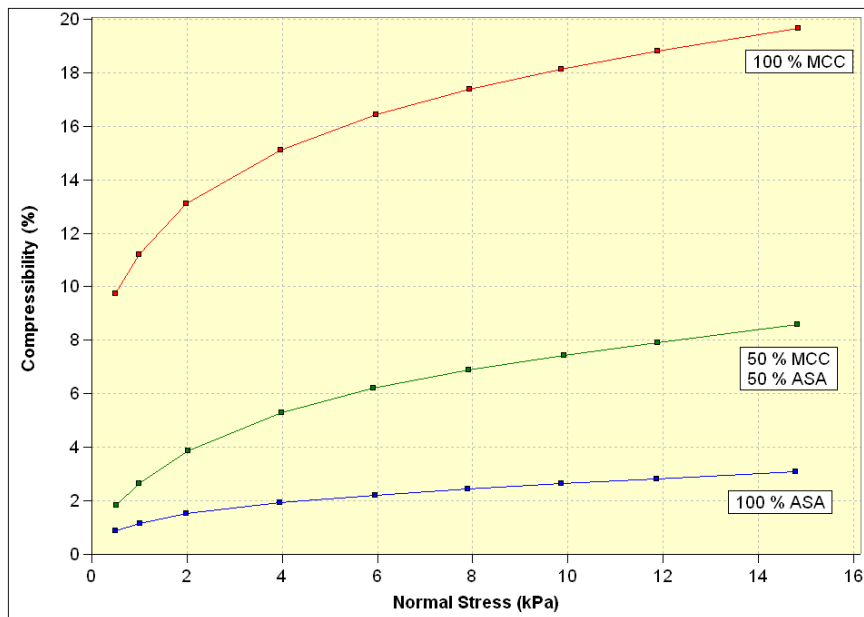
Figure 2.10.: Compressibility for Acetylsalicylic Acid (ASA), Lactose-monohydrate (TAB) and a blend consisting of equal parts of both.

Bulk density under compression

A lot of different models exist for describing the change of powder properties for compressed powders. A simple, yet for a small range of stress approximately good function, to describe the bulk density in dependence of compression is [11]

$$\varrho_c = \varrho_0 + a \ln \left(\frac{\sigma}{\sigma_0} \right), \tag{2.41}$$

where ϱ_c is the compressed bulk density, and ϱ_0 and a are fit parameters. σ_0 is just a comparable stress (here chosen as $1\,\text{kPa}$, to make the expression inside the logarithm dimensionless) [11]. An application of this formula can be found in [19]. In order to use this equation with the CpI-value gained by the FT4, it is reformulated to

$$CpI = \frac{1}{CBD} \left(\varrho_0 + LogC \ln \left(\frac{\sigma}{\sigma_0} \right) \right). \tag{2.42}$$

Examples for such a fit can be found in figure 2.11. The constant of the fitted regression line reflects the density of the powder at $1\,\text{kPa}$. The inclination is a characteristic number representing the Compressibility of a powder. It can clearly be seen that MCC has a much larger Compressibility than ASA, and that the blend can be found in between.
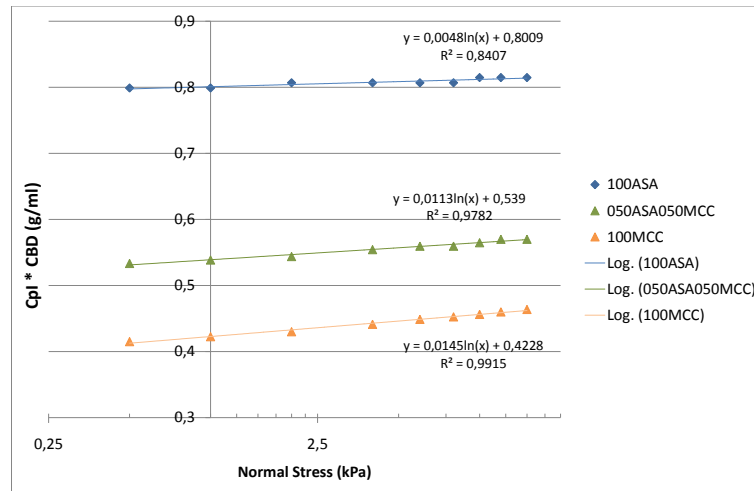
Figure 2.11.: Fit for Compressibility Index on a logarithmic scale, for the same data as in figure 2.10.

18

Permeability

Permeability describes the transmittance of air through a powder bed. Substances with low permeability, often due to small particle sizes, show resistance to passing air. What is actually measured in this test, is the pressure drop across the powder bed, when a certain normal stress is applied on the powder, and a certain amount of air is forced to pass through the powder bed [6].

Further tests

Further tests are available with the FT4, like de-aeration, wall friction etc. [6], which have not been carried out in this work. Shear cell tests have been performed, but have already been explained above.

Comparison between FT4 shear cell module and traditional rotational shear cell

Figure 2.12.: A rotational shear cell

A traditional rotational shear cell as seen in figure 2.12 as well as the FT4 shear cell module, as seen in figure 2.4 have been used. The FT4 comes with its own analysis program, as can be seen in figure 2.6. In contrast, the results of the traditional shear cell are recorded with a printer, as seen in figure 2.5, and then analysed using Excel.

Gained values for measurements on Tablettose 80 can be found in table 2.1. As the consolidation stresses are not the same, the results cannot be directly compared. It can

be seen that increasing the consolidation stress leads to an enlargement of *UYS*, *MPS*, *Coh* and *ffc*. However, *AIF* and *AIFE* should stay roughly the same, as the increase in consolidation enlarges the interparticular forces, but the changes for decreasing stress are still the same.

Comparing both shear systems, both give reasonable results, but the FT4 shows less variance within the same samples. A reason might be found in the many manual steps using the traditional cell, like sieving powder into the cell, tightening screws, and applying weights, which lead to a large chance of error.

BD .... Bulk Density (g/ml)
Cons .... Consolidation Stress (kPa)
UYS .... Unconfined Yield Strength (kPa)
MPS .... Major Principal Stress (kPa)
Coh .... Cohesion Value (kPa)
ffc .... Flow Factor Constant
AIF .... Angle of internal friction (°)
AIFE .... Effective Angle of Internal friction (°)

Device	BD	Cons	UYS	MPS	Coh	ffc	AIF	AIFE
FT4	1.350	9.0	0.522	16.1	0.130	30.9	37.1	37.9
FT4	1.499	9.0	0.488	15.4	0.119	31.6	37.9	38.6
FT4	0.941	15.0	0.727	25.7	0.184	35.4	36.3	37.0
FT4	0.958	15.0	0.922	24.9	0.249	25.2	36.8	37.7
Rotational	0.691	4.5	0.608	7.1	0.153	11.7	36.5	38.5
Rotational	0.669	4.5	0.753	8.0	0.190	10.7	36.6	38.8
Rotational	0.662	5.7	0.474	7.9	0.130	16.6	32.6	34.1
Rotational	0.709	5.7	0.147	7.9	0.037	54.0	35.7	36.1

Table 2.1.: Comparison of shear cell tests with Tablettose 80 on the FT4 and a traditional shear cell. The values are not directly comparable due to different consolidation stresses.

2.2.4. Powder blending

Mechanisms of Mixing

Mixing happens due to two main mechanisms. *Convective transport* is the forced transport of large volumes of the blend, imposed by the mixer. In contrast, *diffusion transport* is a result of particle-particle impacts, and a random process [10, 20].

Convection is largely a result of the geometry and a fast process, it leads to homogeneity of the mixture on a large scale. In contrast, diffusion is a result of the mobility of individual particles and therefore dominantly influenced by cohesion. Diffusion

is rather slow and leads to homogeneity of the mixture on a small scale. Another important factor for mixing is the breaking and forming of agglomerates during the mixing process [20].

Segregation

As mixing needs the relative movement of particles, this also favours segregation. Segregation is the demixing and spatial separation of mixture components [10].

Segregation can be caused by size differences of the particles. Movement of the powder particles lead to an enlargement of the voids in the powder bed. Gravitational force acts on the powder, and smaller particles can pass downwards into the voids. This leads to a net upward motion of the larger particles, known as the "Brazil nut effect" [20].

Further main causes of segregation are found in the shape of particles, as this effects largely the mobility of the particles, and in particle density [20].

Mixture homogeneity

A lot of different indices for mixture homogeneity exist, but most are based on standard deviations, when a certain amount of samples has been taken from the mixture.[3] For a two component mixture with the desired concentration p of one component, and n samples taken from the mixture, giving a concentration x_i, the empirical variance is

$$s_n^2 = \frac{1}{n} \sum_{i=1}^{n} (x_i - p)^2. \tag{2.43}$$

For a completely separated mixture, the variance would be

$$\sigma_0^2 = p(1 - p), \tag{2.44}$$

whereas for a mixture with ideal homogeneity, every sample would have $x_i = p$ and therefore $\sigma_{\text{ideal}} = 0$. However, one cannot hope to achieve ideal homogeneity by a random process. The aim is to achieve stochastic homogeneity, e.g. the possibility of finding a particle of a component is always the concentration and independent of the surroundings. In this case the variance would be [10]

$$\sigma_z^2 = p(1 - p) \frac{V_A}{V_P}, \tag{2.45}$$

where V_A is the volume of a single particle, and V_P is the sample volume taken.

So the possible homogeneity is determined by the size of the sample. Taking sample volumes of the size of the particles would give maximal inhomogeneity, whereas taking the whole mixer as sample volume would of course give maximal homogeneity. A proper sample should therefore be large enough, to avoid the effect of individual particles, but much smaller than the overall mixture [10].

---

[3]A list of different mixture indices and their ranges can be found in [10].

Focus should be put on the mixture performance defined by Ashton and Schmahl M_{AS}, which has a range between 0 (complete de-mixing) and 1 (stochastic homogeneous) [10].

$$M_{AS} = \frac{\log(\sigma_0^2/\sigma^2)}{\log(\sigma_0^2/\sigma_z^2)} \qquad (2.46)$$

Efforts are made, not to stop mixing simply after a given time, but to determine the mixture quality during blending, often via near-infrared-spectroscopy, and stop after a defined end point is reached [7]

A possibility to supervise the progress of a mixing process is *Moving Block Standard Deviation (MBSD)*, often used in combination with infrared spectroscopy. In this procedure, the standard deviation for a certain wavelength, over a block of spectra recorded consecutively is calculated. Then the oldest spectra is removed, a new one added, and the calculation redone, etc. When the moving block standard deviation drops below a certain value, one can assume that the mixture is not changing any more. However, this does not give a statement whether homogeneity has been reached [21, 22].

2.3. Near Infrared Spectroscopy

The range of near infrared is from roughly 1,000 nm to 2,500 nm, or in the more commonly used wavenumbers 10,000 - 4,000 cm^{-1}. In near infrared spectroscopy (NIRS) absorption bands of molecules, due to molecular vibrations are detected, allowing the identification of substances and much more [3].

Modern NIR-spectroscopes are usually based on Fourier-transform NIRS (FT-NIRS). The sample is placed in a Michelson-interferometer and is illuminated by a thermal emitter. An interferogram $I(x)$ of the reflected or transmitted light, in dependence of the arm length is recorded. It is then transformed via Fourier-transformation into $I(\lambda)$, giving the intensity dependent on the wavelength. The advantage of FT-NIRS is the fast recording time, over a large spectral range [3].

Quantitative analysis of spectra usually follows *Beer's law*, which states that the absorbance A is proportional to concentration c of a substance and travelled optical pathlength d, that is to say

$$A = \log\left(\frac{a}{a_0}\right) = \varepsilon \cdot c \cdot d, \qquad (2.47)$$

where a_0 is the original, and a the reflected intensity, and ε the specific absorptivity. This equation can be transformed to the linear so-called "inverse model"

$$c = A \cdot \beta + \beta_0, \qquad (2.48)$$

where the paremeters β and β_0 can be determined by calibration [23].

Powders or granular samples can be looked at in diffuse reflection. A small part of the reflected light stems from direct reflection of the particle surface, however most

recorded photons often have passed several particles and have therefore characteristics of a transmission spectra. However, because of the different distances travelled, Beer's law is not valid anymore. Therefore the data has to be transformed, for example with the Kubelka-Munk transformation [7]. Low absorptivity in the NIR-range allows, to look at diffuse reflected spectra without pretreatment, as diluting, and is therefore suited to look at APIs[4]. However, NIR diffusive spectra do not show a linear relationship over a large range of concentration, additionally baseline variations, multiplicative and scatter effects, complicate the interpretation of NIR-spectra. [7].

2.3.1. Application of NIRS for PAT

NIRS is already widely used in the pharmaceutical industry, as it provides a versatile, non-invasive and non-destructive method, for fast data collection and analysis. On the one hand, it is used for identifying materials, on the other hand for supervising blending, granulating and coating processes, etc.[7].

A lot of examples for the use of NIRS in connection to powders can already be found. Determining the moisture content of powders by NIRS is presented in [24], and determining particle size in [25]. Characterisation of powder flows via NIRS is shown in [26]. The supervising of blending processes can already be found in [21]. An extensive study on blending processes, supervised by NIRS can be found in [27, 28, 29]. Different methods of analysis, for assessing the blend homogeneity via NIRS are presented and compared in [22].

An attempt in connecting NIR-methods and physical powder parameters has recently been done, as presented in [30].

2.3.2. Spectral pretreatment

Often it is necessary to do some pretreatment to the spectral data, to make different spectra comparable. The spectral intensity at a certain wavenumber k is further called a_k [31].

Baseline correction

Systematic deviations of the base line can be caused by scattering loss due to dirt, or a problem of the measuring apparatus. The spectra $\boldsymbol{a}$ can be split up in the important part $\tilde{\boldsymbol{a}}$ containing the chemical information and a polynomial

$$\boldsymbol{a} = \tilde{\boldsymbol{a}} + \alpha + \beta\boldsymbol{k} + \dots . \tag{2.49}$$

To determine the constants α and β, wavelengths containing no information are chosen [31].

---

[4]API is the active pharmaceutical ingredient, e.g. the substance provoking a reaction in the body.

Standard Normal Variate

For Standard Normal Variate Transformation (SNV) the mean $\overline{a}$ and variance of one spectra (over all l wavelengths) is calculated. The transformed spectra are reduced by the mean and divided by the standard deviation as

$$a_{i,\text{SNV}} = \frac{a_i - \overline{a}}{\sqrt{\frac{\sum_{i=1}^{l}(a_i - \overline{a})^2}{l-1}}} \tag{2.50}$$

SNV is performed independently for every spectrum [31].

Multiplicative Scatter Correction

Diffuse reflectance spectra often show differences due to different physical properties of the particles. Different light paths are caused by different particle sizes. Additionally, scattering is wavelength dependent.

To distinguish scatter effects from the chemical information, a mean spectra $\overline{\boldsymbol{a}}$ is created. Then all spectra $\boldsymbol{a}_i$ are adapted to this spectra, using the Least-Squares-Procedure.

$$\boldsymbol{a}_i = \alpha_i + \beta_i \overline{\boldsymbol{a}} + \boldsymbol{e}_i \tag{2.51}$$

The gained coefficients are then used to create the corrected spectra

$$\boldsymbol{a}_{i,\text{MSC}} = \frac{\boldsymbol{a}_i - \alpha_i}{\beta_i}. \tag{2.52}$$

Extended Multiplicative Scatter Correction (EMSC) pursues this ansatz further and models the wavelength dependence by

$$\boldsymbol{a_{i},\text{EMSC}} = \alpha_i + \beta_i \boldsymbol{a}_{i,\text{MSC}} + \delta_i \boldsymbol{\lambda} + \varepsilon_i \boldsymbol{\lambda^2}. \tag{2.53}$$

(E)MSC uses all available spectra, so if a spectrum is added, it has to be recalculated [31].

MSV and SNV should be used, when there is a linear relationship with concentration. Reflection- and transmission spectra should therefore be transformed into absorption spectra [31]. Other possible transformations are centre scaling, smoothing, and taking the derivative and combinations of these pretreatments [31].

3. Methods of analysis

3.1. Design of Experiments

An experiment is performed to test the influence of input factors on the changes of an output of a system. More precisely, the input factors are varied in such a way, that it should be possible to determine, which input factors are most important, and how they influence the output [32].

Often this task is encomplicated by a lot of input factors, which have to be considered, as well as interactions between those input factors. A lot of different strategies exist, to perform a sequence of tests. Most used and widely known are the *best guess* approach and the *one-factor-at-a-time* approach. However, when interactions between input variables appear, those strategies often give poor results. Therefore a more statistical approach is desired [32]. This is provided by statistical experimental design, which is often just called *Design of Experiments (DoE)* [33]. An example is provided by a *factorial design*, in which inputs are varied simultaneously [32].

3.1.1. Performing a Design of Experiments

A Design of Experiments should be carried out similar to the guideline in [32]:

1. *Recognition of and statement of the problem.*

2. *Choice of factors, levels, and ranges.* Everything that has influence on the outcome of an experiment is called a factor, and should be considered in the design. Many of these factors will possibly be controllable in the experiment. If this is true, the ranges, wherein these factors should be varied have to be decided. For screening, this will often be a very large range, whereas for an optimization design, often the number of variable factors and the ranges are reduced, based on past experiences.

3. *Selection of response variable.* One should be sure, that the response variable provides useful information, multiple responses are common. Issues regarding this variables and their measurement should be dealt with before starting the DoE.

4. *Choice of experimental design.* The choice of experimental design is guided by the number of experiments and replicates what should or can be taken. Appropriate software often provides an assortment of experimental designs to choose of. The designs will be discussed more detailed in the next sections.

5. *Performing the experiments.*

6. *Statistical analysis of the data* The benefit of statistical analysis is to provide objective conclusions and to attach a level of confidence to these. Those methods will be discussed in section 3.2

7. *Conclusions and recommendations.* Conclusions of the experiments are often supported by graphical methods. Validation runs should be performed, or a follow-up design of experiments carried out, putting the gained knowledge to use.

3.1.2. Factorial, Central Composite and D-optimal designs

If there are three factors A, B, C, the simplest way is to look at two extrema of these three factors. This results in a number of $2^3 = 8$ experiments, like schematically indicated in figure 3.1. These eight experiments allow to estimate the influence of the three factors on the response, as well as the interaction between factors, e.g. how the effect dependent on one factor varies with another factor. This process can be generalized for k-factors, giving a so called 2^k *full factorial design* [32].
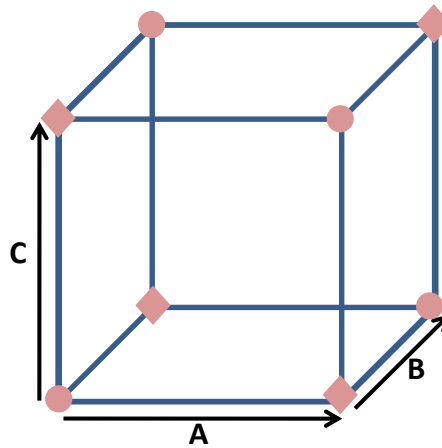
Figure 3.1.: Example for a factorial design with three factors. The factors are varied along the axes and every corner represents an experiment. For a full factorial design all 8 experiments need to be performed. For a fractional factorial design just those symbolized in the figure with diamonds are necessary.

For a large number of factors, the number of experiments to perform grows drastically, and a more time-conserving methodology is preferred. The number of needed experiments can be halved (a so called 2^{3-1}-design), by dropping certain experiments. For example dropping the experiments indicated by circles in figure 3.1. The disadvantage

is, that now the effect of pure factors and the opposing first order interaction terms cannot be distinguished. This is usually noted as $A = BC, B = AC, C = AB$ [32].

This can further be generalized leading to the 2_R^{k-p} *fractional factorial designs*, with k factors, but 2^p dropped experiments leading to unresolved dependencies. R is the resolution of the design, and given in roman numbers.[1] Of course, also the number of levels can be varied, for each factor individually [32].

The basic assumption in these designs is a linear dependence of the responses on the factors and interactions [34]. To test this assumption, usually f center points are added. This also provides a method to estimate the independent error [32].

To model higher order terms, modifications of the factorial designs are necessary. A more often discussed design is the *Central Composite Design* (CCD) [34]. It consists of a 2^k factorial run with a center point and additional "star runs", outside or at the borders of the factorial run. CCD is very popular, because it can be run in two steps. First the factorial run enables to fit a linear model. The additional star runs then enable to fit quadratic models if necessary [32].

An important consideration is the factor matrix X. Roughly, an increase in the determinant $X'X$, increases the information value. This is pursued for *d-optimal* designs, which are such modified factorial designs and include just certain criteria of a full factorial design, or are a combination of factorial and other designs to minimize the determinant of $(X'X)^{-1}$ [34].

A quality criteria for those designs is the *G-efficiency*, which is calculated as

$$\text{G-efficiency} = \frac{100 \cdot k}{N \cdot d_m}, \tag{3.1}$$

where k is the number of factor effects, N the number of runs and d_m the maximum variance of prediction, where the variance of prediction is given by $d = x(X'X)^{-1}x'$, where x is the realisation of a factor [35].

Another criteria is the *condition number*, which is the ratio of the highest and lowest eigenvalue of $X'X$, with the values in X scaled and centered. The condition number represents the sphericity of a design [35].

3.1.3. Mixture Designs

The decisive attribute of mixture designs is, that levels of different factors are not independent anymore. If there are k mixture components, and x_i are their according levels, it must hold that

$$\sum_{i=1}^{k} x_i = 1. \tag{3.2}$$

The sum of all mixture components must always be $100\,\%$. For three mixture components, this can be visualized in a mixture diagram, using a trilinear coordinate system [32], like in figure 3.2. Such a mixture area, whose vertices are pure blends is called a *simplex* [34].

---

[1]For a detailed explanation of the resolution see [32] or [34].
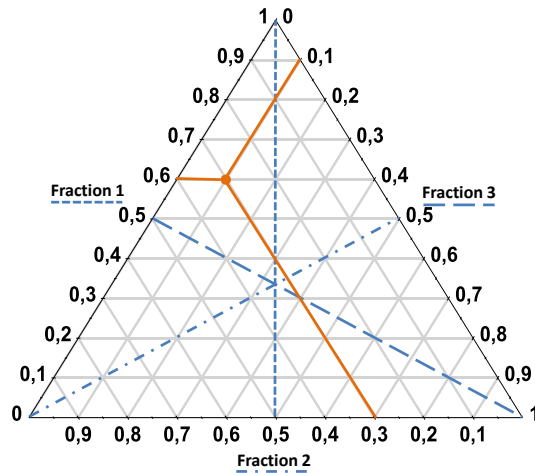
Figure 3.2.: Mixture diagram, a trilinear coordinate system is used. An exemplary point is set in (Fraction 1: 0.6, Fraction 2: 0.3, Fraction 3: 0.1). The solid lines connect the point to the according axes. The dashed lines represent the variation of the according fraction from 0 to 1, the two other fractions are held at constant equal fraction.

In *Extended Axial Designs* a number of $3 \cdot k + f$ runs are located on the axis of the simplex, where k is the number of mixture components and f the number of center runs [35].

Simplex Lattice Designs are created by the following way: For every of k mixture components, $m + 1$ equally spaced proportions between 0 and 1 are taken. This gives for a $\{k, m\}$-simplex lattice design a number of

$$N = \frac{(k + m - 1)!}{m!(k - 1)!} \tag{3.3}$$

experiments. Alternatively, a *simplex centroid design* can be constructed, by the k permutations of $(1, 0, \dots, 0)$, $\binom{k}{2}$ permutations of $(\frac{1}{2}, \frac{1}{2}, 0, \dots, 0)$, etc. up to the centre sample $(\frac{1}{k}, \dots, \frac{1}{k})$ [32].

Because the investigated region is often the whole possible mixture region, higher order terms are frequently needed for a sufficient mixture model [32].

3.2. Multivariate Data Analysis

Assumed are a number of N samples. For every sample i, M independent variables x_{ik} exist, describing those samples [31].

The average value of each variable is given by [36]

$$\overline{x}_j = \frac{1}{N} \sum_i^N x_{ij},$$ (3.4)

and the *sum of squares (SS)* [32]

$$ss_j = \sum_i^N \left(x_{ij} - \overline{x}_j\right)^2,$$ (3.5)

as well as the empirical variable variance

$$s_j^2 = \frac{SS}{\nu} = \frac{\sum_i^N \left(x_{ij} - \overline{x}_j\right)^2}{N - 1}$$ (3.6)

where ν denotes the degrees of freedom.

3.2.1. Variable scaling

Therefore *mean-centred* variables, also called *corrected* variables can be created [31]

$$x_{ij,\text{corr}} = x_{ij} - \overline{x}_j.$$ (3.7)

To unify the scales of the variables, often *Unit Variance Scaling (UV-Scaling)* is used [31, 35, 36].

$$z_{ij} = \frac{x_{ij} - \overline{x}_j}{s_j}.$$ (3.8)

A competitve scaling method is *orthogonal scaling*, which is done by

$$z_{ij} = \frac{x_{ij} - \overline{x}_j}{R},$$ (3.9)

where R is the half range of the factor.

In the following, it is assumed that the variables are scaled, although it is not denoted separately.

3.2.2. Principal Component Analysis

The Principal Component Analysis (PCA) is an important tool for chemometrics. Chemometrics itself can be understood as combination of chemical and statistical thinking, spanning multivariate modelling of chemical data [5]. The purpose of PCA is to reduce the amount of investigated variables. Linear combinations of the original variables are calculated, these are called latent variables, factors, or principal components. Every principal component expresses a part of the variance of the original data [31].
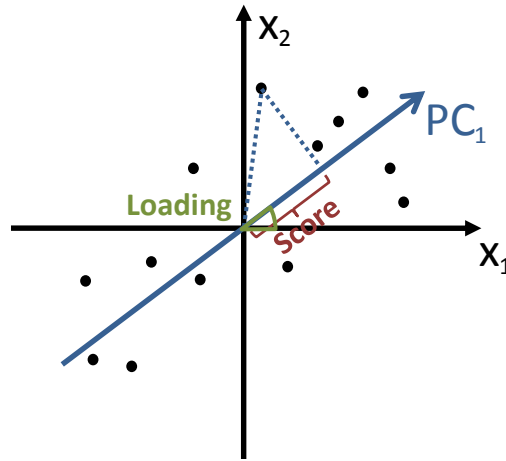
Figure 3.3.: Sketch of a principal component analysis. Every point symbolises a sample, described with the variables x_1, x_2. The principal component PC_1 is a linear combination of the old coordinate system axis. The projection of a data point on the PC is the score. Taking one unit in direction of the principal component, and expressing the coordinates in the old axes, is the loading of the principal component, therefore describing the rotation between the coordinate axis, and the importance of the original variables to the principal components [31].

Geometrical Explanation

The independent variables x are used as dimensions, therefore a N-dimensional space can be created, and every sample i is a point in this space. The variables are scaled and centered and hence form a cloud around the origin. The largest variance within the variables is now found and used as the axis of a new space, this is the first principal component [31].

The normalized vectors describing the direction of the principal component in the old space are called loadings. The greater the loading value, the more the principal component is influenced by this original variable [31].

The projections of the data points on the new axis, are called scores. Often the scores of data points are grouped, and allow classification and distinction of the original data points. To find the location of the original data points, scores and loadings have to be multiplied [31].

The next principal component can always be found by two properties, it has the direction of the largest variance and is normal to all previous components.

Every principle component explains some part of the variation, therefore the more PCs are used, the better the data is described, and the lower is the residual (unexplained variance). Often just a few principle components contain the important information and

are necessary to model the relevant data. Consecutive principal components describe insignificant properties or measurement errors [31].

Mathematical Explanation

The general PCA-model looks like [31]

$$X = TP' + E, \tag{3.10}$$

or for one component

$$x_{ij} = \overline{x}_j + \sum_{a=1}^{A} t_{ia} p_{ja} + e_{ij}(A). \tag{3.11}$$

A is the number of principal components. T is the Scores- and P the Loadings-matrix. Therefore t_{ia} is the score for sample i and principal component a, and p_{ja} is the loading for variable j and principle component a. e_{ij} is the remaining error (residual) and is dependent on the number of principal components used.

As shown in equation (3.10), this is an eigenvalue-problem, which can be solved by different methods, for example with Singular Value Decomposition. One of the most used algorithms for calculating principal components is the *Nonlinear Iterative Partial Least Square (NIPALS) algorithm*[2]. It's advantage is the iterative calculation of the principle components, so it can be stopped any time, when the number of principal components seems sufficient, and additional components can be added easily [31]. To choose the right number of components is a very important task, and this issue will reappear soon.

To calculate the importance of the principle components, it is necessary to know, how much of the variance is explained by a principal component [31]. The total variance is given by [31]

$$s_{\text{corr}}^2 = \frac{1}{NM} \sum_{i=1}^{N} \sum_{j=1}^{M} (x_{ij} - \overline{x}_{\text{total}})^2, \tag{3.12}$$

when $\overline{x}_{\text{total}}$ is the total mean of all samples and variables. On the other hand the scores and loadings of the principle components enable the recovery of the original variable by

$$\hat{x}_{ij} = \overline{x}_j + \sum_{a=1}^{A} t_{ia} p_{ja}, \tag{3.13}$$

which differs from the original variable by $e_{ij}(A)$. For $A = N$, it holds that $e_{ij}(A) = 0$. The contribution of every principle component to the variable is given by

$$\hat{x}_{ij}(a) = t_{ia} p_{ja}, \tag{3.14}$$

so the explained variance by principle component a can be calculated with

$$s_{\text{PCA},a}^2 = s_{\text{corr}}^2 - \frac{1}{N} \frac{1}{M} \sum_{i=1}^{N} \sum_{j=1}^{M} (\hat{x}_{ij} - x_{ij})^2, \tag{3.15}$$

---

[2]For more detail on this algorithm see [31].

and the explained relative variance for component a is then

$$r_a^2 = 1 - \frac{s_{\text{PCA},a}^2}{s_{\text{corr}}^2}. \tag{3.16}$$

Often the overall explained variance $\sum_{a=0}^{A} r_a^2$ is given and called the *coefficient of determination*. As a counterpart, the unexplained variance can be calculated using the residual matrix E [31, 35].

3.2.3. Fitting regression models

Multiple Linear Regression

Now for every of N samples i, there exists a dependent variable y_i to the data, usually called the response. Multiple linear regression assumes a first order relationship between the x variables and the y response

$$y_i = \sum_{j=1}^{m} b_{ij} x_{ij} + g_i, \tag{3.17}$$

respectively in matrice form

$$\boldsymbol{y} = X\boldsymbol{b} + \boldsymbol{g}. \tag{3.18}$$

For the usual case $m < n$ there is no exact solution, but the strategy is to minimize the length of the residual vector $\boldsymbol{g}$. This is usually done with the *least-squares method*, where the parameters are estimated with

$$\boldsymbol{b} = (X'X)^{-1} X'\boldsymbol{y} \tag{3.19}$$

[36].

ANOVA

Having performed a multiple linear regression, responses $\hat{y}_i$ can be calculated out of the factors x_{ij}. The quality of the model can be assessed using *Analysis of Variance (ANOVA)*. ANOVA splits the sum of squares (total variation) into smaller meaningful parts, [34, 35] as can be seen in figure 3.4.

These parts are calculated in the following way,

$$SS_{\text{resid}} = SS_{\text{pe}} + SS_{\text{lof}} = \sum_{i=1}^{N} (y_i - \hat{y}_i) \tag{3.20}$$

$$DF_{\text{resid}} = N - p \tag{3.21}$$

$$SS_{\text{pe}} = \sum_{k} (e_{ki} - e_k)^2 \tag{3.22}$$

$$DF_{\text{pe}} = \sum_{k} (f - 1)^2 \tag{3.23}$$

$$DF_{\text{lof}} = N - p - \sum_{k} (f - 1)^2 \tag{3.24}$$
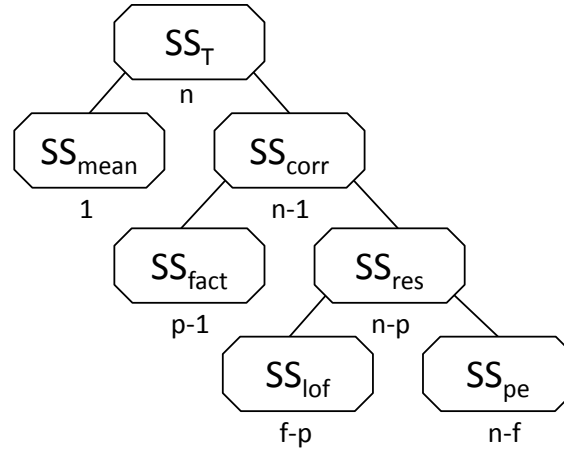
Figure 3.4.: Analysis of Variance Tree [37]. Within the octagons are the sum of squares depicted, below the number of degrees of freedom [38].

where SS is the respective sum of squares, and DF the degrees of freedom. p is the number of used terms in the model. The sums over k are used, when there are k sets of replicates with f repetitions, and e_k is the mean over e_{ik} of the kth set of replicates.

The total sum of squares SS_{tot} is first split into SS_{mean}, describing the SS explained by the means and the SS_{corr}, for the mean corrected. Then, these are further divided in the SS_{reg}, those squares explained by the regression, and the SS_{res} belonging to the residuals [38]. If there are repeated measurements, this sum can further be divided into the SS_{lof}, describing the sum of squares due to the *lack of fit*, meaning the error of the model, and the SS_{pe} (pure error), describing the experimental error [35]. The mean square (MS) is the sum of squares divided by the corresponding degrees of freedom [32].

Significance of Regression

An F-test can be performed to test for the *goodness of fit (gof)*. It holds that [35, 37]

$$F_{(p-1,n-p)} = \frac{\frac{SS_{fact}}{p-1}}{\frac{SS_{resid}}{n-p}}. \tag{3.25}$$

The F-values are tabulated, and determine if the null-hypothesis should be accepted or refused [3]. Here the null-hypothesis is: The factors have no effect on the response, equivalent to the coefficient of correlation being zero [37].

In the same way an F-test for *lack of fit (lof)* can be performed, like

$$F_{(f-p,n-f)} = \frac{\frac{SS_{lof}}{f-p}}{\frac{SS_{pe}}{n-f}}. \tag{3.26}$$

Often not the F-value is given, but the p-value. The p-value is the likelihood of the experimental, or more extreme data, under assumption of the null-hypothesis. An often used level for distinction is $p = 0.05$ [39].

Therefore we want the p_{gof} to be lower than 0.05, rejecting the hypothesis of no influence and the p_{lof} to be larger than 0.05 accepting the null-hypothesis, that the error is experimental and not caused by the model.

3.2.4. Partial Least Squares Regression

Mathematical Description

A connection between an independent variable matrix X, and a matrix Y of M dependent variables y shall now be established, similar to PCA [40].

The same outer relations as for the PCA are now used for both matrices [36]

$$X = TP' + E \tag{3.27}$$

$$Y = UQ' + F^*. \tag{3.28}$$

As a first assumption, an internal linear relationship between the scores is assumed,

$$\hat{\boldsymbol{u}}_a = b_h \boldsymbol{t}_a, \tag{3.29}$$

with

$$b_h = \frac{\hat{\boldsymbol{u}}_a' \boldsymbol{t}_a}{\boldsymbol{t}_a' \boldsymbol{t}_a}. \tag{3.30}$$

This leads to the mixed relationship

$$Y = TBQ' + F, \tag{3.31}$$

where $||F||$ is to be minimized. In an iterative algorithm, the scores between the X-block and Y-block are swapped, to give a better inner relation [36]. After reaching convergence, weights are introduced [40]

$$T = XW^* \tag{3.32}$$

$$W^* = W(P'W)^{-1} \tag{3.33}$$

[40] to give orthogonal X-scores [36].

For predicting new y-values by known x-values, the calculated scores and loadings of the calibration are used and combined to a regression vector $\boldsymbol{b}_k$

$$B = W(P^T W)^{-1} Q^T \tag{3.34}$$

$$\boldsymbol{b_0} = \hat{\boldsymbol{y}} - \hat{\boldsymbol{x}}' B \tag{3.35}$$

and new values can be predicted by

$$\hat{y}_{ik} = b_0 + \boldsymbol{x_i}' \boldsymbol{b}_k \tag{3.36}$$

[31].

When the maximum number of PLS-components $A = N$ is used, the PLS and the multivariate linear regression as presented in section 3.2.3 give the same coefficients. Again the advantage of the PLS is, that the amount of data is reduced [35].

34

Geometrical Interpretation
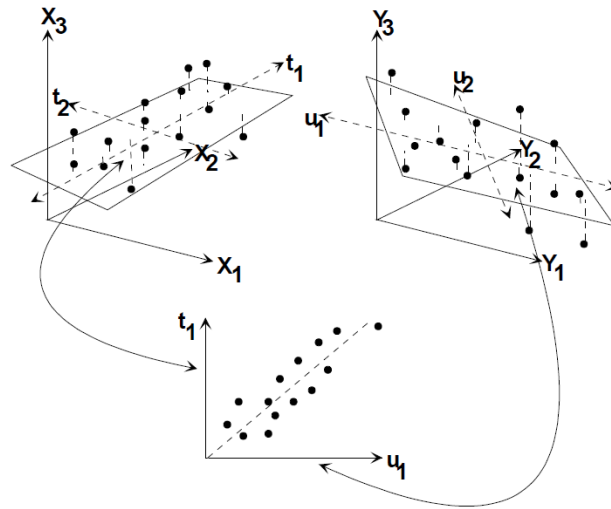
Figure 3.5.: Graphical interpretation of the PLS [35]

The PLS estimates latent variables $\boldsymbol{t}_a$ as linear combinations of the original x-variables and uses them for predicting Y. Geometrically, the X-matrix is reduced to an A-dimensional hyperplane, well approximating X, like indicated in figure 3.5. However, at the same time, the $\boldsymbol{t}_a$, which define the hyperplane, are chosen in such a way, that the scores t_{ia}, e.g., the projection of the data points on this plane, give good predictors for the responses and are related to the responses y_{im} [40].

A PLS can be performed for one or many dependent variables. However, if the responses are not correlated, a separated PLS for every response is preferred [31].

Validating Partial Least Squares Regression

The number of principal components is essential for a model. With increasing number of principal components the residual becomes smaller, (and finally zero for the maximum number of PCs), however the predictive power of the model lessens due to over-fitting [40].

How good the model is explained is usually measured by R^2, the coefficient of

determination. It is calculated by [35]

$$R^2 = \frac{SS_{\text{reg}}}{SS} = 1 - \frac{SS_{\text{resid}}}{SS} \qquad (3.37)$$

$$SS = \sum_{n=1}^{N} \sum_{m=1}^{M} y_{\text{corr}}^2 \qquad (3.38)$$

$$SS_{\text{reg}} = \sum_{n=1}^{N} \sum_{m=1}^{M} \hat{y}_{\text{corr}}^2 \qquad (3.39)$$

$$SS_{\text{resid}} = \sum_{n=1}^{N} \sum_{m=1}^{M} \left(y_{\text{corr}} - \hat{y}_{\text{corr}} \right)^2. \qquad (3.40)$$

SS is the total sum of squares of Y corrected for the mean, and SS_{reg} is the total Sum of Squares of Y explained by the model, whereas SS_{resid} is the fitted residual sum of squares. Therefore R^2 is the fraction of response explained by the model [35].

A possible method to test the predictive power of a model is cross-validation. The data is divided into groups. One group is neglected for building the model, but predicted afterwards. This is then repeated for every group [40].

Another method for estimating the model predictive power is to measure the influence of every data point on the model, this is called the "leverage correction". This is done by

$$Q^2 = 1 - \frac{PRESS}{SS} \qquad (3.41)$$

$$PRESS = \sum_{i=1}^{M} \frac{(\boldsymbol{y}_i - \hat{\boldsymbol{y}}_i)^2}{(1 - h_{ii})^2} \qquad (3.42)$$

$$H = X(X'X)^{-1}X' \qquad (3.43)$$

$PRESS$ is an abbreviation for *Prediction Residual Sum of Squares* [31, 34, 35].

R^2 is therefore an overestimation, and Q^2 an underestimation for the goodness of the fit [35]. A Q^2 of above 0.7 indicates a good predictive power [35]. When choosing the number of principal components, usually the model with the minimum $\frac{PRESS}{N-A-1}$ is preferred [40].

The sums of squares are also expressed as standard deviations. Then

$$SD_{\text{resid}} = \sqrt{\frac{SS_{\text{resid}}}{n-p}}. \qquad (3.44)$$

These quantities do not have to be calculated for the whole model, but can be calculated also for every response separately [35, 40].

Significance of the model

Confidence intervals for PLS are calculated using regression models, actually ANOVA. Those give a little bit larger errors, than would result from the PLS [35].

For predictions, as well as for the coefficients, a confidence interval is calculated with

$$I = \sqrt{h_{ii}} \cdot RSD \cdot t\left(\frac{\alpha}{2}, DF_{\text{resid}}\right) \tag{3.45}$$

where RSD is the residual standard deviation

$$RSD = \frac{SS_{\text{resid}}}{n - p} \tag{3.46}$$

and t is a student-t factor. [32, 35]

The software used in this work, MODDE, determines the validity of a model by

$$\text{Validity} = 1 + 0.57647 \cdot \log(p_{lof}), \tag{3.47}$$

so a value Validity > 0.25 indicates that the experimental errors are not larger than the model errors and the model is considered significant. The reproducibility, e.g. how well experimental results are reproducible under the same conditions is estimated [35] by

$$\text{Reproducibility} = 1 - \frac{MS_{\text{pe}}}{MS_{\text{corr}}}. \tag{3.48}$$

3.2.5. Non-linear models

The usual model used is a linear one, but interaction terms are considered. Therefore, for k factors x_i the model looks like

$$y = \beta_0 + \sum_{i=1}^{k} c_i x_i + \sum_{i=1}^{k-1} \sum_{j=i+1}^{k} \beta_{ij} x_i x_j. \tag{3.49}$$

The linear assumption is often very powerful, because a lot a factors can be modelled very simply, interaction terms are often more influential than higher order terms, and linearity is a good assumption for small ranges.

If a linear model is not sufficient for describing a response two different strategies are applied.

- *Transformation of factors and responses:* Factors and responses can be transformed monotonically, especially if a physical correspondence is known. This does not increase the number of factors.

- *Addition of higher order terms:* New factors can be calculated using the native ones, taking squares or even higher terms, and/or multiple interaction terms. The model is then calculated using these additional terms.

As the R^2 increases with model terms, an adjusted R^2 can be calculated, taking the number of models into account with

$$R^2_{adj} = 1 - \frac{N-1}{N-p}(1 - R^2),$$

(3.50)

[34].

3.2.6. Response Surface Modelling

To visualize a model, the expected response $\hat{y}$ is plotted over the region spanned by the factors, e.g., the mixture components [32]. This gives the possibility to understand the influence of parameters intuitively. Further, a response surface can be the starting point of an optimization process, an interesting part, in terms of process possibilities, could state the borders for a consecutive DoE.

The most extreme measured points of a model, are also its borders of validity. The models described above are not suited for extrapolations [34].

4. Measuring and Modelling Powder Properties

4.1. Powders investigated

A variety of powders has been chosen for performing tests with the FT4, to identify different behaviour of diverse powders. In the following these powders are introduced and an overview of the parameters measured is presented.

4.1.1. General properties of the investigated powders

In-depth research has been performed on with three well-known pharmaceutical powders, which are introduced briefly.

- *Acetylsalicylic acid (ASA)* is a widely used API and the most well known formulation is aspirin [41]. ASA comes in needle shaped bright crystals, up to millimetres in length. For the characterizations with the FT4, Rhodine 3020 crist. was used.

- *Lactose mono-hydrate*; Tablettose (TAB) is granulated α-lactose-monohydrate, and is a widely used excipient[1], available in different size classes [42]. For the experiments Tablettose 80 was used.

- *Microcrystalline Cellulose (MCC)* is a widely used excipient too. For the tests H102 AVO 1002 was used.

An overview of the physical powder parameters of these three powders, summarized in a table, can be found in appendix A.2, as well as some pictures taken with a microscope in figure A.1, clearly showing the difference in shape of these three powders.

Other investigated powders were Ca-Stearate, which is a lubricant, two types of Eudragit, which are usually used for coating and Kollidon, used for coating and other purposes. Furthermore PEG 6000 (Polyethyleneglycole) has been investigated in native and milled form.

The values gained of native PEG are included in the further analysis, although it is actually too large (coming in disks with 10 mm diameter, and up to 2.5 mm thickness), to be measured appropriately. The effects of the cumbersome shape can be seen in figure 4.1, where even consecutive tests exhibit large deviations, due to particles becoming stuck in the gap between the blade and the vessel.

---

[1]Excipients are substances added to a pill beside the API, usually for preservation of the API and improvement of the processability.
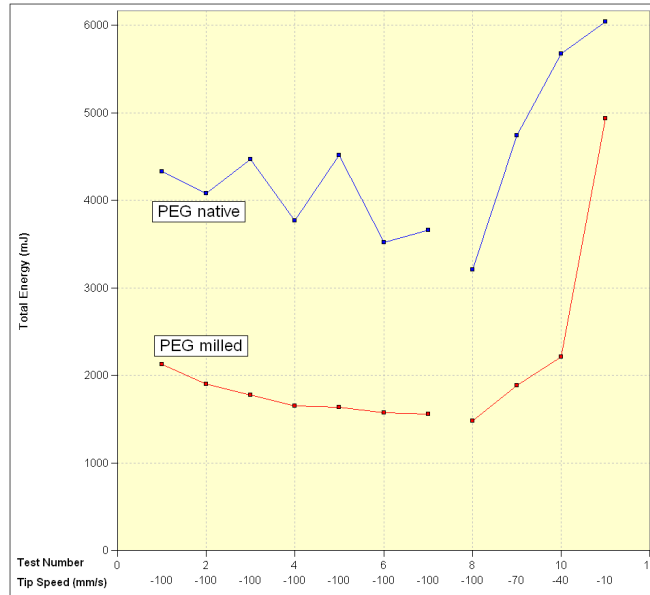
Figure 4.1.: BFE and VFR test of milled and native PEG. The large deviations in the Total Energy for consecutive tests show, that native PEG is unsuitable to be measured with the FT4.

4.1.2. Measured properties of the investigated powders

An assortment of measured properties for very diverse powders can be seen in table 4.1. Most values represent a mean value of several consecutive measurements.

Differences between the powders' properties can be spotted easily, showing that a wide range of parameter variation has to be expected for different powders. First of all, milling has a significant influence on the behaviour of PEG. While the large, clumpy, native PEG showed good flowability, the cohesion increased for the smaller, milled PEG particles. Another outstanding powder is Ca-Stearate, which is employed as a lubricant. This gliding behaviour is reflected in the very low Basic Flow Energy. Moistening TAB seems to have contradictory effects, as at the same time the Basic Flow Energy is lowered, suggesting that water acts as a lubricant, while at the same time Unconfined Yield Strength and Cohesion are rising, indicating that the adhesion increased.

In the following, two examples of possibilities for traditional powder classification methods are given.

Indices comparison

The Carr index allows to asses flowability of a powder and is defined as

$$I_c(\%) = \frac{\varrho_{\text{tap}} - \varrho_0}{\varrho_{\text{tap}}} \cdot 100, \tag{4.1}$$

40

	Bulk Density (g/ml)	Stability Index	Basic Flow Energy (mJ)	Specific Energy (mJ/g)	Flow Rate Index	Unconfined Yield Strength (kPa)	Cohesion (kPa)	Angle of Intenal Friction (°)	Pressure Drop @ 8 kPa (2mm/s)	Compressibility (%) @ 8kPa
PEG Native	0.567	0.85	3659	10.2	1.88	0.00	0.00	58.7	0.0	4
PEG Milled	0.443	0.78	1586	10.1	3.10	5.54	1.25	41.8	1.2	6
MCC PH 102	0.376	1.02	1836	8.1	1.30	0.56	0.37	37.5	1.2	10
TAB	0.632	1.08	1970	5.9	1.05	0.51	0.13	38.3	1.1	7
TAB moistened	0.634	1.02	1682	6.7	1.04	1.12	0.29	38.5	1.5	8
ASA	0.950	0.84	8507	8.0	0.45	0.81	0.28	40.0	0.6	4
Ca-Stearate	0.303	1.16	163	4.7	2.02	4.38	1.24	30.8	12	32
Eudragit RS P0	0.627	0.90	1352	7.3	1.54	0.77	0.21	32.0	10.5	7
Kollidon	0.458	0.98	520	3.4	1.78	0.33	0.11	23.4	4.2	4
Eudragit RL P0	0.548	0.93	1142	6.7	1.78	1.08	0.29	33.6	11.5	8

Table 4.1.: Summary of properties of different powders measured with the FT4

and can be calculated by tapping tests [19]. Additionally, Jenike's flow function constant *ffc* can be used to classify the flowability but is independently determined by shear tests. Both indices are compared in figure 4.2. The investigated powders show good flowability in both indices. However, the Carr index is usually calculated under the assumption, that a stationary state is achieved by tapping, which might not be true for all performed experiments here. Therefore the values should just be taken as a lower limit regarding this index.
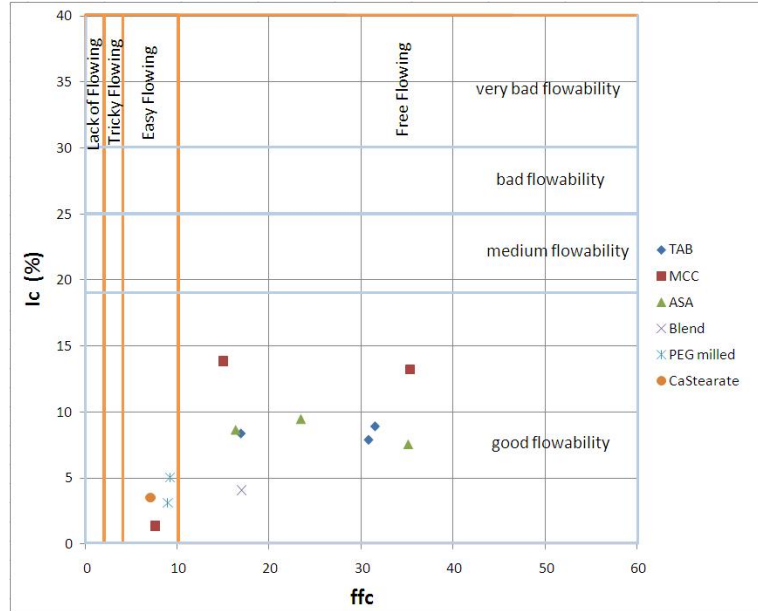
Figure 4.2.: Classification of powders due to two independent indices, Jenike's flow function constant and the Carr index. The powder marked with "Blend" is an equal blend of ASA, TAB, and MCC.

Flow function curves

Shear cell tests with different consolidation stresses allows the construction of flow function curves. These show how the flowability of powders changes, when stress was applied (for example by previous transport steps, etc.). The flow function curves of TAB and MCC are displayed in figure 4.3. Both powders are rather good flowing and change their behaviour just slightly under different compression levels. Nonetheless they differ. MCC tends to be more free flowing under higher consolidation stress, while TAB shows opposite behaviour and becomes decreasingly good flowing under increasing stress.
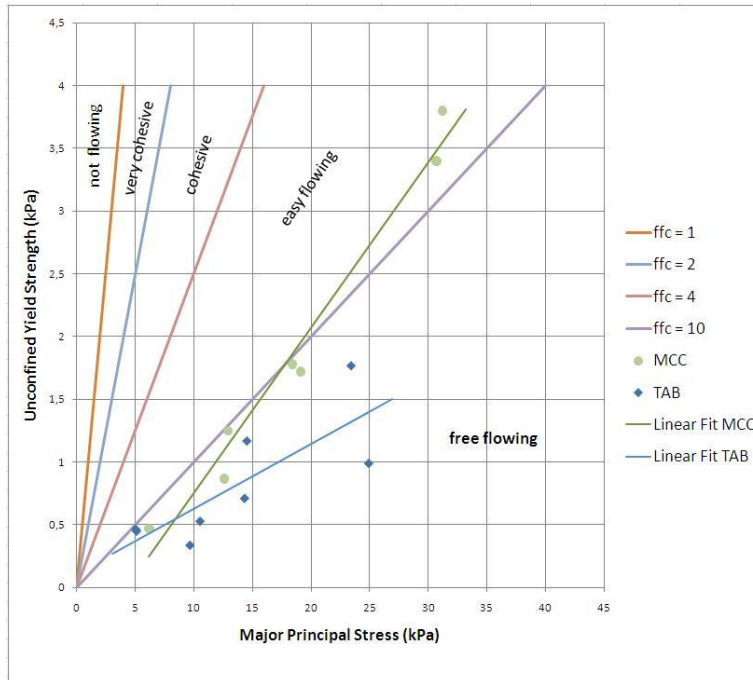
Figure 4.3.: Flow function curves of TAB and MCC

4.2. Considered issues on powder characterization

Before starting the Design of Experiments (DoE), experiments were carried out, to observe the ranges of the responses and to estimate the influence of environment.

4.2.1. Environmental issues

Room humidity

Room Humidity has a strong influence on powder properties. TAB was subjected to tests, both with the FT4 and the traditional annular shear cell, with different preparations regarding moisture.

An exemplary result gained with the FT4 is plotted in figure 4.4. The dry Tablettose has been in the exsiccator for 72 hours, whereas the moistened one has just been put together with a glass of water inside a larger vessel and sealed with parafilm. Clearly a difference in behaviour can be seen, as the dry Tablettose shows a larger resistance in the stirring process.

Different batches

Two different batches of Tablettose 80 were investigated. They were well distinguishable by some of the FT4 parameters, like the permeability, as shown in figure 4.5. The error

43
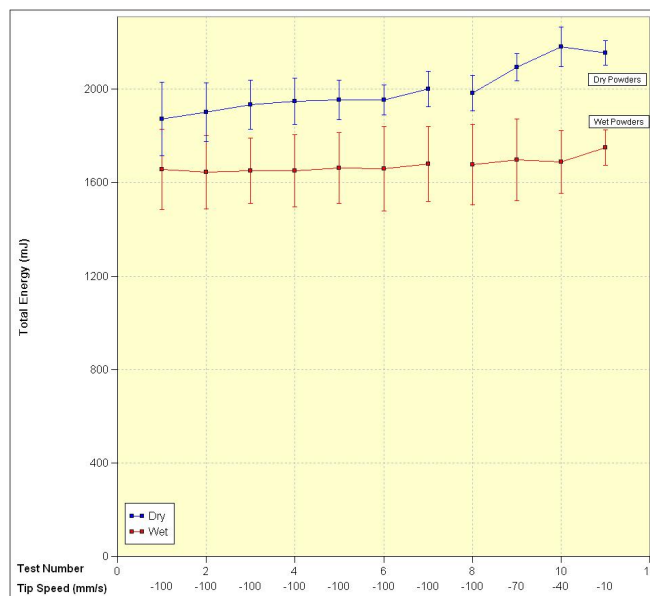
Figure 4.4.: Stability and Variable Flow Rate test for dry and wet TAB

bars represent different tests, performed on different days. The "new" batch shows a significantly lower permeability (e.g., a higher pressure drop), than the "old" batch.

Segregation

Segregation is a big issue and influences the tests. A blend showing a very strong tendency for segregation consists of TAB and ASA. The tendency is indicated by a large stability index of $SI = 1.18$, which is larger than the stability indices of the pure powders.

The dissipated energy at a certain height is displayed in figure 4.6(a). The error bars represent the standard deviation of 8 consecutive tests. It is remarkable, that the blend dissipates less energy than the pure powders, indicating better flowability. This might be a result of large particles losing contact to each other and rolling on the smaller ones.

A kink in the energy gradient is often observed in blends, but not always as clearly as here. This kink might be a result of a powder fraction gathering in one part of the vessel. The absorbed energy of the blend is steadily rising, as indicated in figure 4.6(b).

As segregation cannot be completely avoided, it should at least be minimized. Therefore the blends were prepared with a Turbula mixer, and keeping the number of subsequent steps as low as possible. Filling was done slowly, to minimize segregation, and as an additional provision, the powders were poured against the funnel wall and not directly into the vessel [43].

Unfortunately segregation cannot be avoided in the course of testing the powder
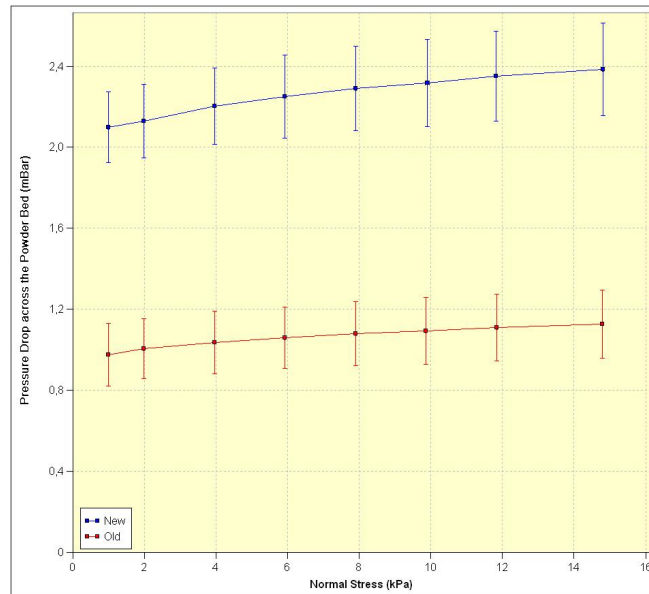
Figure 4.5.: Difference in permeability in between two different batches of TAB. Every batch has been tested several times, resulting in the displayed mean and standard deviation values.

properties. Its effect on model building should be minimized, as all powders share the same treatment, and same degree of segregation.

4.2.2. Powder preparation

Turbula mixer

To ensure that the powders are similarly conditioned before performing the experiments, pure powders as well as blends have been treated in a Turbula® mixer (System Schatz, WKB) before. The aforementioned substances have been treated for 30 min with a frequency of 50.3 rpm.

The turbula mixer provides a good homogeneity of powders with low stresses during blending.

Influence of treatment on particle size distribution

It is possible that the powder treatment changes the particle sizes by attrition or destruction exists. For an assessment QicPic measurements were performed on ASA, TAB and MCC. Measurements were carried out at three different states: i) out from the container, ii) after using the Turbula blender, and iii) after using the FT4. A summary of the measurements is given in table 4.2.
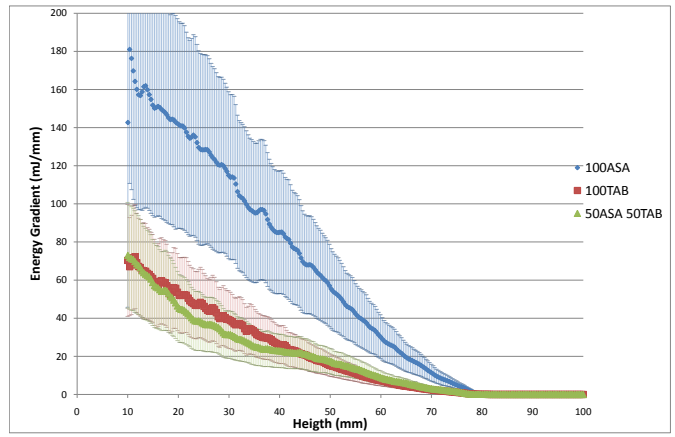
(a) Mean energy gradient for two pure powders and its blend
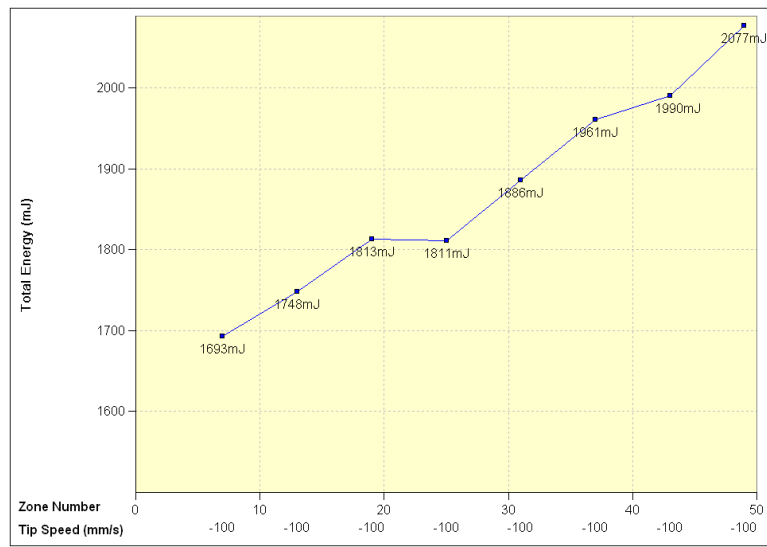
(b) Total energy for a powder blend for consecutive tests

Figure 4.6.: Dissipated Energy during the Stability test for ASA and TAB

ASA	x10	x16	x50	x84	x90	x99	
Pkg	238.32	275.55	425.08	631.00	706.92	1128.61	
Pkg	240.56	277.75	430.02	628.01	695.98	1075.99	
Pkg	237.61	272.98	419.17	611.82	661.40	963.31	
Turbula	252.20	286.58	434.86	638.41	706.37	1073.27	
Turbula	256.36	292.59	448.86	661.71	753.33	992.89	
Turbula	249.04	283.14	432.81	634.74	715.22	947.34	
FT4	222.57	261.30	409.15	595.88	651.80	940.50	
FT4	247.04	283.08	436.74	644.05	727.89	1179.26	$\chi^2 = 13, 4$
FT4	241.35	277.92	429.04	621.70	676.40	940.33	$\chi^2_{((9-1)(6-1),1-\alpha)} = 26.5$
TAB	x10	x16	x50	x84	x90	x99	
Pkg	76.80	94.39	193.65	354.27	417.80	629.78	
Pkg	75.15	92.09	188.95	344.29	405.34	618.31	
Pkg	79.07	97.31	204.70	389.60	454.49	668.55	
Turbula	75.74	92.95	191.73	355.83	422.33	646.73	
Turbula	74.78	91.70	187.85	347.72	413.83	633.63	
Turbula	75.98	93.39	193.80	359.41	424.29	641.17	
FT4	72.23	88.45	181.59	344.44	409.47	641.50	
FT4	72.47	88.92	183.86	354.45	428.48	646.48	$\chi^2 = 2, 16$
FT4	72.03	88.28	183.13	353.80	424.06	636.33	$\chi^2_{((9-1)(6-1),1-\alpha)} = 26.5$
MCC	x10	x16	x50	x84	x90	x99	
Pkg	63.11	74.42	136.24	230.78	259.25	372.97	
Pkg	63.34	74.72	136.86	230.71	259.10	379.79	
Pkg	62.99	74.21	135.94	231.00	258.94	372.76	
Turbula	63.13	74.42	136.07	231.19	259.91	378.76	
Turbula	63.02	74.17	135.00	229.00	256.55	372.52	
Turbula	63.24	74.56	136.42	231.86	260.96	371.62	
FT4	63.51	74.90	136.56	231.58	260.01	372.19	
FT4	63.59	75.12	137.47	230.95	258.79	382.89	$\chi^2 = 0, 14$
FT4	63.78	75.32	138.22	233.82	264.12	373.88	$\chi^2_{((9-1)(6-1),1-\alpha)} = 26.5$

Table 4.2.: Summary of QicPic-Measurements. The powders have been sampled directly from the package (Pkg), after treatment in a turbula mixer (Turbula) and after a complete measurement cycle within the FT4 (FT4). The sizes are all in μm. The χ^2 values for homogeneity are noted, as well as the critical $\chi^2_{((9-1)(6-1),1-\alpha)}$ for the corresponding degrees of freedom and $\alpha = 0.05$.

A χ^2-homogeneity-test was performed, with a confidence level of $\alpha = 0.95$. In all three cases, the null hypothesis, that the samples stem from the same population, was accepted. The conclusion therefore is, that treating the powder in the turbula mixer and in the FT4, does not influence the particle size distribution.

4.3. Model Building on FT4 key parameters

4.3.1. Designs of Experiments

The experimental designs used shall be introduced briefly. All designs are based on four factors. These are the mixture variables, respectively the three powders ASA, TAB and MCC. The fourth factor is the room humidity, which was not controlled but logged. An overview of the factors and their scaling is given in figure 4.7.
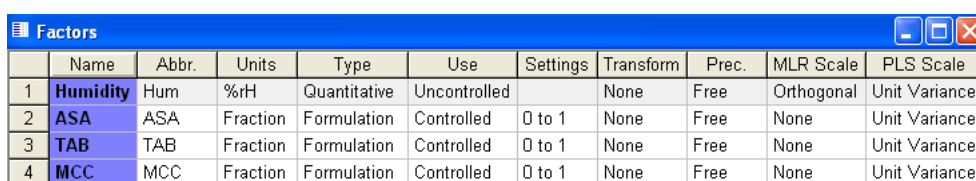
	Name	Abbr.	Units	Type	Use	Settings	Transform	Prec.	MLR Scale	PLS Scale
1	**Humidity**	Hum	%rH	Quantitative	Uncontrolled		None	Free	Orthogonal	Unit Variance
2	**ASA**	ASA	Fraction	Formulation	Controlled	0 to 1	None	Free	None	Unit Variance
3	**TAB**	TAB	Fraction	Formulation	Controlled	0 to 1	None	Free	None	Unit Variance
4	**MCC**	MCC	Fraction	Formulation	Controlled	0 to 1	None	Free	None	Unit Variance

Figure 4.7.: Factors for design of experiments.

Screening: Axial extended design

For the starting experiments, first pure powders, than binary blends, and finally ternary blends have been prepared and tested in the FT4. Finally the data were analysed in the classical way by comparing curves.

Afterwards MODDE (Umetrics AB, Umeå; Sweden) was used, to perform multivariate data analysis and the already gained data were included and complemented by an axial extended design, with a linear model.

Therefore the measurements have not followed a randomized order, as would be suggested. As a result, some properties have more measurement points than others and room humidity is varied over a large range.

Response Surface Modeling: Modified Simplex Centroid Design

A next Design of Experiments has been developed in order to enable appropriate response surface modelling and the inclusion of quadratic terms. Powders have been treated the same way and all measurements have been performed without interruption to minimize external influences. This new DoE was also performed with the second batch of TAB, so that the data gained in the previous design could unfortunately not be used.

Refinement: D-Optimal design

As the whole mixture region was investigated, a cubic model might be necessary to model some of the reponses. Hence, the previous design was further extended to a D-optimal design. If not stated otherwise, the analysis always refers to this model. A summary of the models' properties can be found in appendix A.5.

The investigated responses are summarized in figure 4.8, and will be discussed in more detail in the next but one section. The final workplan, showing the experiments needed to be performed, can be seen in figure 4.9, and a graphical representation of the mixtures can be found in figure 4.10.

	Name	Abbr.	Units	Transform	MLR Scale	PLS Scale	Type
1	Conditioned Bulk Density	CBD	g/ml	None	None	Unit Variance	Regular
2	Basic Flow Energy	BFE	mJ	Log (10Log(Y))	None	Unit Variance	Regular
3	Stability Index	SI		None	None	Unit Variance	Regular
4	Flow Rate Index	FRI		NegLog (-10Log(100-Y))	None	Unit Variance	Regular
5	Specific Energy	SE	mJ/g	NegLog (-10Log(100-Y))	None	Unit Variance	Regular
6	Aeration Ratio	AR		None	None	Unit Variance	Regular
7	Aeration End Energy	AEE	mJ	None	None	Unit Variance	Regular
8	Fluidisation Point	Flu	mm/s	Log (10Log(Y))	None	Unit Variance	Regular
9	Poured Density at -2deg	PD2	g/ml	None	None	Unit Variance	Regular
10	Basic Flow Energy at -2 deg	BFE2	mJ	None	None	Unit Variance	Regular
11	Tapped Density (250 taps)	TD	g/ml	Log (10Log(Y))	None	Unit Variance	Regular
12	Consolidated Energy (250 taps)	CE	mJ	None	None	Unit Variance	Regular
13	Consolidated Energy Index	CEI		None	None	Unit Variance	Regular
14	Hausner Ratio	HR		None	None	Unit Variance	Regular
15	Unconfined Yield Strength	UYS	kPa	None	None	Unit Variance	Regular
16	Major Principal Stress	MPS	kPa	None	None	Unit Variance	Regular
17	Cohesion	Coh	kPa	None	None	Unit Variance	Regular
18	Angle of internal friction	AIF	°	None	None	Unit Variance	Regular
19	Effective Angle of Internal Friction	AIFE	°	None	None	Unit Variance	Regular
20	LogFit of Compressbility	LogC	g/ml	None	None	Unit Variance	Regular
21	Permeability at 8 kPa (Pressure Drop)	P8	mBar	None	None	Unit Variance	Regular
22	Shear Stress at 5 kPa	S5	kPa	Logit (10Log((Y)/(100-Y)))	None	Unit Variance	Regular

Figure 4.8.: Responses investigated with the FT4, scaling methods are also indicated. The parameters are discussed in section 4.3.4.

4.3.2. Information by raw data, variances and covariances

Correlations

It is worth to take a look, which powder properties show correlations. The most important correlations are shown in figure 4.11 in a grouped manner. An illustration for the highest correlations is given in the appendix in figure A.5.

Care has to be taken, when looking at correlations for certain reasons. Firstly, correlation does not mean causality. Two responses can correlate, because they both correlate to a third attribute, which might not even have been measured or identified. Further a lack of correlation does not mean, that there is no connection between two

Figure 4.9.: Workplan for the D-Optimal design, those named with N are part of the original simplex-centroid design, those marked with C are the complement for the d-optimal design.
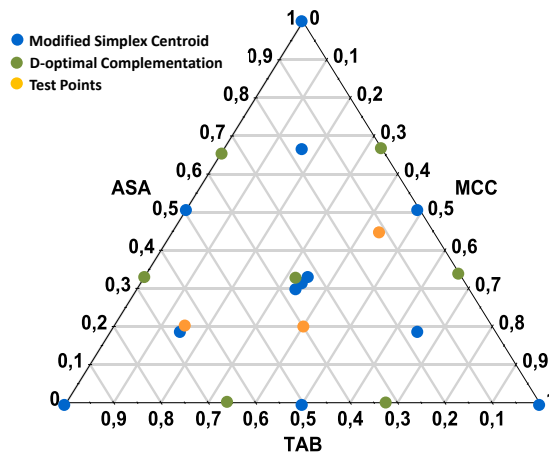
Figure 4.10.: Graphical representation of the mixtures investigated. Every point represents an experiment with a certain composition. The center samples are just seperate for a clear picture and indicate all the same mixture.

parameters, as more complex than linear dependences cannot be recognized. Secondly, the reverse is true, a high correlation indicates most likely a linear relationship.
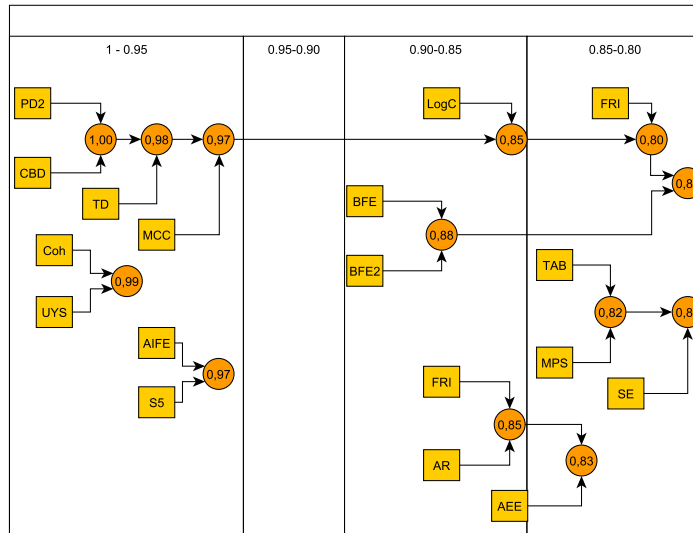
Figure 4.11.: Grouped Correlations, the factors and responses are connected with nodes, showing their correlation coefficient. Terms are just added once to the group with which factor they show correlation. Further correlations inside the group are not shown but likely exist with a lower correlation coefficient than the displayed one. The nodes are arranged with descending correlation coefficients from left to right, with the lowest correlations of 0.8. Quadratic terms are neglected.

An obvious strong correlation is obtained for *Conditioned Bulk Density (CBD)* and *PD2*. As *PD2* is just another Conditioned Bulk Density measurement, taken at a different time during the tests, they should actually be the same. The tapped density also belongs into the same group, so the correlation between poured and tapped density is given. The docking of MCC into this group is also explained easily. As MCC has the lowest bulk density of the investigated powders, its fraction correlates negatively with the bulk density.

The next correlating parameter is the sensitivity of density to compression. That may be the influence of MCC in this group, or the general property, that powders with low bulk density have a higher porosity and therefore higher compressibility. In general the investigated number of powders is too low, to make a clear distinction between general powder properties and properties of the specific investigated powders.

Other obvious correlations exist for the parameters of the shear cell test. *Cohesion*

(Coh) and *Unconfined Yield Strength (UYS)* correlate strongly with each other, because they are a result of the same calculation. The same is true for the *Angle of Internal Friction (AIF)* and the *direct shear stress* value *S5*. More surprisingly is, that there is a rather weak connection between *Coh* and *UYS* on one side, and *AIF* and *S5* on the other side. Their dependence is clearly not linear. Furthermore, the next shear cell parameter *MPS* is weakly linked to these two groups also. However, it is the characteristics of the Tablettose, which establish the connections between the shear cell parameter *MPS* and the specific energy *SE*.

BFE and *BFE2* are both basic flow energy measurements, but done with the stirrer following different helix angles, therefore they should and do correlate. That the consolidated energy *CE* measurements have shown no correlation to the other flow energy measurements, might be explained by insecurity caused by manual tapping.

Interesting and less obvious is the correlation between *Aeration Ratio (AR)* and *Flow Rate Index (FRI)*. The reason behind might be found in the relative particle-particle and particle-blade motions. The relation between *FRI* and *AR* can be seen in figure 4.12.
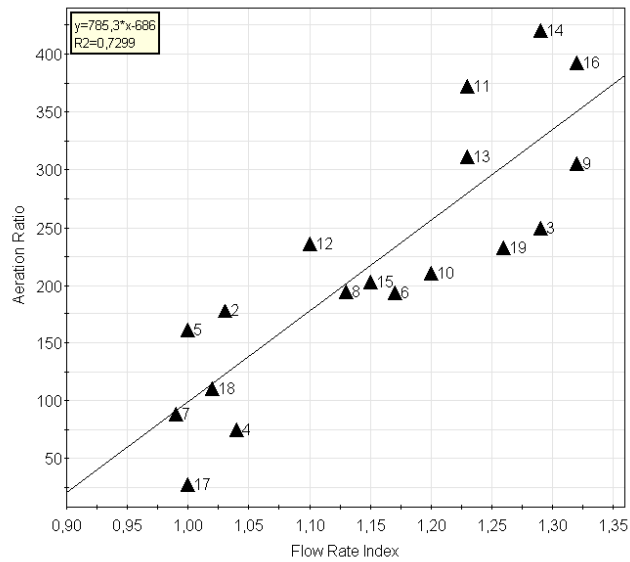
Figure 4.12.: Flow Rate Index versus Aeration Ratio, labelled by experiment number.

Also the fact that humidity is missing in the largest correlation (its strongest correlation is with the *Fluidisation Point (Flu)* with -0.55) is a hint, that the influence of humidity is much less significant, than a change of mixture fractions.

4.3.3. Model building and evaluation exemplary demonstrated for Conditioned Bulk Density

The steps in building a model shall be exercised here on the example of the Conditioned Bulk Density. The experiments have been performed and the values have been entered in the worksheet of MODDE.

A summary of the performed experiments is given in the replicate plot, as can be seen in figure 4.13. Experiments performed under the same conditions (that means for MODDE, with not more than 10 % difference in factors) are plotted on the same index. This allows to see at one glance, if variance is larger in between different or same measurements, or if there is a completely unawaited value. For *CBD* neither is true.
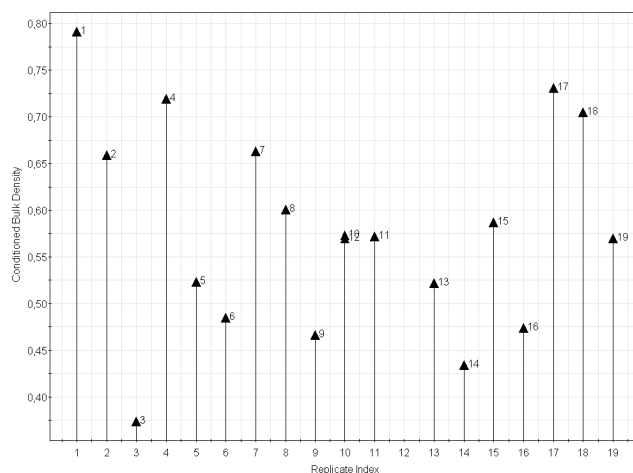
Figure 4.13.: Replication Plot for Conditioned Bulk Density

Further, the distribution of the response values is plotted as a histogram in figure 4.14. It is preferred that the responses follow a normal distribution, if this is not the case, the responses should undergo a transformation. Here, for *CBD*, this is not necessary.

In the next step for model building a PLS was performed. At the beginning this is done for nearly all possible terms, those are listed in table 4.3, and the evaluation of the model is shown in figure 4.15(a). R2, Q2 and Reproducibility are already rather good, but no model validity can be given, as not enough degrees of freedom were left.

For convenience a short summary of the already mathematically defined parameters used in MODDE to asses the fit quality is given here: [35]

- *R*2: The percent of the response explained by the model. The range is between 0 (completely unexplained) to 1 (completely explained).

- *Q*2: The percent of the response explained, according to cross validation or leverage correction. Therefore a measurement how well new values can be
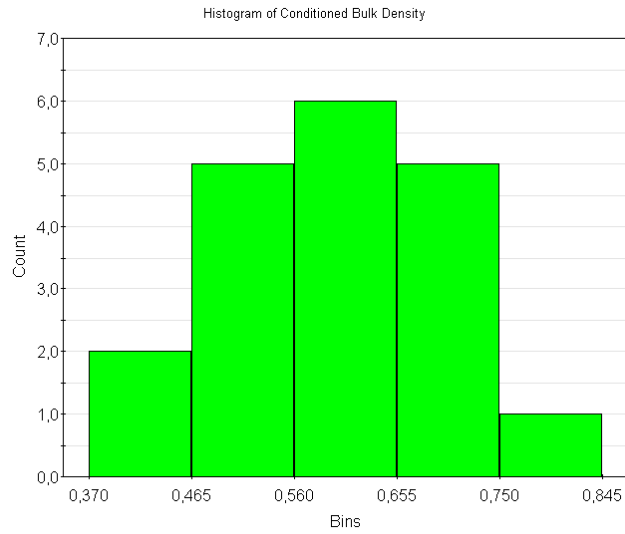
Figure 4.14.: Histogram for Conditioned Bulk Density

Linear Terms	Hum	ASA	TAB	MCC
First Order Interaction	Hum*ASA	Hum*TAB	Hum*MCC	
	ASA*TAB	ASA*MCC	TAB*MCC	
Quadratic Terms	Hum*Hum	ASA*ASA	TAB*TAB	MCC*MCC
Second Order Interaction	Hum*Hum*ASA	Hum*Hum*TAB	Hum*Hum*MCC	Hum*ASA*ASA
	ASA*ASA*TAB	ASA*ASA*MCC	TAB*TAB*MCC	ASA*TAB*TAB
	TAB*MCC*MCC	ASA*MCC*MCC	Hum*TAB*TAB	Hum*MCC*MCC
	Hum*ASA*TAB	Hum*TAB*MCC	Hum*ASA*MCC	
Cubic Terms	Hum*Hum*Hum	ASA*ASA*ASA	TAB*TAB*TAB	MCC*MCC*MCC

Table 4.3.: Possible terms in a cubic model.

(a) All terms included   (b) Superfluous terms removed
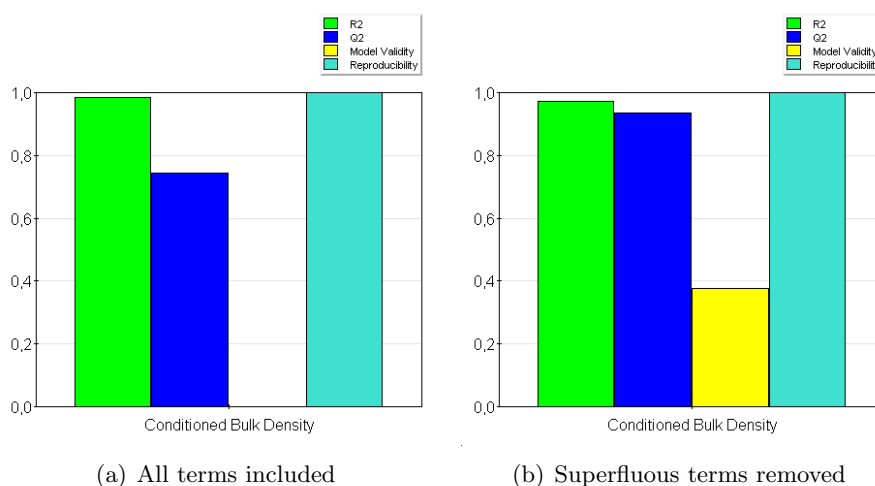
Figure 4.15.: Evaluation of the model for CBD.

predicted.

- *Validity:* Comparison of the error, due to the model, and the experimental error. For > 0.25 there is no lack of fit

- *Reproducibility:* An index for how good experimental results can be reproduced under the same conditions. A value < 0.5 indicates large deviations in the measured results.

To define, which terms are important, the value of the regression coefficient is plotted in the coefficient plot, figure 4.16(a). Clearly the pure powders are dominant, therefore all the other terms are removed, as indicated in figure 4.16(b). As a consequence R2 is reduced, as fewer terms remain for the fit. On the other hand, Q2 has improved, indicating that with fewer terms the model is better suitable for prediction, as less noise is fitted. In general removing the terms is done following these objectives: [34, 35]

- First, higher order terms are investigated, as those usually have the least impact.

- Insignificant terms should be removed. They are recognized by the deviation being larger than the actual value.

- Unimportant terms (whose scaled regression coefficients are much lower than those of other terms) should be removed.

- Main effects should be removed last, however they need to be kept if they appear in higher order terms to ensure model hierarchical integrity.

- Increase of $Q2$ and $R2_{adj}$ is an indicator for an improving model.

(a) All terms included

(b) Superfluous terms removed
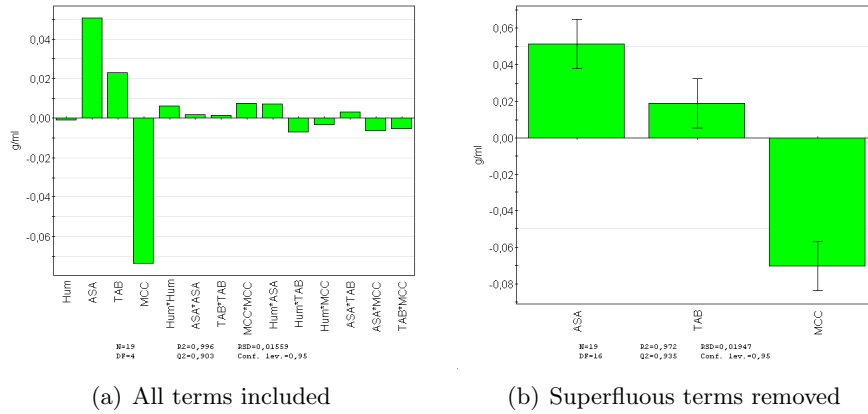
Figure 4.16.: Scaled and centred coefficients for CBD.

- If a physical understanding and model exists, this knowledge should always have priority in preserving factors.

The resulting coefficients now provide the model, which can be displayed in the case of *CBD* as

$$CBD = 0.579 + 0.181 \cdot c_{\text{ASA}} + 0.067 \cdot c_{\text{TAB}} - 0.248 \cdot c_{\text{MCC}}, \qquad (4.2)$$

where the powder fractions c_i range from 0 to 1. The constant is the property value of the reference sample, which in this case is the center sample. Therefore the reference sample is

$$c_{\text{ASA}} = \frac{1}{3}, c_{\text{TAB}} = \frac{1}{3}, c_{\text{MCC}} = \frac{1}{3}. \qquad (4.3)$$

To confirm the suitableness of the model, the curvature of the normal-probability-plot (figure 4.17) is investigated. In this plot the standardized residuals are plotted against a cumulative normal probability scale of their quantiles. If the residuals follow a normal probability, which is the general assumption for unsystematic errors, they will all be on a line. Otherwise, if there are systematic errors, or if the order of the model is not correct, a curvature would appear in the plot [34, 35].

Furthermore, to look for systematic errors, the residuals are plotted against predicted values (figure 4.18(a)), against run order (figure 4.18(b)) and against factors. In either case no pattern should be recognisable. If a pattern is found, this is a strong indication for systematic failure.

After discharging the superfluous terms, another glance at the model evaluation is possible, as can be seen in figure 4.15(b). Now model validity is guessed at 0.39, which indicates a valid model.

A more detailed look can be taken at the lack and goodness of fit. The Lack of Fit-Plot is shown in (figure 4.19(a)), indicating that the LoF is larger than the pure error, but not larger than the pure error taking the critical F-value into account.
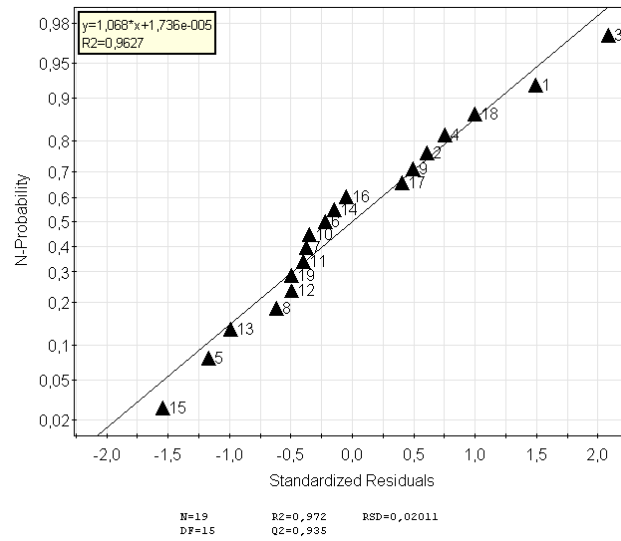
Figure 4.17.: Standardized Residuals against N-probability for Conditioned Bulk Density
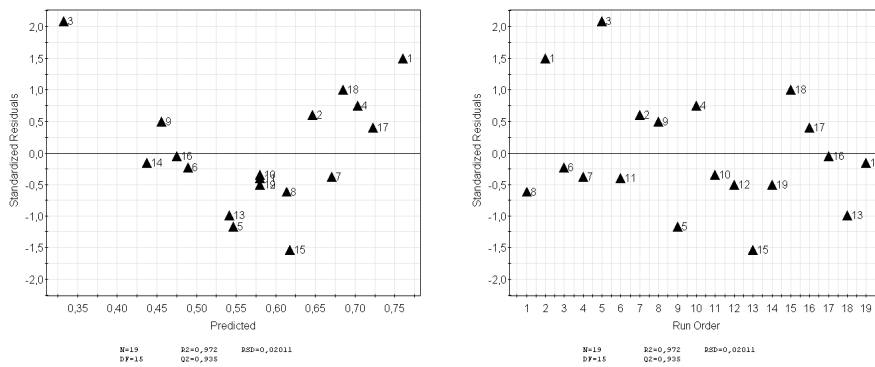
(a) Residuals against predicted values   (b) Residuals against run order

Figure 4.18.: Investigation of residuals of the model for CBD.

The goodness of fit is investigated by ANOVA and more detailed information is gained by the ANOVA plot (figure 4.19(b)). Here the (explained) standard deviation of the regression is much larger than the (unexplained) residual standard deviation (RSD), even multiplied with the critical F-value, therefore indicating a valid model.

(a) Lack of Fit for CBD

(b) ANOVA for CBD
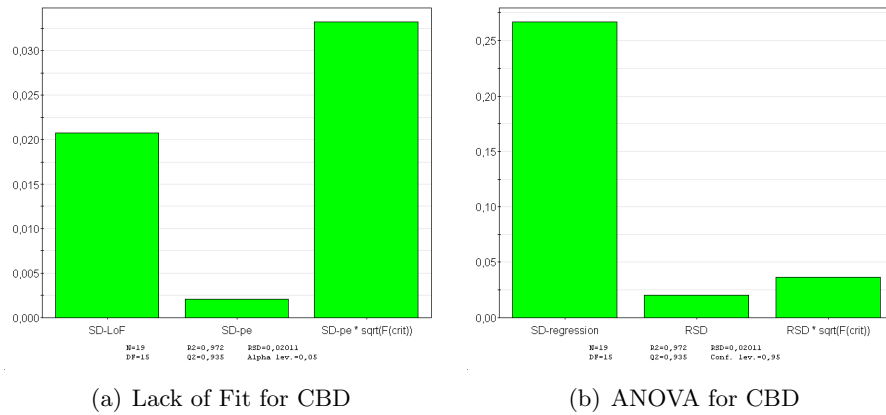
Figure 4.19.: Assessing model quality for CBD
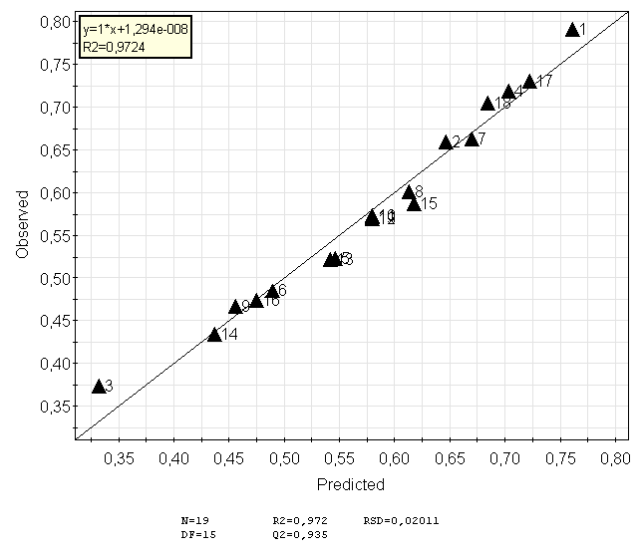
Figure 4.20.: Observed vs. Predicted Plot for Conditioned Bulk Density

Now, that a model is set up, it can be used for predictions. The goodness of the model can be estimated by looking at the observed vs. predicted plot. The values follow the median more or less and no outlier can be identified.

A response surface is created and plotted in figure 4.21, a linear relationship can be

seen. Furthermore lines can be selected from the response surface, where one powder fraction varies from 0 to 1, and the others are held at equal constant fraction, as illustrated in figure 4.22.
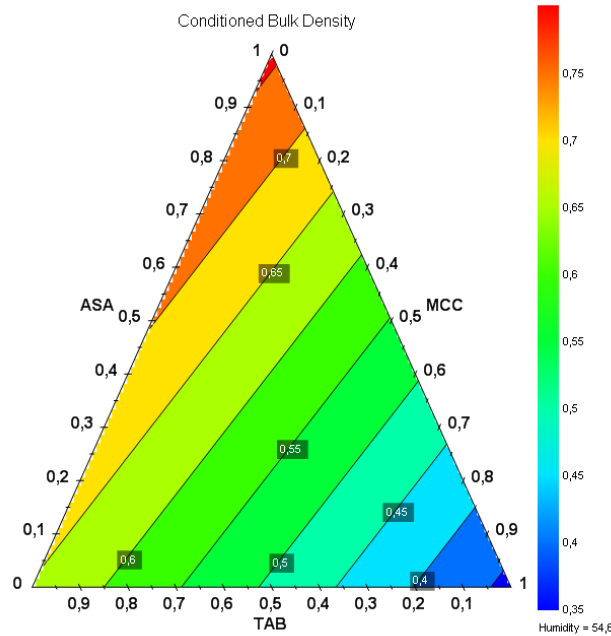
Figure 4.21.: Response Surface for Conditioned Bulk Density

4.3.4. Discussion of parameters and models

The investigated rheological parameters shall now be discussed separately. An overview of the plots and parameters can be found in A.5, also giving exact descriptions on which terms were finally used for the models. An overview of the performance of all models is given in figure 4.23.

If a response for a certain sample is missing, this sample is not included in the MLR. The same is true for PLS, however for PLS, predictions for the missing values of sample can be made [35].

The Conditioned Bulk Density has already been discussed in the previous chapter, and is summarized again in figure 4.24.

4.3.5. Dynamic tests

Basic Flow Energy

The quality of the model, as summarized in figure 4.25, is sufficient, but a large number of terms (including cubic terms) are needed.
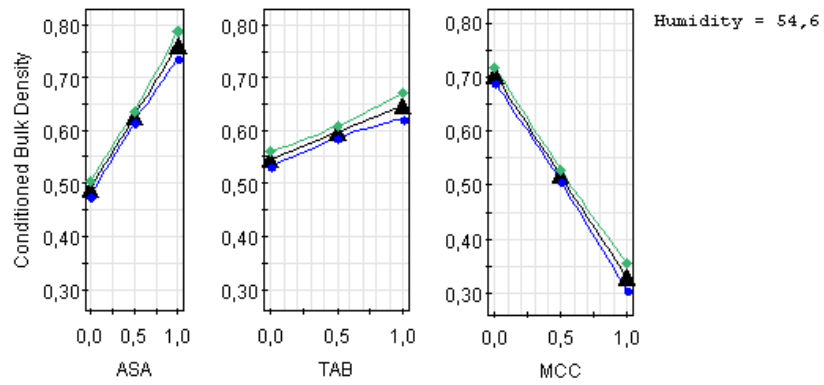
Figure 4.22.: Estimations for the Conditioned Bulk Density for varying mixture fractions. The limits represent a 95% confidence interval.
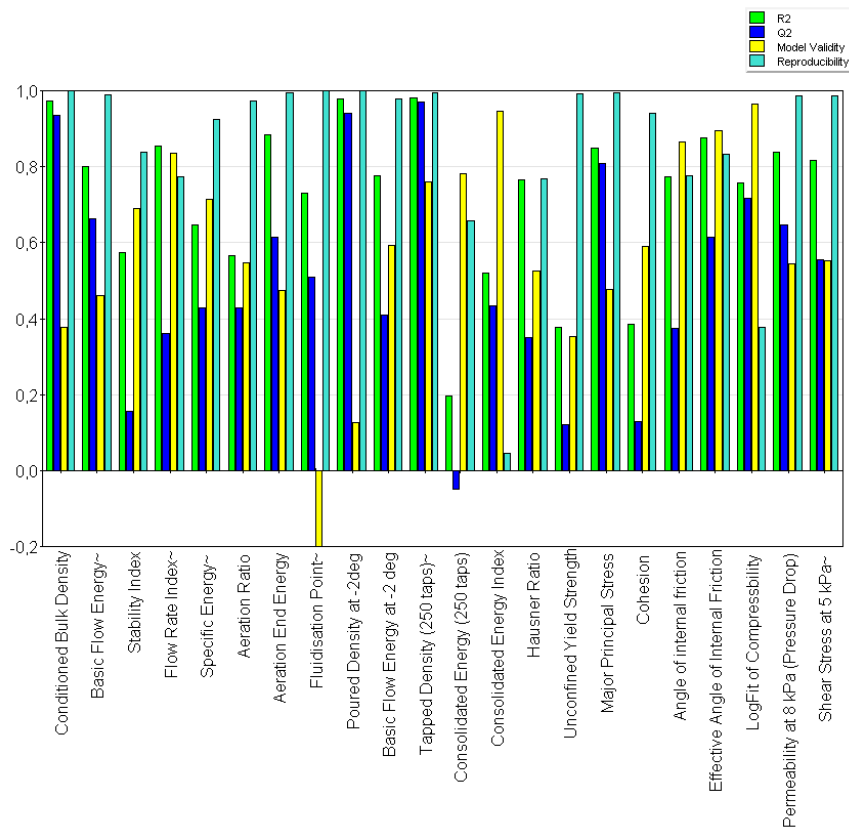
Figure 4.23.: Summary of the model performance for all FT4 parameters

R2:	0.972
Q2:	0.935
Validity:	0.376
Reproducibility:	1.000
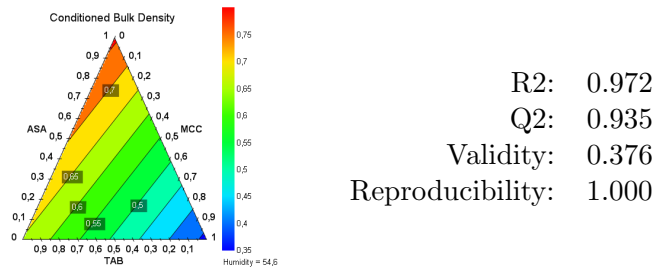
Figure 4.24.: Response Surface and model evaluation parameters for Conditioned Bulk Density

R2:	0.801
Q2:	0.663
Validity:	0.460
Reproducibility:	0.990
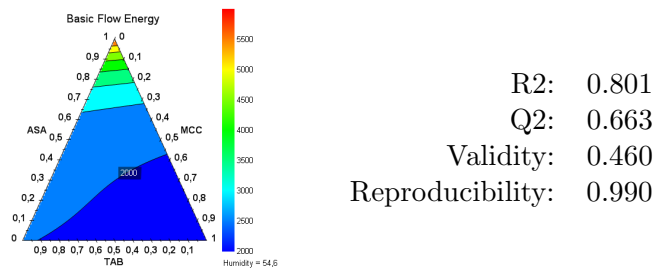
Figure 4.25.: Response Surface and model evaluation parameters for Basic Flow Energy

Here an example is given for the change of the normal probability plot with the model terms. In figure 4.26(a), no quadratic terms were modelled, and clearly a curvature is seen, whereas this curvature is reduced, when quadratic terms are included, as shown in figure 4.26(b). Experiment No. 5 differs from the rest and might indicate an outlier. However, looking at the raw data, it is ensured that it was not.

Stability Index

As shown in figure 4.27, the predictive power for the stability index is rather low. However SI is not a real parameter of powder flow, but just an indicator for changes in the powder bed during testing, insofar it does not directly depend on mixture fractions. The largest deviation from 1, indicating segregation, is given for mixtures of MCC and a decent amount of ASA, which seems reasonable for their largely different particle sizes.

Flow Rate Index

The model for the flow rate index is appropriate, as shown in figure 4.28. However the FRI is dominated by the decreasing FRI with increasing amount of ASA, which is opposed to the rising FRIs of TAB and MCC.

(a) without squared terms

(b) with squared terms
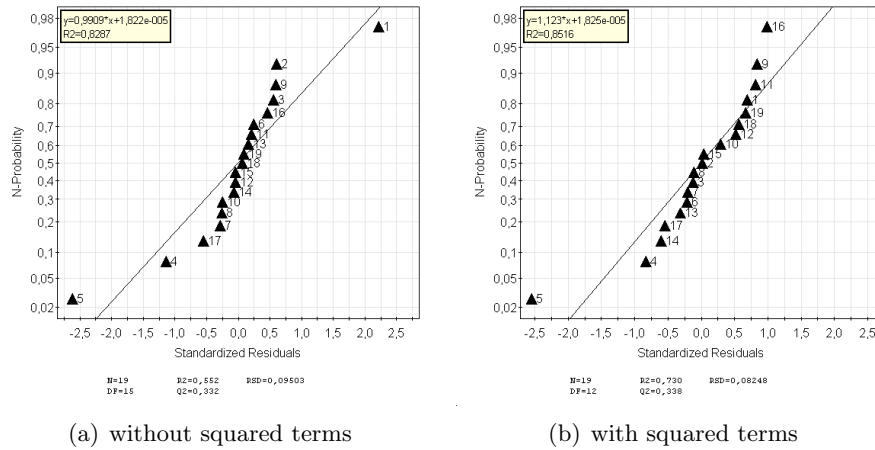
Figure 4.26.: Normal Probability Plot for BFE with different model terms

R2:	0.573
Q2:	0.156
Validity:	0.690
Reproducibility:	0.839
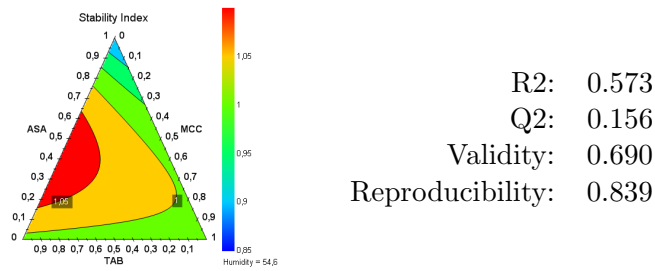
Figure 4.27.: Response Surface and model evaluation parameters for Stability Index

R2:	0.855
Q2:	0.362
Validity:	0.836
Reproducibility:	0.772
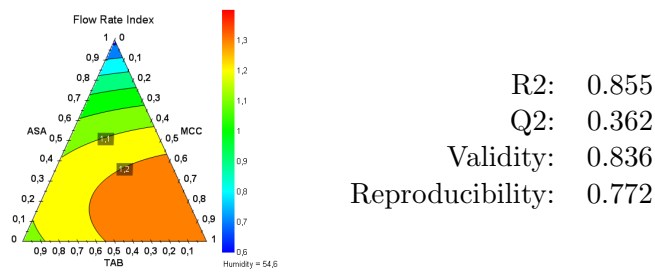
Figure 4.28.: Response Surface and model evaluation parameters for Flow Rate Index

Specific Energy
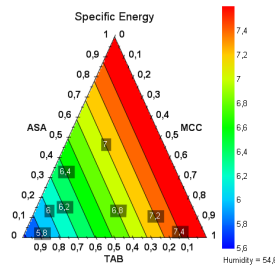
R2:	0.646
Q2:	0.429
Validity:	0.714
Reproducibility:	0.926

Figure 4.29.: Response Surface and model evaluation parameters for Specific Energy

The SE model, summarized in figure 4.29 is rather good and predictive, and only linear terms are needed. The model indicates, that the highest SE appears for MCC. This seems reasonable, as MCC exhibits highest cohesiveness of all three investigated powders.

Aeration Ratio
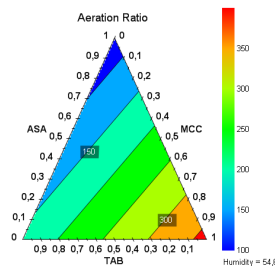
R2:	0.565
Q2:	0.428
Validity:	0.548
Reproducibility:	0.972

Figure 4.30.: Response Surface and model evaluation parameters for Aeration Ratio

The model for aeration ratio, summarized in figure 4.30, is good. As the fluidisation point was not reached for a fraction of 100 % ASA, this AR, AEE and Flu values could not be included in the model. Nonetheless, this values can be now predicted, however as these values are not contained in the measured simplex, those are not validated and should not be relied on. The estimated values by the model are given in table 4.4 and seem to be reasonable. However, due to uncertainties in the measurement, a very large confidence interval is given, relativizing the usefulness of this model.

For the Aeration Ratio linear terms are sufficient, but humidity cannot be neglected.

	Expectation	Lower Limit	Upper Limit
AR	38.4	-16.4	93.2
AEE	74.3	52.6	96.0
Flu	49.3	40.1	60.5

Table 4.4.: Estimated values for the properties in the aeration test of $100\,\%$ ASA, which could not be measured.
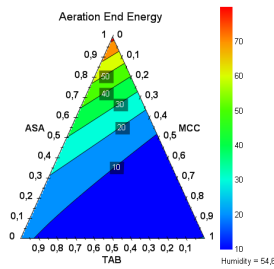
R2: 0.885
Q2: 0.615
Validity: 0.475
Reproducibility: 0.996

Figure 4.31.: Response Surface and model evaluation parameters for Aeration End Energy

Aeration End Energy

The model for the aeration end energy is appropriately good, as shown in figure 4.31. Linear, quadratic and interaction terms are all needed to describe the response. This indicates the complex behaviour of the response, superimposed by the error of the measurements.

Fluidisation Point
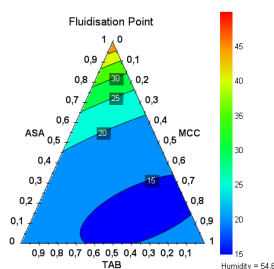
R2: 0.730
Q2: 0.510
Validity: -0.200
Reproducibility: 1.000

Figure 4.32.: Response Surface and model evaluation parameters for Fluidisation Point

The fluidisation point of a powder is reached, when the flow energy is not decreasing further with increasing air flow. However, at such low flow energy values, said energy fluctuates due the powder movement. Hence, to determine the Fluidisation Point, the following criteria was used: The air speed assigned to the fluidisatioin point is reached, when a normalized aeration sensitivity of NAS = 0.005 is under-run. The normalized aeration sensitivity is calculated by the difference of two normalized energy values, divided by the change in air velocity [6].

The model for the fluidisaton point is summarized in figure 4.32. It allows to explain the data and predict it rather well. However the model validity is not given. This might result from the fact, that the fluidisation point is always a distinct point, whose resolution is given by the number of air speed steps in the test program. As these points are set rather sparse, the model describing the fluidisation point has rather large differences between predicted and measured points, as can be seen in figure 4.33.
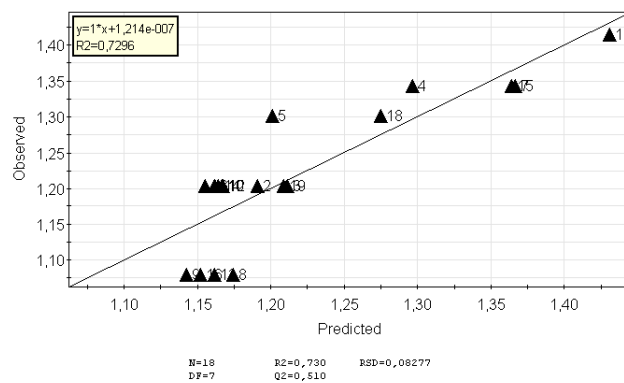
Figure 4.33.: Observed vs. Predicted for the Fluidisation Point

Poured Density at -2 deg

The following parameters carry the assignment -2 deg, because the helix angle of the stirrer path was changed from the standard -5°, to shallower -2°. To have comparable energy values between consolidated and poured powders, both were measured with the shallower angle. This was necessary, as for the consolidated powder the dissipated energy during the stirring process would have been too large to be measured accurately.

As this response is exactly the same as *CBD*, just measured at a different time, it is not surprising, that it does give the same results. The model is summarized in figure 4.34.
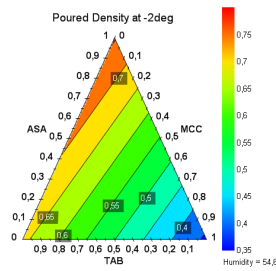
Figure 4.34.: Response Surface and model evaluation parameters for Poured Density at -2deg
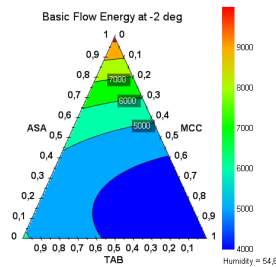
Basic Flow Energy at -2 deg

Figure 4.35.: Response Surface and model evaluation parameters for Basic Flow Energy at -2 deg

BFE2 differs from *BFE* by the angle of the helix the blade follows when measuring the energy. This model does not achieve the same quality, as shown in figure 4.35, as that for *BFE*, otherwise all statements are equally true.

Tapped Density (250 taps)

The model works surprisingly well, as indicated in figure 4.36, and is similar to the model for *CBD*. Nonetheless the powders have been tapped by hand, introducing a large insecurity factor, which might be a result for the mediocre quality of the following models.

Consolidated Energy (250 taps)

The Consolidated Energy is measured with a helix angle of -2 deg, because a larger angle, as used for the standard measurements often led to torque or force overflow, as tapping increases the firmness of powders largely. It turned out, that the model for
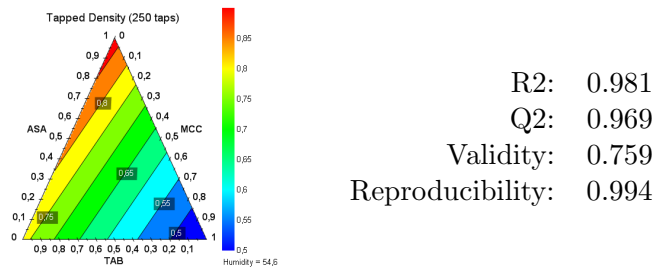
Figure 4.36.: Response Surface and model evaluation parameters for Tapped Density (250 taps)
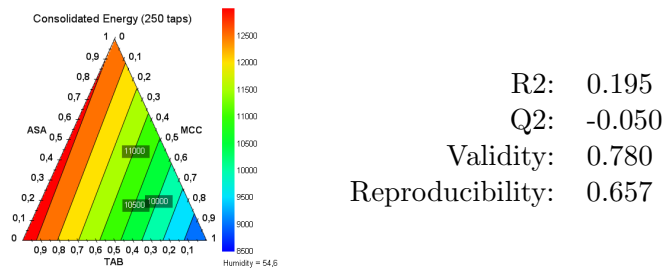
Figure 4.37.: Response Surface and model evaluation parameters for Consolidated Energy (250 taps)

CE, summarized in figure 4.37, is not able to explain the data. This might be a result of the very large deviations introduced by manual tapping.

Consolidated Energy Index

As conditioned and consolidated Basic Flow Energy have been measured, the ConsolidatedEnergy Index can be calculated. Astonishingly this model works better, than predicting the pure consolidated energy. It seems that introducing the information of the *BFE* does improve the model. However, the very low assigned repeatability clearly shows the weakness of this model. The model is summarized in figure 4.38.

Hausner Ratio

Both density measurements, poured and tapped density, allow the development of rather good models, nonetheless, the ratio between those two gives just a mediocre model, as indicated in figure 4.39. This is reflected in the large number of terms, which are taken into account. The model cannot distinguish between significant and insignificant terms. Therefore all terms were included, giving a good fit of the measurements. However predictions are unreliable.
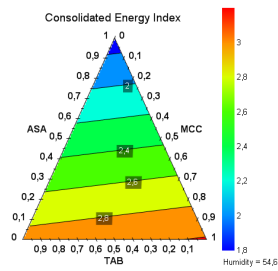
R2:	0.519
Q2:	0.434
Validity:	0.946
Reproducibility:	0.046

Figure 4.38.: Response Surface and model evaluation parameters for Consolidated Energy Index
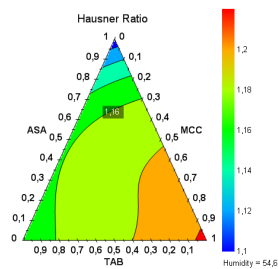
R2:	0.765
Q2:	0.349
Validity:	0.526
Reproducibility:	0.767

Figure 4.39.: Response Surface and model evaluation parameters for Hausner Ratio

4.3.6. Shear Cell tests

Unconfined Yield Strength
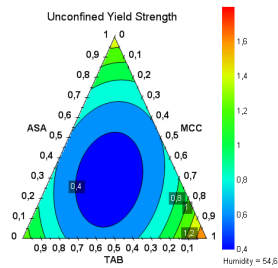
R2:	0.377
Q2:	0.121
Validity:	0.354
Reproducibility:	0.991

Figure 4.40.: Response Surface and model evaluation parameters for Unconfined Yield Strength

The following parameters stem from shear cell tests, which have been performed with a consolidation stress of 9 kPa.

Very ofthen the measured cohesion gave a negative value, resulting in an undefined

unconfined yield strength. Therefore it was set to zero, as this is its physical value. However the assumption of a linear yield locus is not true, especially for very low cohesion and UYS values. The model, summarized in figure 4.40, is therefore not suited for predicting these values.

Major Principle Stress

R2:	0.848
Q2:	0.808
Validity:	0.476
Reproducibility:	0.995
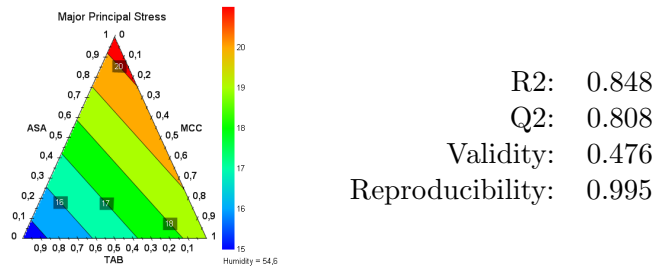
Figure 4.41.: Response Surface and model evaluation parameters for Major Principal Stress

The MPS is a result of the Mohr-plot analysis too, but more a property of compression and powder attributes and offers therefore a better suited model. The model properties are summarized in figure 4.41. For explaining MPS just linear terms were used. However, as shown by the high regression coefficient, humidity seems to have a significant influence.

Cohesion

R2:	0.386
Q2:	0.129
Validity:	0.591
Reproducibility:	0.941
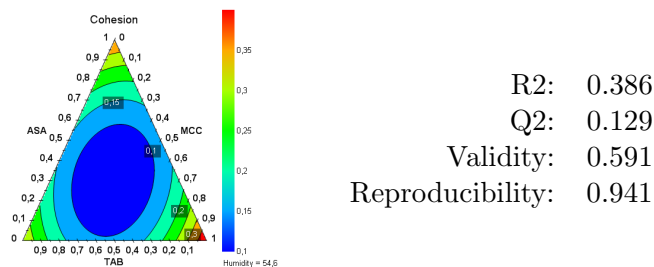
Figure 4.42.: Response Surface and model evaluation parameters for Cohesion

Due to assumptions in the Mohr-plot-analysis, sometimes negative cohesion was achieved. Although this does not make sense in a physical interpretation, those values were accepted, because they reflect nonetheless the measured properties.

Interesting is the indication of a region of blends very good flowing, as indicated in the centre of the response surface infigure 4.42, which accords to the handling experience.

Angle of Internal Friction and Effective Angle of Internal Friction
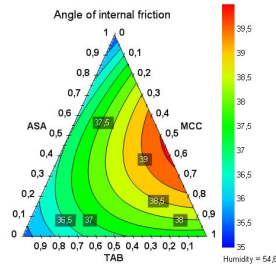
R2:	0.774
Q2:	0.374
Validity:	0.864
Reproducibility:	0.776

Figure 4.43.: Response Surface and model evaluation parameters for Angle of internal friction
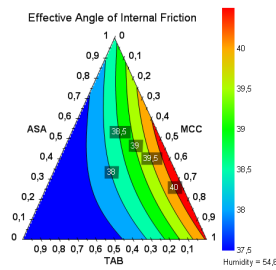
R2:	0.875
Q2:	0.615
Validity:	0.894
Reproducibility:	0.832

Figure 4.44.: Response Surface and model evaluation parameters for Effective Angle of Internal Friction

Both angles are very similar to each other, and based on the same terms for description. Their models are summarized in figure 4.43 and figure 4.44. However, not all of the used terms are significant, but give a sound and quantitative acceptable model.

Shear stress at 5 kPa

As derived parameters of the Mohr-analysis share a certain uncertainty due to the fact, that assumptions and approximations are used, the pure shear stress values were investigated. More exactly the shear stress value at a normal stress of 5 kPa was taken and modelled, shown in figure 4.45. The results show, that this directly measured value gives a better model, than the analytically determined ones.

70

R2:	0.817
Q2:	0.554
Validity:	0.553
Reproducibility:	0.987
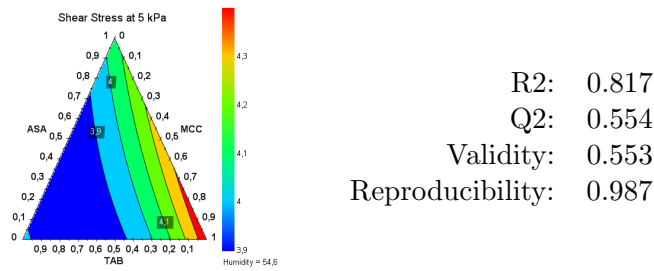
Figure 4.45.: Response Surface and model evaluation parameters for Shear Stress at 5 kPa

4.3.7. Static tests

LogFit of Compressibility

R2:	0.758
Q2:	0.716
Validity:	0.964
Reproducibility:	0.377
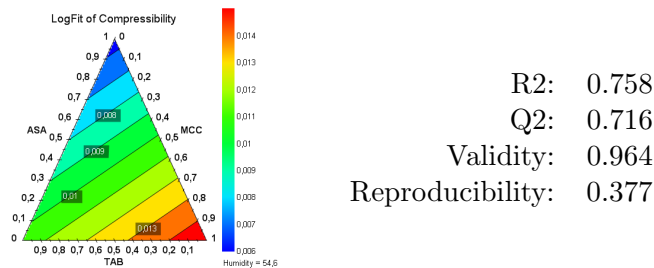
Figure 4.46.: Response Surface and model evaluation parameters for LogFit of Compressbility

LogC is again an analytical parameter, here gained by a compression test. The emerging model is acceptable, as shown in figure 4.46, however a lack of reproducibility is stating a problem in this case.

Pressure Drop at 8 kPa

Pressure drop across the powder bed was measured for various normal stresses, as can be seen in figure 4.48, but just one experimental value was investigated exemplary. The model for the pressure drop works well, as shown in figure 4.47. For pure powders, permeability reflects the particle size well.

Nonetheless, the pressure drop values are very low and might not provide the needed sensitivity, it is therefore recommended to build up a model on permeability with measurements with more air quantum passing the powder bed [44].
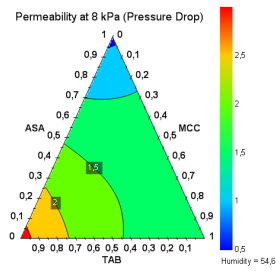
R2:	0.837
Q2:	0.646
Validity:	0.544
Reproducibility:	0.987

Figure 4.47.: Response Surface and model evaluation parameters for Pressure Drop at 8 kPa
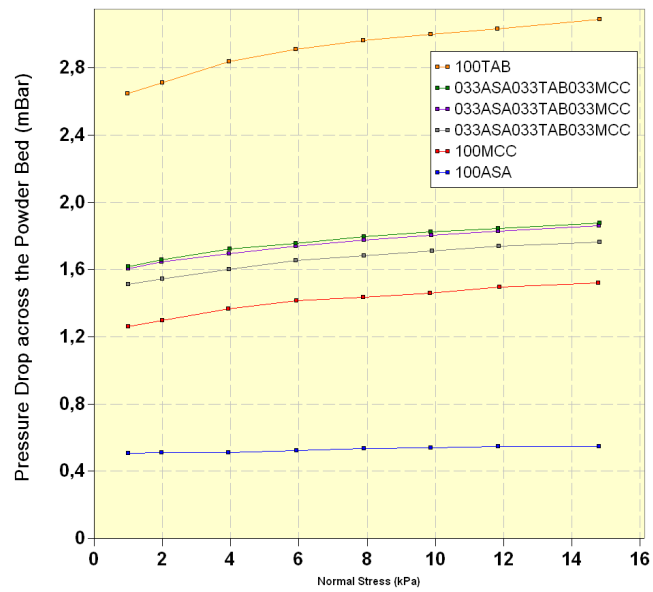
Figure 4.48.: Pressure drop across the powder bed for pure powders and blends.

5. Connecting rheological and blending attributes

5.1. Blending processes investigated by NIR-Spectroscopy

5.1.1. Principle of blending investigations

A blending reactor and a four blade impeller is used for blending the powders. Six optical fibres are connected to the tank, as depicted in in figure 5.1. Fibre 1 is near the centre of the bottom plate, fibre two at half the radius and fibre 3 at the bottom, at the edge of the vessel, three fibres (4, 5 and 6) are attached to the wall at different heights. The fibres are connected to a fibre switch and finally to an NIR-Spectrometer (Perkin Elmer). The collection of a spectrum usually takes $0.3\,\mathrm{s}$, and n spectra are accumulated to increase signal-to-noise ratio. The fibres are subsequently switched onto the NIR spectrometer.

Figure 5.1.: NIR-vessel with optical fibres attached.

As the spectra change with the fractions of powder inside the tank, as exemplary shown in figure 5.2, those can be used for supervising the mixture over time. This is done as follows:
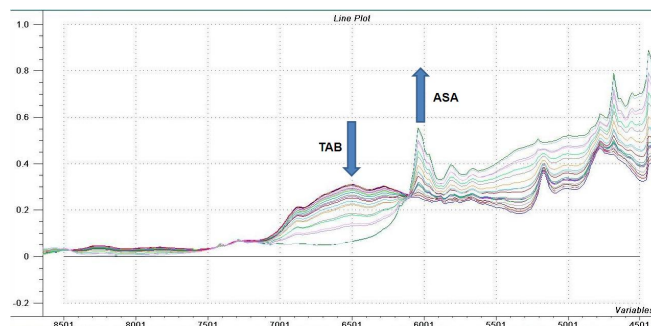
Figure 5.2.: Evolution of the spectra with increase of the fraction of ASA and decrease of the TAB fraction.

1. For calibration, spectra of homogeneous mixtures (prepared with a turbula mixer) are recorded. To address powder subsampling issues, the samples were placed on a rotating disk, while spectra were recorded.

2. Spectra were pretreated: Integrated over time, wavelengths reduced and selected, SNV performed.

3. Using PLS, a calibration model was built out of these spectra.

4. Spectra recorded in the blending reactor are subject to the same treatment than the model spectra.

5. The model is used to predict the concentration out of spectra in the blending reactor.

Exemplary, the model building for channel 4 is shown in figure 5.3. The scores in the upper left show, that the measurements can be distinguished due to their spectral variations, and that the amount of TAB is rising roughly along the first partial least squares component. On the right hand side, the regression coefficients for the first principal component for every wavenumber are plotted. The spectral parts carrying information are weighted stronger than the others. The plot of the unexplained (residual) Y-variance in the lower left corner shows, that with three components, nearly all of the information is explained, and further components do not improve the model. Finally observed and predicted values are in the lower right box, together with the statistics for calibration (top line) and cross validation (lower line). This results in an error level for every channel.

5.1.2. Analysis of the blending experiments.

The blending experiments are evaluated as discussed in section 2.2.4. Focus is put on the experiment where 112 g TAB have been inserted on top of 28 g ASA in the blender.

74

Figure 5.3.: Building of a PLS Model on NIR spectra. Every performed (calibration) experiment is represented by a point and it's amount of TAB. In the upper left window, the scores of the experiments on the first and second partial least squares component are plotted. On the upper right hand side, the regression coefficients for the first component for every wavenumber are plotted. In the lower left section, the unexplained variance for increasing number of components is indicated, and on the lower right, the measured and the predicted values for every experiment are plotted.

The spectra for the different channels are recorded consecutively, and the starting time for each channel has therefore to be corrected. The predictions for the different channels of this experiment are shown in figure 5.4. For each channel a (different) model had to be developed. The error bars indicate the prediction insecurity of these models.
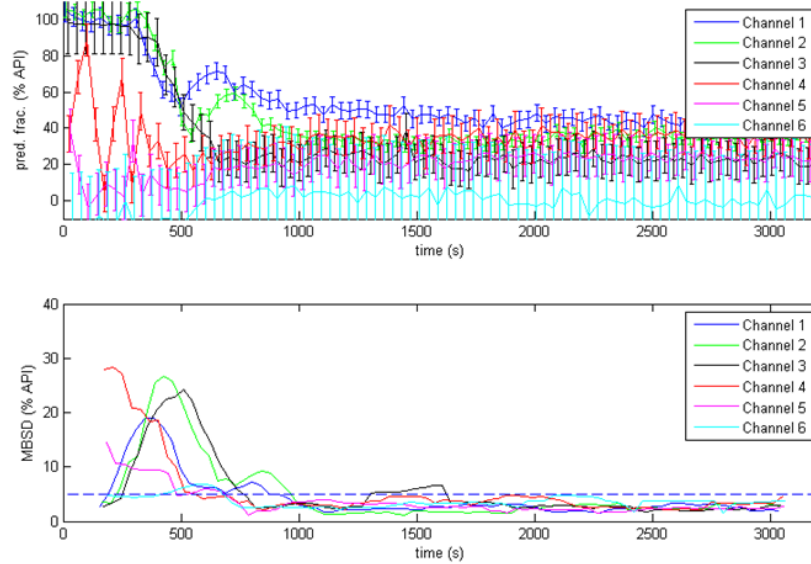
Figure 5.4.: At the top, the predicted values for all six channels for 112 g TAB on top of 28 g ASA, below the MBSD over 9 spectra are shown. A level of 5 % is indicated with a dashed line.

To determine the achieving of a steady state in the blending vessel, when further blending does not change the fraction distribution any more, a moving block standard deviation (MBSD) has been performed. As the PLS is used for already pretreated and filtered spectra, and additionally introduces weights for every wavenumber, the MBSD has not been performed on the raw spectra, but directly on the predictions.

To determine the number of spectra, which defines the block size for the MBSD, an estimation of the sample volume has been performed. The diameter of the scanned area with a fibre is $d_f = 600\,\mu$m. A number of $n = 20$ spectra was accumulated, with an duration of one spectra of $t = 0.3$ s. The diameter of the blending vessel is $d = 0.1$ m, and the impeller rotates with $f = 4.0$ rpm. The estimated sample volume is therefore

$$V_{\text{sample}} = \frac{1}{4}d_f^2\pi \cdot n \cdot t \cdot f \approx 1.13 \cdot 10^{-8}\text{m}^3, \tag{5.1}$$

under the assumption, that the powder is moving as fast as the impeller blades. A tablet with a diameter of 8 mm and a height of 4 mm would result in a tablet volume of $V_{\text{tablet}} \approx 2.01 \cdot 10^{-8}$ m^3. As for such an investigation a volume between 1-3 unit
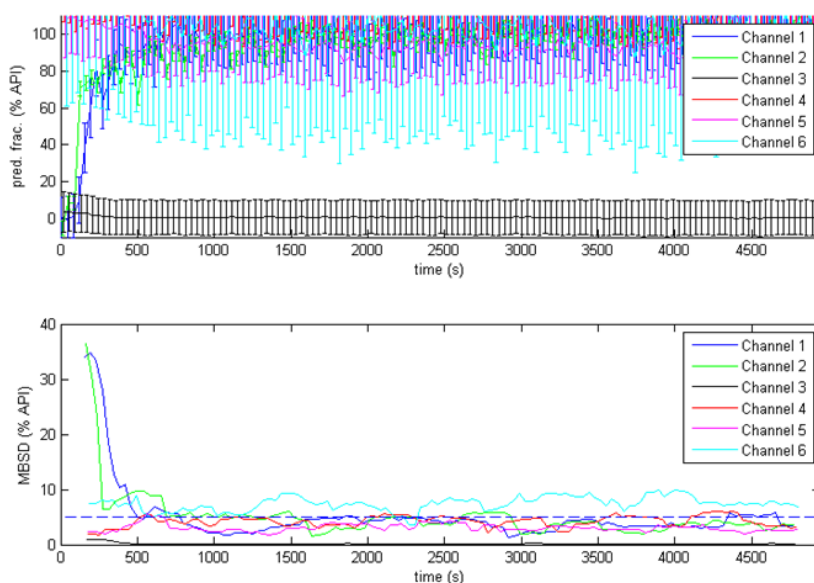
Figure 5.5.: At the top are the predicted values for all six channels for 112 g ASA on top of 28 g TAB, below are the MBSD over 9 spectra. A level of 5 % is indicated with a dashed line.

dosage forms should be monitored [4], the number of spectra used for MBSD was set accordingly.

The results of such an MBSD is shown in the lower parts of figure 5.4 and figure 5.5. When the MBSD value under-runs for five consecutive time steps, a level of 5 %, a channel is considered stationary. Different times until steady state was reached were identified this way, for the different channels and different mixing experiments, with varying amount and composition of powders, as well as filling order.

Some channels appeared to be critical. More precisely, channel 3, located at a position in the corner of the mixing vessel, indicates segregation or powder deposition. Also channel 6 showed deviations, indicated by the large error bars, which are due to a partly covered fibre window at the turnover of powder and air.

5.2. Connecting rheological and blending parameters

The resulting blending times, as discussed in the previous chapter, were then connected to the previously measured rheological parameters. For this purpose, certain rheological parameters of the finished blends, as well as process parameters, like fill order and fill level where considered as factors and time until the steady state was reached as responses. The factors and responses are listed in figure 5.6. Fur further analysis, it always has to be considered, that the limits of the measured blends, also form the

limits of the valid analysis.

Exp No	Exp Name	Run Order	Incl/Excl	Fill Order	Fill Amount	Fraction ASA	Bulk Density	Basic Flow Energy	Flow Rate Index	Specific Energy	Cohesion
1 N1		1 Incl		ASA on TAB	140	0.8	0.738	3270	0.819	7.24	0.232
2 N2		2 Incl		TAB on ASA	140	0.2	0.669	2085	1.12	5.96	0.199
3 N3		3 Incl		ASA on TAB	200	0.5	0.704	2237	1.06	6.61	0.148
4 N4		4 Incl		TAB on ASA	200	0.5	0.704	2237	1.06	6.61	0.148
5 N5		5 Incl		ASA on TAB	400	0.5	0.704	2237	1.06	6.61	0.148

Exp No	Exp Name	Run Order	Incl/Excl		Time Channel 1	Time Channel 2	Time Channel 3	Time Channel 4	Time Channel 5	Time Channel 6	Mean Time
1 N1		1 Incl			1064	1146	926	743	863	340	847
2 N2		2 Incl			951	1676	321	327	334		722
3 N3		3 Incl			604	614	505	574	524	594	569
4 N4		4 Incl				673	683	693	703	653	681
5 N5		5 Incl			458	495	505	516	525	535	506

Figure 5.6.: Factors and responses for rheology and mixing

Further experiments would be needed to separate general powder properties from the distinct properties of the used powders. Nonetheless a simple analysis can be performed estimating the influence parameters. A PLS-regression was used, to establish a connection, and the resulting regression coefficients are presented in figure 5.7.
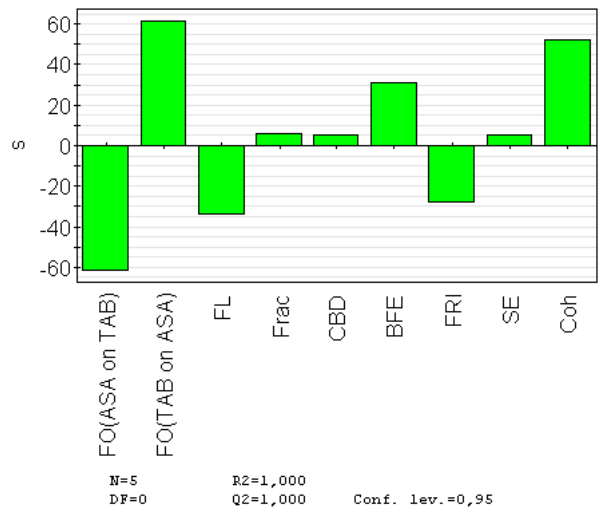
Figure 5.7.: Scaled and Centered Coefficients of Regression for the connection between process and blending parameters for time steady state was reached, averaged over all channels.

It is shown that the fill order has the dominant influence on the time, but that the powder properties cannot be neglected. Unfortunately, the degrees of freedom are too few to allow the estimation of uncertainties.

It is interesting to see, how the importance of factors changes with each channel, as can be seen in figure 5.8. While for the channels at the bottom, cohesion extends the

blending time, it decreases for the channels at the side wall. The fill order dominates all channels, except the second, located in the outer region of the bottom plate, where the cyclic flow around the moving blades may reach its maximum.
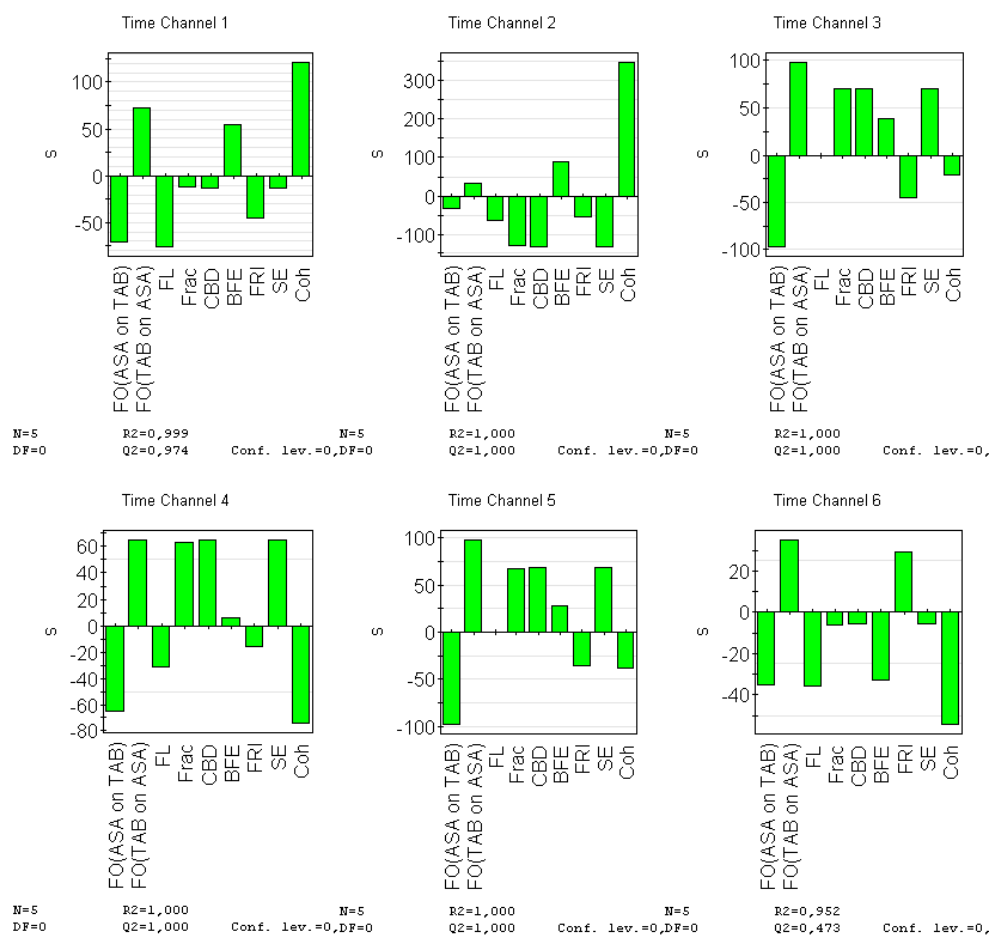
Figure 5.8.: Scaled and Centered Coefficients of Regression for all six different channels

6. Results and discussion

6.1. Rheological models

Models have been built for 22 rheological parameters. A collection of all response surfaces can be found in figure 6.1. Although these models differ widely in quality. Furthermore, three test points were chosen randomly to assess the model predictions. A list of the limits, predicted by the models, can be seen in table 6.1, together with measured properties. To get those measured properties, three tests were taken at every point and the mean value was calculated.

Models for bulk density work best of all. Except the Stability Index, which is not a real powder parameter, the models for the dynamic testing show good quality. More problematic is the Aeration test, where tests underlie from a large uncertainty, as aerated powders are very sensitive to disturbances. A special case is the fluidisation point, which is affected by the sparse discrete measured steps.

Although density of the tapping test is quite predictable, the consumed energy after tapping is not. As the powders were not tapped until a steady state was reached, but just a certain number of times, they might have been put in a not well-defined state of partial-particle rearrangement, causing the energy values to be very variable.

Results from the shear cell test can be put into two groups. Those which are a result of extrapolation, like UYS and Coh, are not useful for appropriate models. On the other hand, the angles of internal friction and the principal stress, as well as the direct shear value, represent decent models. This reflects that the extrapolated values have a much larger deviation range and sensitivity, than the directly measured, respectively interpolated values. This is also the reason, why ffc has not been used to build up a model, as small changes of the cohesion lead to disproportional changes in ffc. Another reason is, that for negative cohesion values, no ffc can be calculated.

Finally there are the models for Compressibility and Permeability. Both give a model of the same quality, although the compressibility model has been developed for a fitted parameter, and the permeability model for a directly measured value. It is necessary to mention, that one of the motivations for introducing the fit-model for Compressibility was, to erase some offset deviations in the original data.

Responses, which show a significant dependence on humidity, can be investigated on its influence. An example is the Major Principle Stress, as seen in figure 6.2, which decreases with increasing humidity. However, as the measurements have been performed in a very limited range of humidity, (53 % rH to 61 % rH), predictions for widespread humidity values are not reliable.

External influences were tried to be eliminated, which might have not happened successfully for all possible disturbances. It is therefore desired to carry out such
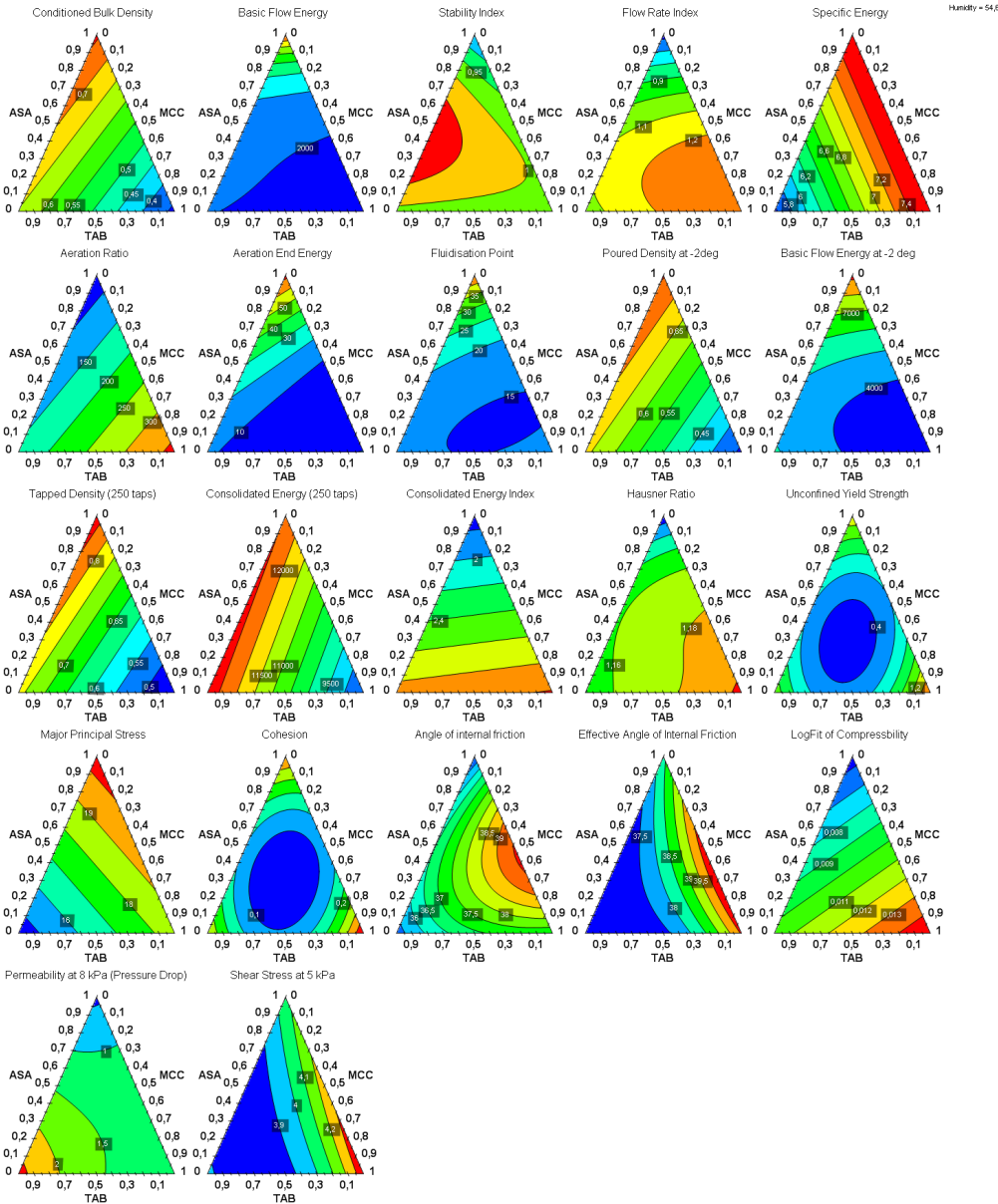
Figure 6.1.: Summary of all response surfaces of the FT4 parameters, for a humidity of 54,6 % rH.

		Conditioned Bulk Density	Basic Flow Energy	Stability Index	Flow Rate Index	Specific Energy	Aeration Ratio	Aeration End Energy	Fluidisation Point	Poured Density at -2deg	Basic Flow Energy at -2 deg	Tapped Density (250 taps)	Consolidated Energy (250 taps)	Consolidated Energy Index	Hausner Ratio	Unconfined Yield Strength	Major Principal Stress	Cohesion	Angle of internal friction	Effective Angle of Internal Friction	LogFit of Compressbility	Permeability at 8 kPa (Pressure Drop)	Shear Stress at 5 kPa
0.2 ASA	Lower	0.533	1873	0.99	1.21	6.57	193	1.95	14	0.541	3108	0.626	9771	2.51	1.17	-0.124	17.3	-0.054	37.27	37.46	0.0105	1.37	3.84
0.4 TAB	Expected	0.544	1960	1.01	1.23	6.83	214	5.94	15	0.550	3804	0.635	10769	2.70	1.18	0.309	17.5	0.060	37.91	37.85	0.0113	1.47	3.91
0.4 MCC	Upper	0.554	2051	1.03	1.25	7.09	236	9.93	16	0.560	4500	0.644	11768	2.90	1.18	0.743	17.7	0.175	38.56	38.24	0.0120	1.56	3.98
53 %rH	Measured	0.527	1786	1.02	1.26	6.30	269	11.75	13	0.534	3404	0.621	9437	2.77	1.16	0.373	17.5	0.049	37.73	37.97	0.0110	1.42	3.91
0.2 ASA	Lower	0.608	1915	0.97	1.15	5.93	114	7.24	16	0.619	3620	0.713	9888	2.40	1.16	0.022	16.6	-0.006	36.18	36.80	0.0091	1.56	3.76
0.65 TAB	Expected	0.622	2168	1.02	1.17	6.29	141	11.37	17	0.632	4327	0.727	11438	2.67	1.17	0.463	16.8	0.110	36.84	37.19	0.0102	1.70	3.83
0.15 MCC	Upper	0.637	2038	0.99	1.19	6.64	169	15.50	18	0.645	5035	0.741	12988	2.94	1.17	0.904	17.0	0.227	37.49	37.59	0.0112	1.84	3.91
50 %rH	Measured	0.618	2024	1.09	1.15	6.27	169	8.75	15	0.626	4543	0.626	12203	2.69	1.14	0.370	16.3	0.093	36.76	37.33	0.0107	1.54	3.87
0.44 ASA	Lower	0.540	1952	0.91	1.16	7.16	134	3.90	17	0.542	3431	0.624	8306	2.19	1.17	-0.048	19.4	-0.042	38.41	39.03	0.0095	0.97	4.05
0.1 TAB	Expected	0.552	2038	0.94	1.19	7.47	177	8.31	17	0.553	4250	0.635	9834	2.43	1.18	0.462	19.7	0.093	39.17	39.49	0.0104	1.10	4.14
0.46 MCC	Upper	0.565	2128	0.97	1.21	7.77	219	12.72	18	0.564	5068	0.646	11363	2.66	1.19	0.971	20.0	0.228	39.93	39.95	0.0113	1.23	4.23
49 %rH	Measured	0.533	2243	1.07	1.21	7.45	166	13.74	16	0.537	4877	0.537	12744	2.60	1.18	0.160	19.2	0.030	39.56	39.73	0.0123	1.28	4.20

Table 6.1.: Predicted and measured data for random samples
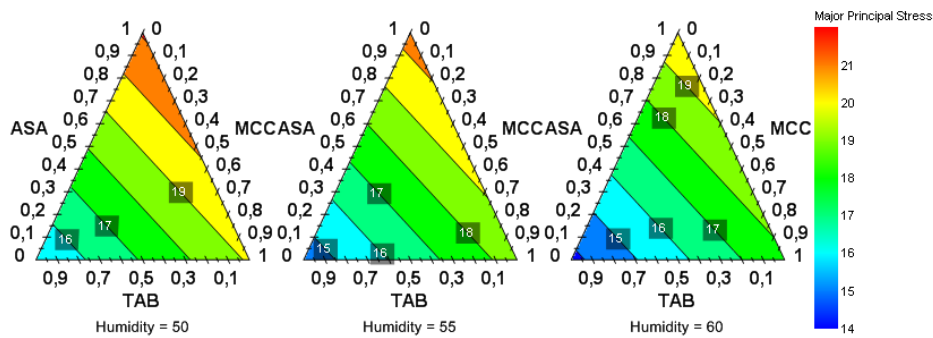
Figure 6.2.: Influence of Humidity on Major Principle Stress

experiments in conditioned environments.

6.2. Crosslinking with mixing

The models used for prediction of the mixture concentrations show a rather large error, up to 10 %. However further improvement increases the model performance, based on additional training samples and more distinguished choice of selected wavenumbers.

The time until a steady state was reached was linked to rheological parameters. This clearly reflects the importance of process parameters, like fill order, for the blending process. Additionally, it can be seen, that segregation cannot be neglected, and that after a certain time, although a stationary state is reached, it does not represent overall blend uniformity. In contrast, areas largely differing from the desired composition exist, although the mixing times become extended.

More experiments are clearly needed to develop robust models for this process, and able clear statements for the complex process of powder mixing.

A grade for the homogeneity of powders can be gained by looking at the standard deviations over all six fibres. For the experiment of 100 g ASA on top of 100 g TAB the empirical variance (over all six fibres) is shown in figure 6.3. Under the same assumption for sample volume as in equation (5.1), and a particle volume of around $1\,mm^3$, the empirical variance can be transformed to the mixture goodness criteria of Ashton and Schmal, as introduced in section 2.2.4. This is shown in figure 6.4.

However, the six positions investigated do not reflect six samples taken randomly (for example with a thief probe), as they give access to the powder composition at the wall and bottom of the vessel, but the dynamics interior are still unknown.
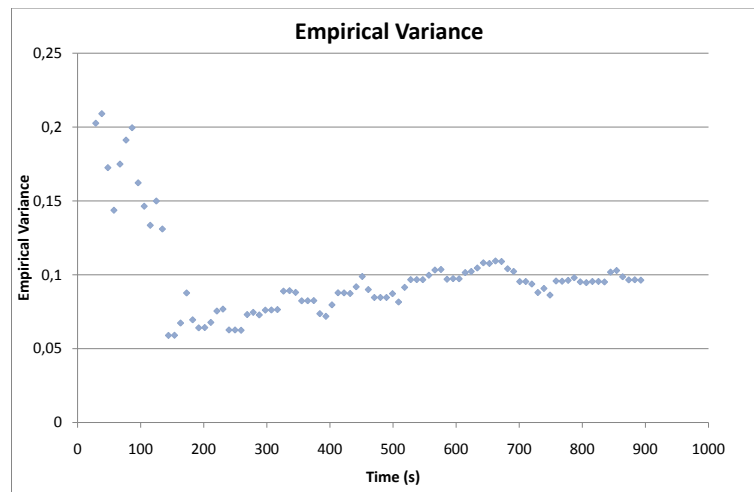
Figure 6.3.: Empirical variance for $100\,\mathrm{g}$ TAB on top of $100\,\mathrm{g}$ ASA
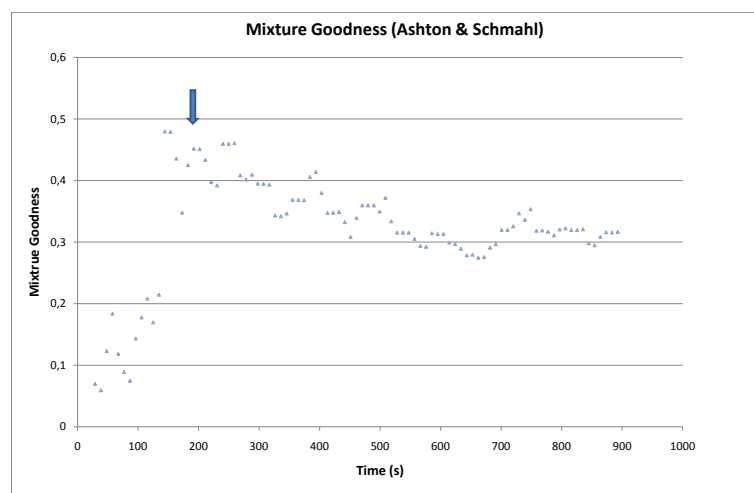
Figure 6.4.: Mixture goodness according to Ashton and Schmal [10] for $100\,\mathrm{g}$ TAB on top of $100\,\mathrm{g}$ ASA, the arrow indicates the best achieved value, for a mean over 9 points.

7. Summary and prospects

- Not only pure powders, but also blends have been investigated to establish predictive models for their attributes. Blend properties determined confidently with the FT4, were modelled using DoE and MVDA.

- It has been shown, that some properties are not convenient for a model, while for others models can be developed allowing predictions for unknown blends.

- Hence, a whole formulation instead of single powders can be characterized and optimized.

- Finally these knowledge can be carried over to mixing experiments for the same blends. An example would be the Basic Flow Energy determined with the FT4, which is an indicator for the energy, which is needed for powder agitation.

- Different mixing properties like powder segregation, mixing time until blend uniformity, etc. can be monitored with Process Analytical Technology (PAT) tools as Near-Infrared Spectroscopy and correlated to the FT4 key parameters.

- It is possible to cross-link rheological and process parameters in a meaningful way. However, further blending experiments need to be performed, to break down the relationship between distinct powders and general powder properties. Thereafter direct dependencies between rheological properties and mixture assessments, as blending time and achieved concentration ratio can be constructed.

List of Figures

List of Tables

References

[1] (Picture: F. Meyer, 13.03.2008). WSL Institute for Snow and Avalanche Research SLF. `http://www.slf.ch/lawineninfo/wochenbericht/2007-08/Jahresbericht/Lawinenaktivitaet/index_DE`, 2008. (accessed on 2010-08-18).

[2] I.C. Sinka, F. Motazedian, A.C.F. Cocks, and K.G. Pitt. The effect of processing parameters on pharmaceutical tablet properties. *Powder Technology*, 189(2):276 – 284, 2009. Special Issue: 3rd International Workshop on Granulation: Granulation across the Length Scales, 3rd International Workshop on Granulation across the Length Scales.

[3] R. W. Kessler, editor. *Prozessanalytik - Strategien und Fallbeispiele aus der industriellen Praxis*. Wiley-VCH, 2006.

[4] U.S. Department of Health and Human Services. Guidance for Industry PAT — A Framework for Innovative Pharmaceutical Development, Manufacturing, and Quality Assurance. 2004.

[5] K. A. Baakev, editor. *Process Analytical Technology - Spectroscopic Tools and Implementation Strategies for the Chemical and Pharmaceutical Industries*. John Wiley & Sons Ltd., 2nd edition, 2010.

[6] Freeman Technology. *FT4 Support Documents*, 2010.

[7] D. E. Pivonka, J. M. Chalmers, and P. R. Griffiths, editors. *Applications of Vibrational Spectroscopy in Pharmaceutical Research and Development*. John Wiley & Sons Ltd., 2007.

[8] R. Clift. Powder technology and particle science. *Powder Technology*, 88:335–339, 1996.

[9] J.K. Prescott and R.A. Barnum. On powder flowability. *Pharmaceutical Technology*, 24(10):60–85, 2000.

[10] M. Stieß. *Mechanische Verfahrenstechnik - Partikeltechnologie 1*. Springer, 3rd edition, 2009.

[11] D. Schulze. *Pulver und Schüttgüter - Fließeigenschaften und Handhabung*. Springer, 2nd edition, 2009.

[12] B. N. J. Persson. Capillary adhesion between elastic solids with randomly rough surfaces. *Journal of Physics: Condensed Matter*, 20(31):315007, 2008.

[13] Sympatec GmbH System-Partikel-Technik. *Windox 5 Help*, 2009.

[14] W. Witt, U. Köhler, and J. List. Die Bildverarbeitung von sehr schnellen Partikeln ermöglicht die Anwendung der leistungsfähigen (Trocken-)Dispergierung für Größen- und Formanalyse. Technical report, Sympatec GmbH, System-Partikel-Technik, 2004.

[15] A. Steland. *Basiswissen Statistik*. Springer, 2010.

[16] D. Schulze. Zur Fließfähigkeit von Schüttgütern - Definition und Meßverfahren. *Chemie Ingenieur Technik*, 67(1):60–68, 1995.

[17] R. E. Smallman and R. J. Bishop. *Modern Physical Metallurgy and Materials Engineering*. Butterworth Heinemann, 6th edition, 1999.

[18] V. Ganesan, K.A. Rosentrater, and K. Muthukumarappan. Flowability and handling characteristics of bulk solids and powders - a review with implications for DDGS. *Biosystems Engineering*, 101(4):425 – 435, 2008.

[19] E. Guerin, P. Tchoreloff, B. Leclerc, D. Tanguy, M. Deleuil, and G. Couarraze. Rheological characterization of pharmaceutical powders using tap testing, shear cell and mercury porosimeter. *International Journal of Pharmaceutics*, 189(1):91 – 103, 1999.

[20] R. Hogg. Mixing and segregation in powder evaluation, mechanisms and processes. *KONA Powder and Particle Journal*, 27:1–15, 2009.

[21] SS Sekulic, HW Ward, DR Brannegan, ED Stanley, CL Evans, ST Sciavolino, PA Hailey, and PK Aldridge. On-line monitoring of powder blend homogeneity by near-infrared spectroscopy. *Analytical Chemistry*, 68(3):509–513, FEB 1 1996.

[22] I. Storme-Paris, I. Clarot, S. Esposito, J. C. Chaumeil, A. Nicolas, F. Brion, A. Rieutord, and P. Chaminade. Near infra-red spectroscopy homogeneity evaluation of complex powder blends in small-scale pharmaceutical preformulation process, a real life application. *European Journal of Pharmaceutics and Biopharmaceutics*, 72:189–198, 2009.

[23] H. W. Siesler, Y. Ozaki, S. Kawata, and H. M. Heise, editors. *Near-Infrared Spectroscopy: Principles, Instruments, Applications*. Wiley-VCH, 3rd edition, 2006.

[24] J. Beyer and K.-J. Steffens. Kalibrationsmodelle zur Bestimmung des Wassergehalts pharmazeutischer Hilfsstoffe mittels Nah-Infrarot-Spektroskopie (NIRS). *Die pharmazeutische Industrie*, 65(2):186–192, 2003.

[25] M. Otsuka. Comparative particle size determination of phenacetin bulk powder by using Kubelka-Munk theory and principal component regression analysis based on near-infrared spectroscopy. *Powder Technology*, 141:244–250, 2004.

[26] C. Benedetti, N. Abatzoglou, J.-S. Simard, L. McDermott, G. Léonard, and L. Cartilier. Cohesive, multicomponent, dense powder with flow characterization by NIR. *International Journal of Pharmaceutics*, 336:292–301, 2007.

[27] A. S. El-Hagrasy, F. D'Amico, and J. K. Drennen. A Process Analytical Technology Approach to Near-Infrared Process Control of Pharmaceutical Powder Blending. Part I: D-Optimal Design for Characterization of Powder Mixing and Preliminary Spectral Data Evaluation. *Journal of Pharmaceutical Sciences*, 95(2):392–406, 2006.

[28] A. S. El-Hagrasy, M. Delgado-Lopez, and J. K. Drennen. A Process Analytical Technology Approach to Near-Infrared Process Control of Pharmaceutical Powder Blending: Part II: Qualitative Near-Infrared Models for Prediction of Blend Homogeneity. *Journal of Pharmaceutical Sciences*, 95(2):407–421, 2006.

[29] A. S. El-Hagrasy and J. K. Drennen. A Process Analytical Technology Approach to Near-Infrared Process Control of Pharmaceutical Powder Blending. Part III: Quantitative Near-Infrared Calibration for Prediction of Blend Homogeneity and Characterization of Powder Mixing Kinetics. *Journal of Pharmaceutical Sciences*, 95(2):422–434, 2006.

[30] M. C. Sarraguça, A. V. Cruz, S. O. Soares, H. R. Amaral, P. C. Costa, and João A. Lopes. Determination of flow properties of pharmaceutical powders by near infrared spectroscopy. *Journal of Pharmaceutical and Biomedical Analysis*, 52(4):484 – 492, 2010.

[31] W. Kessler. *Multivariate Datenanalyse für die Pharma-, Bio- und Prozessanalytik.* Wiley-VCH, 2007.

[32] D. C. Montgomery. *Design and Analysis of Experiments.* Wiley VCH, 1996.

[33] L. Eriksson, E. Johansson, and C. Wikströn. Tutorial: Mixture design - design generation, PLS analysis, and model usage. *Chemometrics and Intelligent Laboratory Systems*, 43:1–24, 1998.

[34] K. Siebertz, D. van Bebber, and T. Hochkirchen. *Statistische Versuchsplanung - Design of Experiments (DoE).* Springer, 2010.

[35] Umetrics AB. *User Guide to MODDE Version 9*, 2009.

[36] P. Geladi and B. R. Kowalski. Partial least-squares regression: A tutorial. *Analytica Chemica Acta*, 185:1–17, 1986.

[37] S. N. Deming and S. L. Morgan. The use of linear models and matrix least squares in clinical chemistriy. *Clinical Chemistry*, 25(6):840–855, 1979.

[38] S. N. Deming. Chemometrics: an Overview. *Clinical Chemistry*, 32/9:1702–1706, 1986.

[39] L. Sachs and J. Hedderich. *Angewandte Statistik*. Springer Verlag, 2006.

[40] S. Wold, M. Sjöström, and L. Eriksson. PLS-regression: a basic tool of chemometrics. *Chemometrics and Intelligent Laboratory Systems*, 58:109–130, 2001.

[41] German Social Accident Insurance. Gestis-database on hazardous substances. `www.dguv.de/ifa/gestis-database`, accessed on: 29 July 2010.

[42] T. Friedl. Lactosen - Anwendungsbreite und physiologische Verträglichkeit. *Meggle Articles Database, Meggle GmbH*, 1990. `www.meggle-pharma.de/de/literature/articles/370/370.pdf`.

[43] A. Levy and H. Kalman, editors. *Handbook of Powder Technology*, volume 10: Handbook of conveying and handling of particulate solids. Elsevier Science B.V., 2001.

[44] J. Clayton, Freeman Technology. Personal correspondance, 2010.

[45] V. Ganesan, K. Muthukumarappan, and K.A. Rosentrater. Flow properties of DDGS with varying soluble and moisture contents using jenike shear testing. *Powder Technology*, 187(2):130 – 137, 2008.

A. Appendix

A.1. Used devices and programs

FT4 Powder Rheometer: Freeman Technology; Boulters Farm Centre; Castlemorton Common; Welland, Malvern; Worcestershire; WR13 6LE, UK

QicPic: Sympatec GmbH, System-Partikel-Technik; Am Pulverhaus 1; D-38678 Clausthal-Zellerfeld; Germany

Spectrum 400 FT-IR/FT-NIR Spectrometer: Perkin Elmer; 940 Winter Street; Walthm; Massachusetts 02451; USA

Scherzelle RO-200: IPT

Controlled Impeller: Heidolph RZR 2102 Control

Turbula System Schatz: Willy A. Bachofen AG, Maschinenfabrik, Switzerland

MODDE 9.0.0.0: Umetrics AB; Box 7960; SE-907 19 Umeå; Sweden

The Unscrambler v9.8: CAMO Software AS, Nedre Vollgate 8, N-0158 Oslo, Norway

Microsoft Office Excel 2007: Microsoft

MATLAB R2009b: Version 7.9.0.529; MathWorks, Inc.

A.2. General properties of the investigated powders

The general properties of the used pharmaceutical powders are listed here, for ASA in table A.1, for TAB in table A.2 and for MCC in table A.3. Microscope images taken from the powders are shown in figure A.1.

A.3. QicPic-Measurements

Exemplary QicPic-Measurements can be found in figure A.2, figure A.3 and figure A.4.

A.4. Flow Function Classification

The flow function constant can be classified as listed in table A.4.

Name	Acetylsalecylic acid
Form	needles
Colour	white
Odour	weak acidic
Characterisation:	Combustible solid Slightly soluble in water Not volantile
Formula:	C9-H8-O4
Melting Point	136 °C
Density	1.35 g/ml
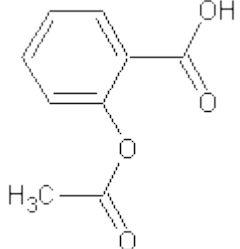
Table A.1.: Properties of ASA by [41]
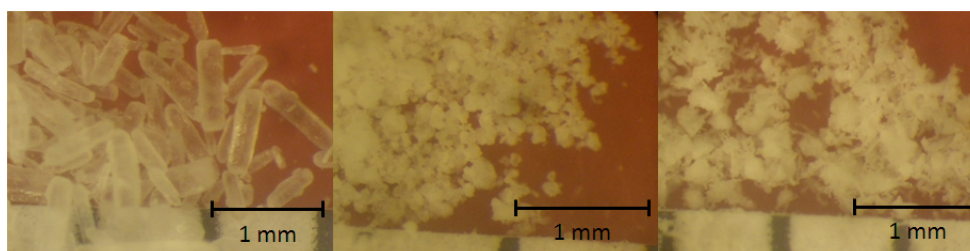
Figure A.1.: Pictures taken in a reflected-light microscope. ASA (left), TAB (center), MCC (right);

Name	Lactose
Form	crystals
Colour	colourless
Odour	odourless
Characterisation:	Combustible solid
	Very soluble in water
	Below 93.5 °, lactose is present as alpha lactose monohydrate, in solution alpha- and beta-lactose are in equilibrium.
Formula:	C12-H22-O11
Melting Point	130 °C
Density	1,525 g/ml
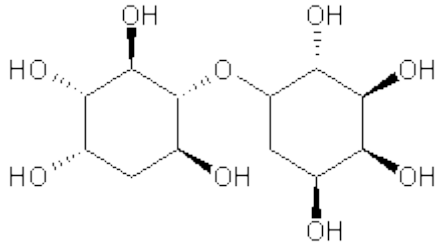
Table A.2.: Properties of TAB by [41]

Name	Cellulose
Form	powder
Colour	white
Odour	odourless
Characterisation:	Combustible solid
	Practically insoluble in water
	Hygroscopic
Formula:	(C6-H10-O5)n
	n = 1000 - 10000
Ignition temperature	232 °C (microcrystalline)
Density	0.2 - 0.4 g/ml (Bulk)
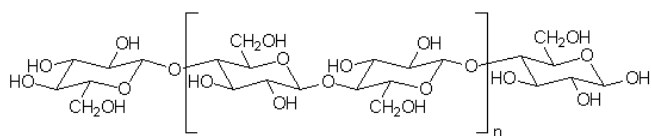
Table A.3.: Properties of MCC by [41]

SYMPATEC

Sympatec GmbH
System-Partikel-Technik

QICPIC-Partikelgrößenanalyse
WINDOX 5

QICPIC (QP0112) & OASISDRY/L, 2.00 63.0 mm - M8 (20...6820μm)
Tablettose Partikelanzahl:1345016   **2010-07-15, 14:54:57**,468

$x_{10} = 72,47$ μm $x_{50} = 183,86$ μm $x_{90} = 428,48$ μm   **SMD = 140,17 μm   VMD = 218,76 μm**
$x_{16} = 88,92$ μm $x_{84} = 354,45$ μm $x_{99} = 646,49$ μm
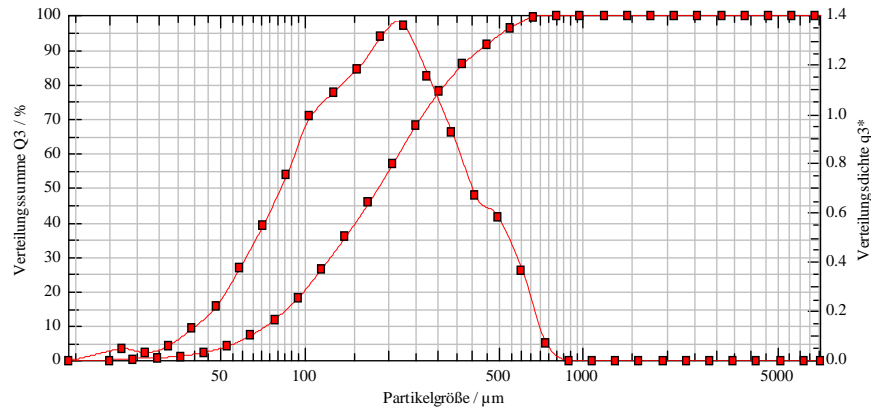
Kommentar:

Benutzerparameter:
Benutzer: Johannes Hofer
Probenbezeichnung: Tablettose FT 4
Anmerkung 1: Probe von Otto Scheibelhofer
Anmerkung 2: wahre Dichte aus Literatur

Verteilungssumme

x_0/μm	Q_3/%	x_0/μm	Q_3/%	x_0/μm	Q_3/%	x_0/μm	Q_3/%
20,00	0,00	94,72	18,20	448,57	91,43	2124,39	100,00
24,29	0,39	115,04	26,55	544,83	96,32	2580,23	100,00
29,50	0,64	139,73	35,74	661,73	99,40	3133,89	100,00
35,84	1,13	169,71	45,70	803,73	100,00	3806,35	100,00
43,52	2,23	206,13	56,77	976,19	100,00	4623,11	100,00
52,86	4,07	250,36	68,22	1185,65	100,00	5615,12	100,00
64,21	7,22	304,08	77,96	1440,07	100,00	6820,00	100,00
77,98	11,85	369,32	85,78	1749,08	100,00	7307,77	100,00

Verteilungsdichte (log.)

x_m/μm	$q_3$lg	x_m/μm	$q_3$lg	x_m/μm	$q_3$lg	x_m/μm	$q_3$lg
14,14	0,00	85,94	0,75	407,02	0,67	1927,62	0,00
22,04	0,05	104,39	0,99	494,36	0,58	2341,24	0,00
26,77	0,03	126,79	1,09	600,44	0,36	2843,62	0,00
32,52	0,06	153,99	1,18	729,28	0,07	3453,79	0,00
39,49	0,13	187,03	1,31	885,77	0,00	4194,90	0,00
47,97	0,22	227,17	1,36	1075,83	0,00	5095,03	0,00
58,26	0,37	275,91	1,15	1306,68	0,00	6188,31	0,00
70,76	0,55	335,12	0,93	1587,07	0,00	7059,67	0,00

Auswertung: WINDOX 5.6.0.0
Berechnungsmodus: EQPC

Produkt: Tablettose
Dichte: 1,5700 g/cm³

Figure A.2.: Q_3-Distribution of TAB after an FT4-test, obtained with QicPic.

Sympatec GmbH
System-Partikel-Technik

**SYMPA
TEC**

QICPIC-Partikelgrößenanalyse
WINDOX 5

QICPIC (QP0112) & OASISDRY/L, 2.00 63.0 mm - M8 (20...6820µm)
ASA Partikelanzahl:56909   2010-07-15, 13:02:06$_{781}$

x_{10} = 222,57 µm	x_{50} = 409,15 µm	x_{90} = 651,80 µm	SMD = 347,53 µm	VMD = 427,15 µm
x_{16} = 261,31 µm	x_{84} = 595,88 µm	x_{99} = 940,50 µm		
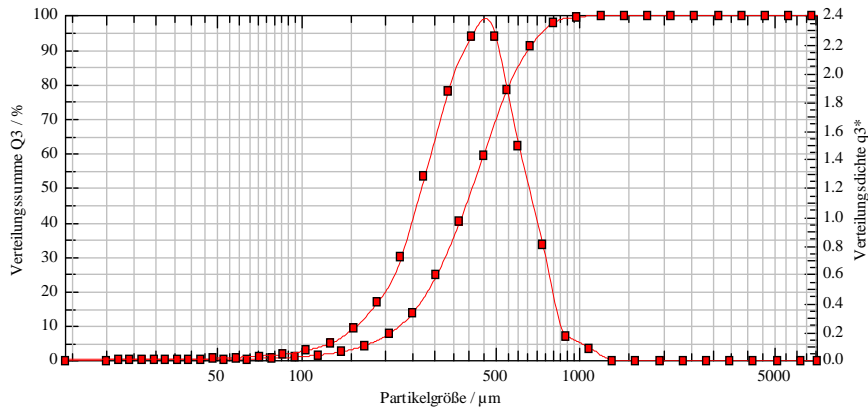
Kommentar:

Benutzerparameter:
Benutzer: Johannes Hofer
Probenbezeichnung: ASA aus FT 4
Anmerkung 1: Probe von Otto Scheibelhofer
Anmerkung 2: wahre Dichte aus Literatur

Verteilungssumme

x_0/µm	Q_3/%	x_0/µm	Q_3/%	x_0/µm	Q_3/%	x_0/µm	Q_3/%
20,00	0,00	94,72	0,89	448,57	59,47	2124,39	100,00
24,29	0,02	115,04	1,48	544,83	78,52	2580,23	100,00
29,50	0,03	139,73	2,45	661,73	91,07	3133,89	100,00
35,84	0,05	169,71	4,34	803,73	97,88	3806,35	100,00
43,52	0,10	206,13	7,75	976,19	99,29	4623,11	100,00
52,86	0,18	250,36	13,80	1185,65	100,00	5615,12	100,00
64,21	0,33	304,08	24,61	1440,07	100,00	6820,00	100,00
77,98	0,56	369,32	40,43	1749,08	100,00	7307,77	100,00

Verteilungsdichte (log.)

x_m/µm	$q_3$lg	x_m/µm	$q_3$lg	x_m/µm	$q_3$lg	x_m/µm	$q_3$lg
14,14	0,00	85,94	0,04	407,02	2,25	1927,62	0,00
22,04	0,00	104,39	0,07	494,36	2,26	2341,24	0,00
26,77	0,00	126,79	0,12	600,44	1,49	2843,62	0,00
32,52	0,00	153,99	0,22	729,28	0,81	3453,79	0,00
39,49	0,01	187,03	0,40	885,77	0,17	4194,90	0,00
47,97	0,01	227,17	0,72	1075,83	0,08	5095,03	0,00
58,26	0,02	275,91	1,28	1306,68	0,00	6188,31	0,00
70,76	0,03	335,12	1,87	1587,07	0,00	7059,67	0,00

Auswertung: WINDOX 5.6.0.0
Berechnungsmodus: EQPC

Produkt: ASA
Dichte: 1,4200 g/cm³

Figure A.3.: Q_3-Distribution of ASA after an FT4-test, obtained with QicPic.

QICPIC-Partikelgrößenanalyse
WINDOX 5

QICPIC (QP0112) & OASISDRY/L, 2.00 63.0 mm - M8 (20...6820µm)
MCC Partikelanzahl:1074387   **2010-07-15, 13:44:01**,671

x_{10} = **63,59 µm**	x_{50} = **137,47 µm**	x_{90} = **258,79 µm**	**SMD** = **112,80 µm**	**VMD** = **151,88 µm**
x_{16} = 75,12 µm	x_{84} = 230,95 µm	x_{99} = 382,89 µm		
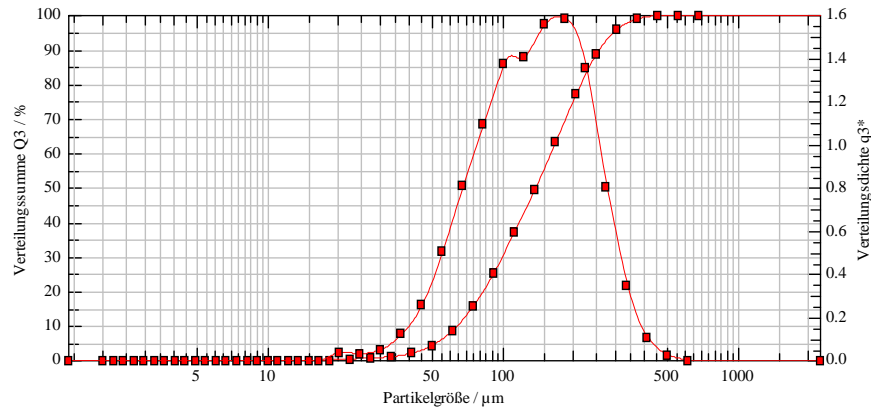
Kommentar:

Benutzerparameter:
Benutzer: Johannes Hofer
Probenbezeichnung: MCC FT 4
Anmerkung 1: Probe von Otto Scheibelhofer
Anmerkung 2: wahre Dichte aus Literatur

Verteilungssumme

x_0/µm	Q_3/%	x_0/µm	Q_3/%	x_0/µm	Q_3/%	x_0/µm	Q_3/%
2,00	0,00	9,99	0,00	49,94	4,29	249,52	88,83
2,45	0,00	12,22	0,00	61,06	8,69	305,10	95,85
2,99	0,00	14,94	0,00	74,66	15,74	373,06	98,89
3,66	0,00	18,27	0,00	91,29	25,31	456,15	99,80
4,47	0,00	22,34	0,32	111,62	37,30	557,76	100,00
5,47	0,00	27,32	0,58	136,49	49,56	682,00	100,00
6,68	0,00	33,40	0,99	166,89	63,18	7307,77	100,00
8,17	0,00	40,84	2,05	204,06	77,01		

Verteilungsdichte (log.)

x_m/µm	$q_3$lg	x_m/µm	$q_3$lg	x_m/µm	$q_3$lg	x_m/µm	$q_3$lg
1,41	0,00	9,04	0,00	45,16	0,26	225,65	1,35
2,21	0,00	11,05	0,00	55,22	0,50	275,91	0,80
2,70	0,00	13,51	0,00	67,52	0,81	337,37	0,35
3,31	0,00	16,52	0,00	82,56	1,10	412,52	0,10
4,04	0,00	20,20	0,04	100,95	1,37	504,41	0,02
4,94	0,00	24,70	0,03	123,43	1,40	616,76	0,00
6,04	0,00	30,20	0,05	150,93	1,56	2232,47	0,00
7,39	0,00	36,93	0,12	184,54	1,58		

Auswertung: WINDOX 5.6.0.0
Berechnungsmodus: EQPC

Produkt: MCC
Dichte: 1,3500 g/cm³

Figure A.4.: Q_3-Distribution of MCC after an FT4-test, obtained with QicPic.

ffc < 1	not flowing
1 < ffc< 2	very cohesive
2 < ffc < 4	cohesive
4 < ffc < 10	intermittent flow
10 < ffc	free flowing

Table A.4.: Classification of the flow function constant according to Jenike [45].

A.5. Plots and parameters of the rheological models

A.5.1. Parameters of the DoEs properties

The DoE-concerning model parameters are shown in table A.5, table A.6 and table A.7.

Maximum Runs	2048
Objective	Screening
Process Model	–
Mixture Model	Linear
Design	Axial Extended
Runs in Design	9
Center points	3
Replicates	0
N = Actual Runs	12

Table A.5.: Summary of properties of the screening DoE

A.5.2. Correlations

An overview of the largest 50 correlations is given in figure A.5.

A.5.3. Parameters of the final response models

The quality parameters gained for the responses can be found in table A.8, and the coefficients are tabulated together with their confidence levels in table A.9, table A.10, table A.11, table A.12 and table A.13. Non-significant parameters are indicated by a red p-value. Not for all parameters enough degrees of freedom of repeated experiments exist to estimate uncertainties, this is especially true, when humidity cannot be neglected.

Maximum Runs	2048
Objective	RSM
Process Model	–
Mixture Model	Quadratic
Design	Modified Simplex Centroid
Runs in Design	9
Center points	3
Replicates	0
N = Actual Runs	12

Table A.6.: Summary of properties of the RSM-DoE

Candidate set			
Extreme Vertices	3		
Edge points	9		
Centroids of high dim. surfaces	2		
Total Runs	14		
D-Optimal			
Objective	RSM		
Model Type	Cubic		
Potential Terms			
Number of Inclusions	12		
Constraints	No		
Design Runs	18		
Selected Design Number	21		
Design Statistics	G-Efficiency	56.1592	
	log(Det. of X'X)	0.270353	
	Norm. log(Det. of X'X)	-1.22824	
	Condition Number	65.438	

Table A.7.: Summary of properties of the d-optimal DoE

Figure A.5.: Overview of the 50 most important correlations within factor and response parameters.

	N	Comp.	Cond. No.	R2	R2 Adj.	Q2	SDY	RSD	Validity	Reproduc.
Conditioned Bulk Density	19	1	1.732	0.972	0.969	0.935	0.111	0.019	0.376	1.000
Basic Flow Energy	19	2	1.732	0.801	0.601	0.663	0.130	0.082	0.460	0.990
Stability Index	19	2	6.015	0.573	0.040	0.156	0.086	0.084	0.690	0.839
Flow Rate Index	19	2	3.469	0.855	0.715	0.362	0.001	0.000	0.836	0.772
Specific Energy	19	1	1.732	0.646	0.593	0.429	0.004	0.002	0.714	0.926
Aeration Ratio	18	2	2.520	0.565	0.431	0.428	109.540	82.639	0.548	0.972
Aeration End Energy	18	2	9.504	0.885	0.837	0.615	11.681	4.714	0.475	0.996
Fluidisation Point	18	2	11.21	0.730	0.343	0.510	0.102	0.083	-0.200	1.000
Poured Density at -2deg	19	1	1.732	0.977	0.975	0.941	0.110	0.018	0.127	1.000
Basic Flow Energy at -2 deg	19	2	3.469	0.777	0.691	0.408	1.617	899.304	0.592	0.979
Tapped Density (250 taps)	19	1	1.732	0.981	0.978	0.969	0.077	0.011	0.759	0.994
Consolidated Energy (250 taps)	19	2	1.834	0.195	-0.035	-0.050	2.824	2,872.470	0.780	0.657
Consolidated Energy Index	19	1	1.732	0.519	0.459	0.434	0.500	0.368	0.946	0.046
Hausner Ratio	19	2	22.44	0.765	-1.119	0.349	0.029	0.043	0.767	0.767
Unconfined Yield Strength	19	2	3.469	0.377	0.137	0.121	0.603	0.560	0.354	0.991
Major Principal Stress	19	2	1.834	0.848	0.804	0.808	1.818	0.804	0.476	0.995
Cohesion	19	2	3.469	0.386	0.150	0.129	0.161	0.148	0.591	0.941
Angle of internal friction	19	2	5.822	0.774	0.688	0.374	1.493	0.834	0.864	0.776
Effective Angle of Internal Friction	19	2	5.822	0.875	0.827	0.615	1.208	0.502	0.894	0.832
LogFit of Compressbility	19	1	1.732	0.758	0.728	0.716	0.003	0.001	0.964	0.377
Pressure Drop at 8 kPa	19	2	2.609	0.837	0.734	0.646	0.540	0.278	0.544	0.987
Shear Stress at 5 kPa	19	2	3.469	0.817	0.746	0.554	0.021	0.011	0.553	0.987

Table A.8.: Summary of the parameters describing the fit quality for the responses

Unscaled coefficients, adjusted to reference mixture

Conditioned Bulk Density	Coeff.	Std. Err.	P	Conf. int(±)	Ref.Mixt.
Constant	0.579947	0.0199767	2.87E-15	0.0423487	(Original units)
ASA	0.181	0.0222658	4.50E-07	0.0472014	0.333333
TAB	0.0668464	0.0222658	0.00844071	0.0472014	0.333333
MCC	-0.247846	0.0222658	6.06E-09	0.0472014	0.333334

N = 19	Q2 =	0.935	Cond. no. =	1.732	
DF = 16	R2 =	0.972	RSD =	0.01947	
Comp. = 1	R2 Adj. =	0.969			
			Conf. lev. =	0.95	

Basic Flow Energy~	Coeff.	Std. Err.	P	Conf. int(±)	Ref.Mixt.
Constant	3.32297	--	--	--	(Original units)
ASA	-0.0736669	--	--	--	0.333333
TAB	-0.0156468	--	--	--	0.333333
MCC	-0.104864	--	--	--	0.333334
ASA*ASA	0.149469	--	--	--	
ASA*TAB	0.183576	--	--	--	
ASA*MCC	0.330018	--	--	--	
ASA*ASA*ASA	0.36689	--	--	--	
ASA*ASA*TAB	-0.462279	--	--	--	
ASA*ASA*MCC	-0.648204	--	--	--	

N = 19	Q2 =	0.663	Cond. no. =	1.732	
DF = 9	R2 =	0.801	RSD =	0.08188	
Comp. = 2	R2 Adj. =	0.601			
			Conf. lev. =	0.95	

Stability Index	Coeff.	Std. Err.	P	Conf. int(±)	Ref.Mixt.
Constant	0.397967	--	--	--	(Original units)
Hum	0.011554	--	--	--	
ASA	0.0573289	--	--	--	0.333333
TAB	0.0771562	--	--	--	0.333333
MCC	-0.0843985	--	--	--	0.333334
ASA*ASA	-0.242913	--	--	--	
TAB*TAB	-0.125935	--	--	--	
MCC*MCC	0.0343181	--	--	--	
ASA*TAB	0.312622	--	--	--	
ASA*MCC	0.0640948	--	--	--	
TAB*MCC	-0.117317	--	--	--	

N = 19	Q2 =	0.156	Cond. no. =	6.015	
DF = 8	R2 =	0.573	RSD =	0.08442	
Comp. = 2	R2 Adj. =	0.04			
			Conf. lev. =	0.95	

Flow Rate Index~	Coeff.	Std. Err.	P	Conf. int(±)	Ref.Mixt.
Constant	-1.99468	--	--	--	(Original units)
ASA	-0.000648692	--	--	--	0.333333
TAB	-0.000283638	--	--	--	0.333333
MCC	0.000578076	--	--	--	0.333334
ASA*ASA	-0.00227726	--	--	--	
TAB*TAB	-0.00046082	--	--	--	
MCC*MCC	-0.000262182	--	--	--	
ASA*TAB	0.00191985	--	--	--	
ASA*MCC	0.00161179	--	--	--	

N = 19	Q2 =	0.362	Cond. no. =	3.469	
DF = 10	R2 =	0.855	RSD =	0.0004124	
Comp. = 2	R2 Adj. =	0.715			
			Conf. lev. =	0.95	

Table A.9.: Summary of the coefficients of the response parameters Conditioned Bulk Density, Basic Flow Energy, Stability Index, Flow Rate Index

Unscaled coefficients, adjusted to reference mixture

Specific Energy~	Coeff.	Std. Err.	P	Conf. int(±)	Ref.Mixt.
Constant	-1.96863	0.00228154	0	0.00483664	(Original units)
ASA	0.0032805	0.00254297	0.215377	0.00539086	0.333333
TAB	-0.00665825	0.00254297	0.0186349	0.00539086	0.333333
MCC	0.00337757	0.00254297	0.202749	0.00539086	0.333334

N = 19	Q2 =	0.429	Cond. no. =	1.732	
DF = 16	R2 =	0.646	RSD =	0.002224	
Comp. = 1	R2 Adj. =	0.593			
			Conf. lev. =	0.95	

Aeration Ratio	Coeff.	Std. Err.	P	Conf. int(±)	Ref.Mixt.
Constant	-178.205	--	--	--	(Original units)
Hum	7.15868	--	--	--	
ASA	-141.32	--	--	--	0.333333
TAB	-51.4049	--	--	--	0.333333
MCC	155.259	--	--	--	0.333334

N = 18	Q2 =	0.428	Cond. no. =	2.52	
DF = 13	R2 =	0.565	RSD =	82.64	
Comp. = 2	R2 Adj. =	0.431			
			Conf. lev. =	0.95	

Aeration End Energy	Coeff.	Std. Err.	P	Conf. int(±)	Ref.Mixt.
Constant	9.43554	5.22367	0.0959956	11.3813	(Original units)
ASA	25.3768	7.01419	0.00352793	15.2825	0.333333
TAB	1.59873	6.91927	0.821165	15.0757	0.333333
MCC	-26.9755	6.91926	0.00211539	15.0757	0.333334
ASA*ASA	39.5311	10.8142	0.00329328	23.562	
TAB*TAB	0.159848	6.97765	0.982096	15.2029	
MCC*MCC	28.7864	6.97763	0.00140671	15.2029	
ASA*TAB	-10.9044	13.1408	0.422845	28.6312	
ASA*MCC	-68.1576	13.1408	0.000226805	28.6311	
TAB*MCC	10.5847	11.2139	0.363844	24.4329	

N = 18	Q2 =	0.615	Cond. no. =	9.504	
DF = 12	R2 =	0.885	RSD =	4.714	
Comp. = 2	R2 Adj. =	0.837			
			Conf. lev. =	0.95	

Fluidisation Point~	Coeff.	Std. Err.	P	Conf. int(±)	Ref.Mixt.
Constant	1.53329	--	--	--	(Original units)
Hum	-0.00595438	--	--	--	
ASA	-0.00365617	--	--	--	0.333333
TAB	-0.00851983	--	--	--	0.333333
MCC	-0.123106	--	--	--	0.333334
ASA*ASA	0.46086	--	--	--	
TAB*TAB	0.0141473	--	--	--	
MCC*MCC	0.136804	--	--	--	
ASA*TAB	-0.000587585	--	--	--	
ASA*MCC	-0.281085	--	--	--	
TAB*MCC	-0.0231926	--	--	--	

N = 18	Q2 =	0.51	Cond. no. =	11.21	
DF = 7	R2 =	0.73	RSD =	0.08277	
Comp. = 2	R2 Adj. =	0.343			
			Conf. lev. =	0.95	

Table A.10.: Summary of the coefficients of the response parameters Specific Energy, Aeration Ration, Aeration End Energy, Fluidisation Point

A 12

Unscaled coefficients, adjusted to reference mixture

Poured Density at -2deg	Coeff.	Std. Err.	P	Conf. int(±)	Ref.Mixt.
Constant	0.584631	0.0179931	4.88E-16	0.0381437	(Original units)
ASA	0.171539	0.0200549	2.30E-07	0.0425145	0.333333
TAB	0.0783079	0.0200549	0.00126131	0.0425145	0.333333
MCC	-0.249846	0.0200549	1.19E-09	0.0425145	0.333334

N = 19	Q2 =	0.941	Cond. no. =	1.732	
DF = 16	R2 =	0.977	RSD =	0.01754	
Comp. = 1	R2 Adj. =	0.975			
			Conf. lev. =	0.95	

Tapped Density (250 taps)~	Coeff.	Std. Err.	P	Conf. int(±)	Ref.Mixt.
Constant	-0.173859	0.0116611	8.37E-11	0.0247204	(Original units)
ASA	0.117072	0.0129973	1.15E-07	0.0275531	0.333333
TAB	0.0586689	0.0129973	0.000353232	0.0275531	0.333333
MCC	-0.175741	0.0129973	3.58E-10	0.0275531	0.333334

N = 19	Q2 =	0.969	Cond. no. =	1.732	
DF = 16	R2 =	0.981	RSD =	0.01137	
Comp. = 1	R2 Adj. =	0.978			
			Conf. lev. =	0.95	

Consolidated Energy (250 taps)	Coeff.	Std. Err.	P	Conf. int(±)	Ref.Mixt.
Constant	3272.11	--	--	--	(Original units)
Hum	146.136	--	--	--	
ASA	1240.38	--	--	--	0.333333
TAB	1593.56	--	--	--	0.333333
MCC	-2833.96	--	--	--	0.333334

N = 19	Q2 =	-0.05	Cond. no. =	1.834	
DF = 14	R2 =	0.195	RSD =	2872	
Comp. = 2	R2 Adj. =	-0.035			
			Conf. lev. =	0.95	

Consolidated Energy Index	Coeff.	Std. Err.	P	Conf. int(±)	Ref.Mixt.
Constant	2.53579	0.377119	4.89E-06	0.799457	(Original units)
ASA	-0.843077	0.420333	0.062099	0.891065	0.333333
TAB	0.350769	0.420333	0.416285	0.891065	0.333333
MCC	0.492307	0.420333	0.258654	0.891065	0.333334

N = 19	Q2 =	0.434	Cond. no. =	1.732	
DF = 16	R2 =	0.519	RSD =	0.3676	
Comp. = 1	R2 Adj. =	0.459			
			Conf. lev. =	0.95	

Shear Stress at 5 kPa~	Coeff.	Std. Err.	P	Conf. int(±)	Ref.Mixt.
Constant	-1.39794	0.0129229	1.35E-20	0.0279182	(Original units)
ASA	0.0600993	0.0260637	0.0382402	0.0563071	0.333333
TAB	-0.102177	0.0260637	0.00175742	0.0563071	0.333333
MCC	0.0420782	0.0260636	0.130431	0.0563071	0.333334
ASA*ASA	-0.034709	0.0304539	0.274966	0.0657917	
TAB*TAB	0.112404	0.0304539	0.00271654	0.0657917	
MCC*MCC	0.016806	0.0304539	0.590411	0.0657917	

N = 19	Q2 =	0.554	Cond. no. =	3.469	
DF = 13	R2 =	0.817	RSD =	0.01076	
Comp. = 2	R2 Adj. =	0.746			
			Conf. lev. =	0.95	

Table A.11.: Summary of the coefficients of the response parameters Poured Density at -2 deg, Tapped Density, Consolidated Energy, Consolidated Energy Index, Shear stress at 5 kPa

Unscaled coefficients, adjusted to reference mixture

Hausner Ratio	Coeff.	Std. Err.	P	Conf. int(±)	Ref.Mixt.
Constant	1.17065	--	--	--	(Original units)
ASA	0.00914188	--	--	--	0.333333
TAB	0.0101316	--	--	--	0.333333
MCC	0.0291377	--	--	--	0.333334
ASA*ASA	-0.041998	--	--	--	
TAB*TAB	-0.0433052	--	--	--	
MCC*MCC	-0.029546	--	--	--	
ASA*TAB	-0.0100798	--	--	--	
ASA*MCC	0.0172461	--	--	--	
TAB*MCC	-0.0171763	--	--	--	
ASA*ASA*ASA	-0.0542561	--	--	--	
MCC*MCC*MCC	0.0382086	--	--	--	
ASA*ASA*TAB	0.0511135	--	--	--	
ASA*ASA*MCC	0.113106	--	--	--	
MCC*MCC*ASA	-0.0783964	--	--	--	
TAB*TAB*MCC	0.0719611	--	--	--	
MCC*MCC*TAB	-0.0372514	--	--	--	

N = 19	Q2 =	0.349	Cond. no. =	22.44	
DF = 2	R2 =	0.765	RSD =	0.04264	
Comp. = 2	R2 Adj. =	-1.119			
			Conf. lev. =	0.95	

Unconfined Yield Strength	Coeff.	Std. Err.	P	Conf. int(±)	Ref.Mixt.
Constant	-0.271018	0.672803	0.693627	1.4535	(Original units)
ASA	0.331272	1.35695	0.810941	2.93152	0.333333
TAB	0.0814957	1.35695	0.953021	2.93152	0.333333
MCC	-0.412766	1.35695	0.7658	2.93151	0.333334
ASA*ASA	1.32197	1.58552	0.419465	3.42531	
TAB*TAB	1.35075	1.58552	0.409674	3.42531	
MCC*MCC	2.35866	1.58552	0.1607	3.42531	

N = 19	Q2 =	0.121	Cond. no. =	3.469	
DF = 13	R2 =	0.377	RSD =	0.5601	
Comp. = 2	R2 Adj. =	0.137			
			Conf. lev. =	0.95	

Major Principal Stress	Coeff.	Std. Err.	P	Conf. int(±)	Ref.Mixt.
Constant	24.9786	--	--	--	(Original units)
Hum	-0.131342	--	--	--	
ASA	2.70671	--	--	--	0.333333
TAB	-3.41833	--	--	--	0.333333
MCC	0.711626	--	--	--	0.333334

N = 19	Q2 =	0.808	Cond. no. =	1.834	
DF = 14	R2 =	0.848	RSD =	0.8043	
Comp. = 2	R2 Adj. =	0.804			
			Conf. lev. =	0.95	

Cohesion	Coeff.	Std. Err.	P	Conf. int(±)	Ref.Mixt.
Constant	-0.0998837	0.178057	0.584362	0.38467	(Original units)
ASA	0.0683779	0.359118	0.851933	0.775827	0.333333
TAB	0.0555047	0.359118	0.879542	0.775827	0.333333
MCC	-0.123882	0.359117	0.735639	0.775826	0.333334
ASA*ASA	0.394053	0.419609	0.364802	0.90651	
TAB*TAB	0.352785	0.419609	0.415686	0.90651	
MCC*MCC	0.635165	0.419609	0.154027	0.90651	

N = 19	Q2 =	0.129	Cond. no. =	3.469	
DF = 13	R2 =	0.386	RSD =	0.1482	
Comp. = 2	R2 Adj. =	0.15			
			Conf. lev. =	0.95	

Table A.12.: Summary of the coefficients of the response parameters Hausner Ratio, Unconfined Yield Strength, Major Principle Stress, Cohesion

Unscaled coefficients, adjusted to reference mixture

Angle of internal friction	Coeff.	Std. Err.	P	Conf. int(±)	Ref.Mixt.
Constant	38.2265	0.914101	3.02E-15	1.9748	(Original units)
ASA	0.760292	1.21902	0.543619	2.63353	0.333333
TAB	-2.74791	1.21902	0.0420804	2.63353	0.333333
MCC	1.98763	1.21902	0.126971	2.63353	0.333334
ASA*ASA	-4.08712	1.1954	0.004572	2.5825	
TAB*TAB	-0.290645	1.1954	0.811694	2.5825	
MCC*MCC	-3.1931	1.1954	0.0192218	2.5825	
ASA*TAB	1.18465	1.78184	0.517768	3.84943	
ASA*MCC	6.98957	1.78184	0.00174954	3.84943	
TAB*MCC	-0.603356	1.78184	0.740307	3.84943	

N = 19	Q2 =	0.374	Cond. no. =	5.822	
DF = 13	R2 =	0.774	RSD =	0.8343	
Comp. = 2	R2 Adj. =	0.688			
			Conf. lev. =	0.95	

Effective Angle of Internal Friction	Coeff.	Std. Err.	P	Conf. int(±)	Ref.Mixt.
Constant	38.0977	0.549932	4.39E-18	1.18806	(Original units)
ASA	1.08515	0.733374	0.162783	1.58436	0.333333
TAB	-3.0692	0.733374	0.00106895	1.58436	0.333333
MCC	1.98406	0.733373	0.0180077	1.58436	0.333334
ASA*ASA	-0.830807	0.719164	0.268784	1.55366	
TAB*TAB	2.46699	0.719164	0.0044737	1.55366	
MCC*MCC	-0.000562478	0.719162	0.999311	1.55366	
ASA*TAB	-1.63674	1.07197	0.150756	2.31586	
ASA*MCC	3.29835	1.07197	0.00883079	2.31585	
TAB*MCC	-3.29722	1.07197	0.00884863	2.31585	

N = 19	Q2 =	0.615	Cond. no. =	5.822	
DF = 13	R2 =	0.875	RSD =	0.5019	
Comp. = 2	R2 Adj. =	0.827			
			Conf. lev. =	0.95	

LogFit of Compressbility	Coeff.	Std. Err.	P	Conf. int(±)	Ref.Mixt.
Constant	0.0103158	0.00143875	2.23E-06	0.00305002	(Original units)
ASA	-0.00484616	0.00160362	0.00809878	0.00339952	0.333333
TAB	0.000153842	0.00160362	0.924764	0.00339952	0.333333
MCC	0.0046923	0.00160362	0.00989072	0.00339952	0.333334

N = 19	Q2 =	0.716	Cond. no. =	1.732	
DF = 16	R2 =	0.758	RSD =	0.001402	
Comp. = 1	R2 Adj. =	0.728			
			Conf. lev. =	0.95	

Permeability at 8 kPa (Pressure	Coeff.	Std. Err.	P	Conf. int(±)	Ref.Mixt.
Constant	-0.611164	--	--	--	(Original units)
Hum	0.0376803	--	--	--	
ASA	-1.06979	--	--	--	0.333333
TAB	1.25226	--	--	--	0.333333
MCC	-0.2258	--	--	--	0.333334
ASA*TAB	-0.402178	--	--	--	
ASA*MCC	1.99468	--	--	--	
TAB*MCC	-1.5275	--	--	--	

N = 19	Q2 =	0.646	Cond. no. =	2.609	
DF = 11	R2 =	0.837	RSD =	0.2784	
Comp. = 2	R2 Adj. =	0.734			
			Conf. lev. =	0.95	

Table A.13.: Summary of the coefficients of the response parameters Angle of Internal Friction, Effective Angle of Internal Friction, Parameter of the logarithmic fit of Compressibility, Permeability at 8 kPa